



NRL/MR/7322--19-9960

Development and Implementation of a Langmuir Turbulence Parameterization

MIGUEL SOLANO

*NRC Postdoctoral Fellowship
Washington, DC*

YALIN FAN
PAUL MARTIN

*Ocean Dynamic & Prediction Branch
Oceanography Division*

October 28, 2019

DISTRIBUTION STATEMENT A: Approved for public release; distribution is unlimited.

REPORT DOCUMENTATION PAGE

Form Approved
OMB No. 0704-0188

Public reporting burden for this collection of information is estimated to average 1 hour per response, including the time for reviewing instructions, searching existing data sources, gathering and maintaining the data needed, and completing and reviewing this collection of information. Send comments regarding this burden estimate or any other aspect of this collection of information, including suggestions for reducing this burden to Department of Defense, Washington Headquarters Services, Directorate for Information Operations and Reports (0704-0188), 1215 Jefferson Davis Highway, Suite 1204, Arlington, VA 22202-4302. Respondents should be aware that notwithstanding any other provision of law, no person shall be subject to any penalty for failing to comply with a collection of information if it does not display a currently valid OMB control number. **PLEASE DO NOT RETURN YOUR FORM TO THE ABOVE ADDRESS.**

1. REPORT DATE (DD-MM-YYYY) 28-10-2019			2. REPORT TYPE NRL Memorandum Report			3. DATES COVERED (From - To) April 2018 – September 2019			
4. TITLE AND SUBTITLE Development and Implementation of a Langmuir Turbulence Parameterization						5a. CONTRACT NUMBER			
						5b. GRANT NUMBER			
						5c. PROGRAM ELEMENT NUMBER 0601153N			
6. AUTHOR(S) Miguel Solano*, Yalin Fan, and Paul Martin						5d. PROJECT NUMBER 73-1G35-20-5			
						5e. TASK NUMBER BE-031-0342			
						5f. WORK UNIT NUMBER 1G35			
7. PERFORMING ORGANIZATION NAME(S) AND ADDRESS(ES) Naval Research Laboratory 1005 Balch Boulevard Stennis Space Center, MS 39529-5004						8. PERFORMING ORGANIZATION REPORT NUMBER NRL/MR/7322--19-9960			
9. SPONSORING / MONITORING AGENCY NAME(S) AND ADDRESS(ES) Office of Naval Research One Liberty Center 875 North Randolph Street, Suite 1425 Arlington, VA 22203-1995						10. SPONSOR / MONITOR'S ACRONYM(S) ONR			
						11. SPONSOR / MONITOR'S REPORT NUMBER(S)			
12. DISTRIBUTION / AVAILABILITY STATEMENT DISTRIBUTION STATEMENT A: Approved for public release; distribution is unlimited.									
13. SUPPLEMENTARY NOTES *NRC Postdoctoral Fellowship, 500 Fifth Street, NW, Washington, DC 20001									
14. ABSTRACT Langmuir turbulence (LT) occurs under the influence of wave and wind forcing, which arises as an additional vortex force in the momentum equations according to the theory of Craik and Leibovich (1976). Although LT is now regarded as a contributing and often dominant factor driving turbulent processes that transport heat and momentum in the upper layer of oceans and lakes, our understanding on this physical process is still limited. Current attempts to represent the LT effect in ocean models are all based on idealized study with simplified oceanic and wind conditions, and thus can have limited practical application in real ocean modeling. This report describes the development of a parameterization that represents the eddy viscosity difference due to the presence of LT based on real case studies, and its implementation in the Navy Coastal Ocean Model (NCOM). The new parameterization overcomes two significant limitations by previous attempts that presume wind-wave alignment and constant Stokes depth penetration ratio (). The model proposed here includes an additional function to account for the wind-wave angle of misalignment and variable Stokes decay scales base on real case simulations. Although model comparisons at the Ocean Weather Station Papa show comparable skill between the newly developed parameterization and the turbulence closure models by Kantha-Clayson (2004) and Harcourt (2015), given the relative simple ocean dynamics at the station, we expect better performance from the new parameterization in more complicated atmospheric and ocean conditions.									
15. SUBJECT TERMS Turbulent mixing Langmuir turbulence NCOM Turbulet mixing scheme Parameterization									
16. SECURITY CLASSIFICATION OF:				17. LIMITATION OF ABSTRACT		18. NUMBER OF PAGES		19a. NAME OF RESPONSIBLE PERSON Yalin Fan	
a. REPORT Unclassified Unlimited		b. ABSTRACT Unclassified Unlimited		c. THIS PAGE Unclassified Unlimited				19b. TELEPHONE NUMBER (include area code) (228) 688-4655	
				Unclassified Unlimited		72			

This page intentionally left blank.

Table of Contents

LISTING OF TABLES AND FIGURES.....	IV
EXECUTIVE SUMMARY.....	E-1
1. INTRODUCTION.....	1
1.1 PHYSICAL INTERPRETATION OF LANGMUIR TURBULENCE.....	1
1.2 TURBULENCE MODELING	1
<i>1.2.1 Langmuir Turbulence in LES.....</i>	<i>2</i>
<i>1.2.2 Langmuir Turbulence in RANS.....</i>	<i>2</i>
1.3 DOCUMENT OVERVIEW.....	3
2. REVIEW OF LANGMUIR TURBULENCE PARAMETERIZATIONS	4
2.1 MELLOR-YAMADA (MY)	4
2.2 KANTHA-CLAYSON (KC).....	5
2.3 HARCOURT (HC)	5
2.4 THE NON-LOCAL KPP MODEL.....	6
3. LT PARAMETERIZATION	7
3.1 IMPORTANT DEFINITIONS.....	8
3.2 LARGE EDDY SIMULATIONS AT STATION PAPA.....	10
3.3 STATISTICS AND AVERAGING	14
3.4 DIMENSIONAL ANALYSIS FOR LT.....	15
3.5 PARAMETER DEVELOPMENT.....	16
3.6 NON-DIMENSIONAL VARIABLES.....	22
3.7 LT SURFACE PARAMETERIZATION	25
3.8 LT BOUNDARY LAYER PARAMETERIZATION	32
<i>3.8.1 The KPP model.....</i>	<i>34</i>
<i>3.8.2 The enhanced KPP model.....</i>	<i>35</i>
<i>3.8.3 The new KPP model.....</i>	<i>37</i>
4. IMPLEMENTATION.....	45
5. RESULTS AND DISCUSSION	47
5.1 COMPUTING MLD AND BLD	48
5.2 NCOM SIMULATION SET-UP	50
5.3 SIMULATIONS WITHOUT LT	52
5.4 SIMULATIONS WITH LT.....	54
5.5 OWS PAPA (1961).....	57
5.6 CLOSING REMARKS.....	59
6. SUMMARY AND CONCLUSIONS.....	59
7. GLOSSARY	60
ACKNOWLEDGEMENTS.....	61
REFERENCES.....	62

Listing of tables and figures

Table 1: Length, time and velocity scales typically used to represent wind stress, buoyancy and Stokes drift.....	19
Table 2: List of NCOM simulations at OWS-P.....	50
Figure 1: Location of Ocean Water Station Papa.....	11
Figure 2: Vertical grid for Large Eddy Simulation at Ocean Water Station Papa.....	12
Figure 3: Initial temperature and salinity profiles for Large Eddy Simulation at Ocean Water Station Papa.....	12
Figure 4: Surface forcing at OWS-P. (Top) Wind stress magnitude in Pascals. (Bottom) Surface heat flux in Watts per square meter.....	13
Figure 5: Stokes drift at OWS-P. (Top-left) Time series of Eastward surface Stokes drift. (Bottom left) Time series of Northward Stokes drift. (Right) Stokes drift current profile at initialization.....	13
Figure 6: (Top) Water side friction velocity. (Middle) Surface Stokes drift. (Bottom) Surface buoyancy flux at Ocean Water Station Papa for the 6.5 day averaging period. Background shaded rectangles are used to denote different inertial periods.....	14
Figure 7: (Top) Stoke drift e-folding depth. (Bottom) wind-wave misalignment angle at Ocean Water Station Papa from November 16, 2011 at 7:12:01 to November 22, 2011 at 19:25:19. ...	14
Figure 8: Vertical Turbulent Kinetic Energy budget at Ocean Water Station Papa from the LES model averaged over 10 inertial oscillations (6.5 day period). (Left) Without LT. (Right) With LT.....	17
Figure 9: Difference in the Vertical Turbulent Kinetic Energy budget, between simulations with and without LT.....	18
Figure 10: Correlation coefficient of physical parameters with the difference in shear production from simulations with and without Stokes drift.....	20
Figure 11: (Top) Turbulent Langmuir number. (Bottom) Hoenikker number for Ocean Water Station Papa simulations.....	23
Figure 12: Parameter space (La-Ho) for OWS-P simulations.....	24
Figure 13: Scaling of turbulent Langmuir number and non-dimensional eddy viscosity difference.....	26
Figure 14: Scaling of turbulent Langmuir number and non-dimensional eddy viscosity difference. (Left) Colored by wind-wave misalignment angle. (Right) Colored by e-folding depth.....	26
Figure 15: Scaling of surface layer Langmuir number and non-dimensional eddy viscosity difference.....	28
Figure 16: Scaling of e-folding depth averaged Langmuir number and non-dimensional eddy viscosity.....	28
Figure 17: (Left) Scaling of modified Langmuir number $u * \beta S_0$. (Right) Scaling of penetration depth ratio $(hm\beta)$ with non-dimensional eddy viscosity difference.....	29
Figure 18: Scaling of modified Langmuir $u * S_0hm$ number and non-dimensional eddy viscosity difference.....	30

Figure 19: Surface layer parameterization showing the scaling between modified Langmuir number and non-dimensional eddy viscosity difference. The black line is the non-linear regression (power fit). 31

Figure 20: Scaling of modified Langmuir number with non-dimensional eddy viscosity colored by wind-wave misalignment angle..... 32

Figure 21: Profiles of inertially averaged scalar eddy viscosity from estimated from LES at Station Papa. (Left) Without LT. (Right) With LT..... 33

Figure 22: Profiles of inertially averaged eddy viscosity difference, between LES with and without LT. 34

Figure 23: Profiles of inertially averaged eddy viscosity for 10 periods estimated from LES (blue) and from the KPP model of Smyth et al. (2002) (red). 37

Figure 24: (Left) Profiles of scalar eddy viscosity and (Right) eddy viscosity difference for idealized LES under different wind-wave angles. 38

Figure 25: Wind-wave modulation function $g(\theta)$ in range $-\pi < \theta < \pi$ 40

Figure 26: Profiles of eddy viscosity difference between simulations with and without LT at different wind-wave misalignment angles. Solid lines are estimated from LES and dashed lines are calculated using the wind-wave modulation function. 41

Figure 27: Generalized shape function $G(\sigma) = \sigma^1 - \sigma^n$ with different degrees (n)..... 42

Figure 28: Preliminary BL parameterization without modification of shape function using values from LES at OWS-P..... 44

Figure 29: Final BL parameterization using preliminary values computed from LES at OWS-P. 45

Figure 30: (Top) Surface buoyancy flux at OWS-P. (mid-top) MLD and BLD from LES without LT. (mid-bottom) MLD and BLD from LES with LT. (bottom) MLD and BLD difference, from LES with LT minus LES without LT..... 48

Figure 31: Color contours of \log_{10} of eddy viscosity from LES with LT, superimposed with the BLD estimated from the bulk Richardson number ($Ric = 0.3$) using the mean velocity (white line), Lagrangian velocity (green line) and the parameterization suggested by Li and Fox-Kemper (2017; black line). 49

Figure 32: Vertical grid with 150 layers used for NCOM simulations. 51

Figure 33:(Top) wind vectors at 10m height. (Bottom) Surface Stoke drift vectors at OWS-P. . 52

Figure 34: Inertially averaged eddy viscosity profiles from LES (black), MY (blue), KC (red), HC (green) and KPP (magenta). 53

Figure 35: Color contours of \log_{10} of eddy viscosity from LES and NCOM simulations..... 54

Figure 36: Inertially averaged eddy viscosity profiles from LES (black), KC (red), HC (green) and KPP (magenta) 55

Figure 37: Color contours of \log_{10} of eddy viscosity from LES and NCOM simulations..... 56

Figure 38: Surface forcing used for the OWS-P simulations during 1961. (Top) Wind stress, (middle) surface heat flux, and (bottom) surface Stokes drift velocity magnitude..... 57

Figure 39: SST at station Papa during 1961 from BT observations (black) and NCOM simulations with LT using Mellor-Yamada 2.5 (magenta), Kantha-Clayson (red), Harcourt (green) and our enhanced KPP model (blue). 58

This page intentionally left blank.

Executive Summary

Langmuir turbulence (LT) occurs under the influence of wave and wind forcing, which arises as an additional vortex force in the momentum equations according to the theory of Craik and Leibovich (1976). Although LT is now regarded as a contributing and often dominant factor driving turbulent processes that transport heat and momentum in the upper layer of oceans and lakes, our understanding on this physical process is still limited. Current attempts to represent the LT effect in ocean models are all based on idealized study with simplified oceanic and wind conditions, and thus can have limited practical application in real ocean modeling. This report describes the development of a parameterization that represents the eddy viscosity difference due to the presence of LT based on real case studies, and its implementation in the Navy Coastal Ocean Model (NCOM). The new parameterization overcomes two significant limitations by previous attempts that presume wind-wave alignment and constant Stokes depth penetration ratio (βh). The model proposed here includes an additional function to account for the wind-wave angle of misalignment and variable Stokes decay scales base on real case simulations. Although model comparisons at the Ocean Weather Station Papa show comparable skill between the newly developed parameterization and the turbulence closure models by Kantha-Clayson (2004) and Harcourt (2015), given the relative simple ocean dynamics at the station, we expect better performance from the new parameterization in more complicated atmospheric and ocean conditions

This page intentionally left blank.

1. Introduction

This report documents efforts in developing a parameterization to model the enhanced mixing due to Langmuir Turbulence under realistic forcing conditions, which arise from the interaction of non-breaking surface gravity waves and ocean currents, to improve vertical mixing schemes used in the oceanic surface boundary layer (OSBL) for models solving the Reynolds-Averaged Navier-Stokes (RANS) equations.

1.1 Physical interpretation of Langmuir Turbulence

LT occurs under the influence of wave and wind forcing, which arises as an additional vortex force in the momentum equations according to the theory of Craik and Leibovich (Craik & Leibovich, 1976), hereafter named the Craik-Leibovich Vortex Force (CL-VF). Although LT is now regarded as a contributing and often dominant factor driving turbulent processes that transport heat and momentum in the upper layer of oceans and lakes, it is not included in most ocean general circulation models. Several laboratory, modeling, and observational studies attribute the under prediction of vertical mixing in mixed layer models to the absence of a LT parameterization (D'Asaro et al. 2014).

Throughout this report, Langmuir Circulation, or Langmuir Cells (LC), refer to the dominant coherent structure of LT composed of “large” counter-rotating vortices formed at the ocean surface as first described by Irving Langmuir (1938). A distinction is made with Langmuir turbulence, which refers more specifically to the additional terms in the phase-averaged governing equations solved by Large Eddy Simulations for oceanic currents in the surface Planetary Boundary Layer (PBL), where the average is over the high-frequency surface gravity waves (McWilliams et al. 1997). This distinction is important because LT exhibits similar characteristics observed in other turbulent flows, namely shear and convective turbulence, which have been extensively studied in the PBL. It is therefore reasonable to assume that LT follows Kolmogorov’s similarity hypothesis, Rotta’s energy redistribution hypothesis (Rotta 1951), and Crow’s distortion by shear (Crow 1968), which are widely used assumptions in modeling turbulence.

The dynamical framework of LT arises from the interpretation of LC proposed by Craik and Leibovich (1976) and later expanded by Leibovich (1983). In the ocean, LC are characterized by elongated streaks of surface particles approximately aligned with the direction of the wind, as observed by Langmuir (1938). LC have been observed in the ocean (Gargett & Wells 2007) and are now recognized as an important process contributing to the mixing of stratified layers in the surface of the ocean, and thus important in the ocean-atmosphere exchange of heat. In the model of Craik and Leibovich, LC are formed by the interaction of the phase average of non-breaking surface waves (i.e., Stokes drift) and ocean currents generated by wind-shear.

1.2 Turbulence Modeling

Langmuir turbulence is modeled similarly to a shear production term in turbulence closure models and is equal to the product of the horizontal momentum fluxes and the mean vertical gradient of the Stokes drift. In this study, we assume a horizontally homogeneous ocean such that LT only affects vertical mixing and is not influenced by horizontal gradients. This section

gives a brief overview of how turbulence induced by LC is modeled in LES and in RANS models.

1.2.1 Langmuir Turbulence in LES

Large-Eddy Simulations take advantage of the energy cascade process of turbulence by explicitly simulating the larger energy containing eddies and parameterizing sub-grid scale variability, which according to Kolmogorov's similarity theory is more homogeneous and isotropic. This approach solves important grid scale variables (e.g., Reynold stresses) and models sub-grid scale eddies which are believed to be less flow dependent and act primarily to dissipate energy through viscosity. (Moeng 1984).

The LES model in this study is based on the National Center for Atmospheric Research (NCAR) LES model, and is described in detail by McWilliams (McWilliams et al. 1997, pp. 3-4). The filtered Craik-Leibovich momentum equations include additional terms of the LES Navier-Stokes equations, namely the CL-VF represented by the cross product of the Stokes drift and Eulerian vorticity, modifications to the Coriolis force and generalized pressure as well as additional advection of any material property by wave-induced Lagrangian motion. A Stokes production term is included in the sub-grid scale (SGS) model, the details of this implementation can be found in Sullivan (Sullivan and McWilliams 2007)

1.2.2 Langmuir Turbulence in RANS

Models based on the Reynolds Average Navier-Stokes equations only solve the mean velocity field and require a turbulence closure model to simulate unresolved fluctuations. These unresolved fluctuations affect the mean flow through the Reynold stresses, which are a flow of heat and momentum from the small scale (unresolved) motions affecting the large scale (mean flow). The turbulent momentum fluxes are usually modeled as:

$$\overline{\mathbf{u}'w'} = K_m \partial_z \mathbf{U} \quad (1)$$

Where $\overline{\mathbf{u}'w'}$ represents the Reynold stress, $\partial_z \mathbf{U}$ is the vertical shear of velocity and K_m is the local eddy viscosity, which encapsulates the capacity of the flow to mix momentum in the vertical direction. In this report, variables in bold are used to represent vectors. Turbulent vertical mixing in RANS models are often called Mixed Layer (ML) models, which can be categorized as bulk or diffusion models.

Bulk ML models are based on the assumption that properties within the boundary layer (BL) are well mixed and the governing equations are integrated over the ML under the influence of surface fluxes. These models parameterize the evolution of the ML as a function of surface fluxes of momentum and buoyancy, but give no information of the vertical structure within the ML. Moreover, these parameterizations are not universal and it is often necessary to adjust entrainment coefficients under different conditions. Most bulk ML models are based on those proposed by Niiler (Niiler and Kraus 1977) and Price (Price et al. 1986), which use the bulk or gradient Richardson numbers to determine the evolution of the ML.

On the other hand, diffusion ML models attempt to directly parameterize the turbulent mixing and diffusion, and thus give information about the vertical variability of properties within the

ML. Two approaches are generally used in diffusion models: the K-profile parameterization (Large et al. 1994), hereafter LMD, or Mellor-Yamada type models (Mellor and Yamada 1974).

Mellor-Yamada type models or General Length Scale (GLS) models, use prognostic equations to solve the evolution of turbulent quantities, typically a turbulent velocity scale (q) and a turbulent length (l) or dissipation (q^2l) scale in the specific case of Mellor-Yamada. In second moment (or second order) closure (SMC) models the turbulence equations are closed at the second moment and higher moments are modeled based on Kolmogorov's similarity hypothesis, Rotta's energy redistribution hypothesis (Rotta 1951), and Crow's distortion by shear (Crow 1968). SMC models are empirical since coefficients are usually tuned to different types of turbulent flows and generally yield good results. However, it requires explicit iteration of additional prognostic equations which are computationally expensive to solve, especially when the number of grid points is large. The most commonly used SMC models for ocean applications are the ones introduced by Mellor and Yamada (1974, 1984), Kantha and Clayson (1994, 2004), and more recently Harcourt (2013, 2015).

A second approach of diffusion ML models is the K-profile parameterization (KPP), in which turbulent mixing and diffusion are specified within the ML based on semi-empirical formulations, originally derived from the Atmospheric Boundary Layer (ABL). This approach offers the advantage of being computationally inexpensive compared to SMC models and based on physically relevant theories, such as Monin-Obukhov similarity relations in the constant flux layer. The most notable model using this approach applied to the OSBL is the non-local KPP of LMD, in which vertical fluxes are linearly proportional to the local property gradient plus a nonlocal transport term to circumvent the down gradient flux assumption (Large et al. 1994).

1.3 Document Overview

The objective of this report is to document the development of a Langmuir Turbulence parameterization based on LES results using observed quantities at Ocean Water Station Papa (OWS-P) and the implementation on the NCOM model. We are interested only in diffusion ML models, because we want to resolve important processes in the OSBL. Furthermore, LES results used to develop the parameterization are initialized from observed temperature and salinity profiles, forced with time-varying wind stress and surface heat fluxes, and a Stokes drift is computed using a full 2D wave frequency spectra, which differs from other studies that assume a monochromatic wave field aligned with steady winds and a constant surface buoyancy flux.

Section 2 views the important aspects of LT and previous parameterization efforts in diffusion ML models. Theory of Mellor-Yamada type models is discussed in the context of LT. The non-local KPP scheme of LMD (Large et al. 1994) is discussed briefly along with previously suggested modifications to include LT parameterization (McWilliams and Sullivan 2001; Smyth et al. 2002).

Section 3 shows the development of the LT parameterization to be implemented in NCOM. LES experiments are performed at Station Papa under realistic forcing conditions, and the results are used to develop the enhanced KPP model presented here. Dimensional analysis is used to determine the relevant physical parameters and non-dimensional numbers used in the

parameterization, which are compared with previously well-established parameters such as the turbulent Langmuir number (McWilliams et al. 1997) and the Hoenikker number (Li and Garrett 1995; Li et al. 2005). The KPP model suggested by McWilliams and Sullivan (2000), and Smyth et al. (2002) are taken as the basis of the LT parameterization, using a modified Langmuir number developed here instead of the turbulent Langmuir number. A set of idealized LES are used to include the effect of wind-wave misalignment. The original shape function from LMD is modified to resemble eddy viscosity profiles estimated from LES under realistic forcing conditions at station Papa. Preliminary results of the proposed model are shown, using values from LES.

Section 4 presents the implementation of the KPP model in NCOM. The overall structure of the code is presented with emphasis on the computation of the mixed and boundary layer depth.

Section 5 presents results from the LT parameterization developed here, compared with LES and other SMC schemes implemented in NCOM. One dimensional simulations are performed using NCOM at Ocean Water Station Papa (OWS-P), using Mellor-Yamada 2.5, Kantha and Clayson, Harcourt and the KPP model. Results are discussed in terms of inertially-averaged eddy viscosity, mixed layer depth, sea surface temperature (SST), and temperature and salinity profiles. The final subsection presents closing remarks about the KPP implementation with LT and how these compare with other ML models.

2. Review of Langmuir Turbulence parameterizations

LT parameterizations have been developed and successfully implemented in GLS models by Kantha and Clayson (2004) and Harcourt (2015), and in the KPP model by McWilliams and Sullivan (2000). In order to understand how these parameterizations work, it is important to understand the theoretical principles and assumptions used for their development. Of special interest is the use of LES to develop and improve model parameterizations, since these models resolve important turbulent quantities within the BL, and have been used to adjust model coefficients to yield accurate results. This section presents an overview of the turbulence closure schemes implemented in NCOM, which are used as reference for the new LT parameterization.

2.1 Mellor-Yamada (MY)

The Mellor-Yamada (MY) turbulence closure model (Mellor and Yamada 1974, 1984) is one of the most widely used schemes to simulate the dynamics of the atmospheric and oceanic boundary layers. In their model the full mean Reynolds stress model equations, composed of 8 Partial Differential Equations (PDE, Eqns. 4, 5 and 6 in Mellor and Yamada 1974), are reduced to only 2 PDE's, also known as the Mellor-Yamada level 2 model (hereafter MY2). The more popular Mellor-Yamada level 2.5 (hereafter MY2.5) solves two transport PDE's, one for twice the Turbulent Kinetic Energy (q^2) and one for dissipation ($q^2 l$), where q is the turbulent velocity and l is a master length scale. The remaining equations are solved algebraically to determine stability functions (S_m, S_h) and define the eddy viscosity (K_m):

$$K_m = S_m q l \quad (2)$$

The main advantage of this scheme is that it considers the energetics of the mixing explicitly by solving prognostic equations for turbulent kinetic energy and length scale. In doing so, the mixing estimates carry information about the time history of the flow and can effectively both advect and diffuse. However, this scheme does not account for the interaction between surface waves and ocean currents, so simulations of the OSBL become inaccurate as Langmuir turbulence dominates over shear or convective turbulence. Another disadvantage is the computational cost associated with solving 2 additional three dimensional PDE's, which poses a problem when simulating large domains at high resolution.

2.2 Kantha-Clayson (KC)

The SMC model by Kantha and Clayson (KC) solves the same prognostic equations of MY2.5, but uses the modified expansion of Galperin et al. (1988) and includes shear-instability induced mixing in the strongly stratified region below the mixed layer which addresses some of the shortcomings of the MY model (Kantha and Clayson 1994). Despite this improvement, the first model by KC does not include the effects of surface gravity waves, and after strong modeling evidence from LES studies (Skylningstad and Denbo 1995; McWilliams et al. 1997), an improved SMC model was introduced to include the effects of breaking and non-breaking surface gravity waves. In their second model (Kantha and Clayson 2004), additional turbulence production terms are added to the prognostic equations for TKE and dissipation to simulate the effects of LT, as well as a new model constant used to adjust the relative contribution of the CL-VF term in the prognostic PDE for dissipation.

The model by KC offers some additional features over the MY model. First, it is derived for ocean applications, which includes the effect of Langmuir turbulence and other physics relevant to the OSBL. The model captures important processes of wave-current interactions: their results show that breaking waves have a significant impact on TKE and dissipation levels close to the surface, and more importantly that the inclusion of LT in the turbulent transport equations yield elevated TKE and dissipation rate levels throughout the ML. This increased mixing deepens the ML and sea surface temperature drops at seasonal scales, although variation at diurnal scales is less evident. Second, the model constants are tuned to simulations of the ocean and adjusted by replicating the idealized LES study by McWilliams et al. (1997). However, this LES experiment uses steady surface forcing (momentum and heat fluxes are constant) and Stokes drift calculated from a monochromatic wave aligned with the wind, which are not a good approximation of the real ocean. As with the MY model, it also requires solving transport equations for two variables so a major disadvantage of KC is also the computation cost.

2.3 Harcourt (HC)

The SMC model by Harcourt (HC, 2013, 2015) also attempts to include the effects of LT in the two equation model of Mellor and Yamada. As in the MY and KC models, two prognostic equations are dynamically solved for TKE and dissipation, and the remaining Reynold stresses are solved through stability functions solved algebraically. Harcourt points out that the derivation of the stability functions derived in Kantha and Clayson (2004) only include the local forcing effects by stratification and shear, but not the CL-VF. In his paper (Harcourt 2013) he derives the stability functions from the algebraic Reynold stress model (ARSM) to include the vortex force

terms, and tunes the model constants using the new derivation. Pressure-strain rate correlation which include return to isotropy (Rotta 1951) and a term for distortion by shear (Crow 1968) include an additional term by Stokes shear, and pressure-scalar correlation (Moeng and Wyngaard 1986) are also extended to include the additional vertical gradient of the Stokes drift. These augmentations introduce two additional constants to the turbulence closure models. Closure assumptions for the third moment and pressure-velocity transport terms are the same as in KC (Harcourt 2013).

The most notable difference in the HC scheme is the use of a separate eddy diffusivity for the Stokes shear, which allows part of the vertical momentum flux to be directed down the gradient ($\partial_z \mathbf{U}^s$) of the Stokes drift in addition to the conventional component down the gradient ($\partial_z \mathbf{U}$). The eddy diffusivity for the Stokes shear is:

$$K_s = S_m^s q l \quad (3)$$

Therefore, the momentum fluxes are not computed as in (1), but rather as:

$$\overline{\mathbf{u}'\mathbf{w}'} = K_m \partial_z \mathbf{U} + K_s \partial_z \mathbf{U}_s \quad (4)$$

Where $\partial_z \mathbf{U}_s$ is the Stokes shear. This presents the advantage that local momentum fluxes are sensitive to both the Eulerian and Stokes shear separately, allowing them to evolve independently. As with the other SMC schemes its advantage lies in the accuracy of its results and the disadvantage lies in the computational cost associated with solving two additional PDE's.

2.4 The non-local KPP model

The non-local K-Profile Parameterization introduced by Large et al. (1994) is very appealing for three main reasons: It is based on semi-empirical formulations (i.e., based on Monin-Obukhov similarity theory and functions adjusted from observations), it is computationally inexpensive compared to SMC models and it can be easily adapted to include the additional effects of LT (McWilliams and Sullivan 2001). The most significant disadvantage of this model is the computation of an appropriate boundary layer depth, which in practice requires an initial guess and enough vertical grid resolution at the base of the ML.

The motivation behind this model was that boundary layer models failed to replicate important physics observed in the ABL and OSBL, namely the fact that the surface layer, roughly the upper 10% of the OSBL, does not extend all the way to the surface because at a finite distance roughness begins to directly influence turbulence. Another important motivation behind its development, was the fact that turbulence is fundamentally non-local so that local fluxes of momentum and heat depend on boundary layer depth and surface fluxes in addition to local properties and gradients characteristic of pure shear turbulence. Based on observations and LES experiments that resolve a large portion of momentum and heat fluxes, convective and Langmuir turbulence have been shown to exhibit important characteristics of nonlocal behavior in the form of coherent structures (Mahrt and Gibson 1976; Gargett and Wells 2007). A third motivation is given by observations and simulations indicating that the vertical diffusivity profile for passive

scalars is significantly different when property fluxes are driven by entrainment or surface fluxes. The LES study of Wyngaard and Brost (1984) shows that in the ABL surface driven diffusivities are significantly larger than entrainment driven diffusivities, which implies that a single diffusivity for the total process may be ill-behaved. They attribute this asymmetry to the observation that in the ABL upward vertical plumes are horizontally narrower and have larger vertical velocities than the more diffuse return flows. Interestingly, LC in the ocean are also characterized by horizontally narrow downward flows with higher velocities than the larger and lower velocity upward flows found in between cells (Gargett and Wells 2007), suggesting similar (non-local) behavior of LT.

Consequently the non-local KPP model parameterizes momentum fluxes proportional to the product of an eddy viscosity (K_m) and the mean velocity gradient plus a non-local transport term (γ_m):

$$\overline{\mathbf{u}'w'} = -K_m \partial_z \mathbf{U} + \gamma_m \quad (5)$$

The parameterization consists on prescribing the eddy viscosity at depth (K-profile) and the non-local term as functions of surface fluxes and entrainment. The K-profile is divided in two regimes: the mixed layer under the influence of surface conditions and the ocean interior driven by internal waves, shear instability and double diffusion. In the first regime, the eddy viscosity is proportional to the product of the BL depth (h), a depth dependent turbulent velocity scale (w_m) and a non-dimensional vertical shape function (σ).

$$K_m = hw_m(\sigma)G(\sigma) \quad (6)$$

These variables are discussed in detail in later sections. The parameterization developed here neglects the non-local component of the eddy viscosity, such that the turbulent fluxes are only linearly proportional to mean gradient and the eddy viscosity in order for the scheme to be relevant to other models that use the downgradient assumption.

3. LT Parameterization

While the SMC schemes are able to solve the prognostic equations for turbulent kinetic energy and length scale explicitly, their approach of adding the vortex force to the turbulent closure models is not valid in high resolution simulations. Because the assumption for the Craik and Leibovich theory is based on wave period averaged currents, and it becomes invalid in high resolution models. On the other hand, turbulence models based on the KPP are less computationally demanding but current implementations are based on idealized LES experiments that make unrealistic assumptions about the ocean, namely a Stokes drift computed from a monochromatic wave aligned with the wind direction. Using LES experiments initialized and forced by observed quantities, offers an opportunity to improve the shortcomings of previous parameterizations based on the KPP scheme while maintaining a low computational cost.

In this section, we are interested in parameterizing the *difference* in vertical mixing in the ocean due to the additional turbulence generated by LC under realistic forcing conditions. In order to

develop a robust and accurate model, it must be both computationally inexpensive and based on ocean physics theory and observations. We use dimensional analysis paired with LES simulation results at OWS-P to parameterize the additional turbulent mixing induced by this wave-current interaction. We start by discussing some important definitions used in the parameterization.

3.1 Important definitions

It is important to keep in mind that due to the large number of publications and practices throughout history, as well as distinct physics between the atmosphere and the ocean, authors have used different criteria to define important parameters used in modeling vertical mixing the ABL and OSBL. Most notably, the mixed layer depth (MLD) may vary significantly depending on the application, with some authors choosing a temperature or density criteria to define it. Another crucial definition is that of the turbulent eddy viscosity, which is usually assumed to be down-gradient in turbulence models but this is not always the case. These quantities will be briefly discussed here with a justification for its definition and use.

Entrainment depth (h_e): Depth at which the negative buoyancy flux ($\overline{w'b'}$) is maximum. This parameter has been widely used in ABL dynamics, because in the atmosphere buoyancy flux is the dominant production term of TKE in the vertical direction and controls most of the turbulent characteristics. For more details, refer to the discussion in Large et al. (1994, pp. 366-367).

$$h_e = z \left(\max(\overline{w'b'}) \right) \quad (7)$$

Mixed Layer Depth (h_m): Although MLD may be defined differently depending on its use, for the purpose of this document it is more generally defined as the “depth of active mixing”. The question that every author must answer is: active mixing of which property? Even under this definition, there are significant discrepancies on what parameter is used to define active mixing. Another confusion arises from the fact that boundary layer depth (BLD) and mixed layer depth (MLD) are sometimes (incorrectly) used interchangeably. This distinction is discussed in Sutherland et al. (2014), in which they define the “mixed layer” based on a density criteria, and the “mixing layer” determined from direct measurements of dissipation. To clarify, BLD (“mixing layer”) is used to quantify the ability of a flow to mix vertical layers in the ocean due to turbulent motions (e.g., convective turbulence) and MLD is a measure of vertical stratification (temperature, salinity), which does not require fluid motion. From this perspective the “mixed layer” is affected by the “mixing layer”, and under steady conditions these quantities should reach equilibrium. This distinction is important because it implies that MLD is used to draw conclusions on how tracers are mixed by turbulent motions, which are (mostly) resolved by LES models and only modeled in RANS resolving models by a choice of parameterization. For a detailed discussion on the difference of MLD, BLD and entrainment depth, see Pearson et al. (2018). In this report we define the MLD as the depth at which the potential density changes by 0.125kg/m^3 from the surface.

$$h_m = z(\rho(0) - \rho(z) = 0.125\text{kg/m}^3) \quad (8)$$

Boundary Layer Depth (h): BLD is directly used in ML models to parameterize surface fluxes and its definition is still under much debate (Pearson et al. 2018). Three quantities are repetitively used: bulk/gradient Richardson number, TKE and dissipation. Some authors use the Richardson number, which involves both density and velocity gradients to define BLD, but this poses a problem in the case of pure convection where vertical velocity gradients are absent resulting in an infinite Richardson number. In this document we define BLD as the shallowest depth (d) at which the bulk Richardson number reaches a critical Richardson number, which varies from 0.2 to 0.5.

$$Ri_b = \frac{(B_r - B(d))d}{(v_r - v(d))^2 + v_t^2(d)} \quad (9)$$

Where d is the distance from the surface, $B(d) = -g\rho(d)/\rho_0$ is the buoyancy, $V(d) = \sqrt{u^2 + v^2}$ is the velocity magnitude and the quantities B_r and V_r are the velocities averaged over the surface layer, which is taken as the top 10% of the BLD. In order to avoid unrealistic values under pure convection a turbulent velocity scale V_t is added to the denominator to represent the unresolved velocity shear parameterized in Large et al. (1994) as:

$$V_t = C_v Ri_c^{-1} \kappa^{-2} (-\beta_T)^{\frac{1}{2}} (c_s \epsilon)^{-1/2} d N w_s \quad (10)$$

Note that equation (10) attempts to parameterize the unresolved velocity shear due to shear and convection, but the effect of the Stokes drift and LT is not taken into account. Li and Fox-Kemper (2017) suggest a parameterization based on the surface layer averaged Langmuir number to model the effects of LT on the BLD. Other suggestions include the use of the Lagrangian velocity (i.e., Eulerian + Stokes) to compute the resolved velocity shear.

Eddy Viscosity (K_m): The turbulent viscosity, also known as eddy viscosity, measures the transfer of momentum by turbulent motions (e.g., eddies) in a flow. It is analogous to the molecular viscosity in a laminar flow, which is a measure of the internal friction created in the presence of velocity gradients (shear). An important distinction between the molecular viscosity and the eddy viscosity, is that the first is a property of the fluid and the latter is a property of the flow, that is, a theory that aims at modeling the transfer of energy from unresolved small scale motions to the mean flow. In a local K-profile parameterization, the eddy viscosity relates the vertical momentum fluxes to the mean velocity gradients, as shown in equation (1). This definition stems from the gradient-diffusion hypothesis that assumes that the momentum flux vector is aligned with the mean gradient vector (Pope 2000, p. 94). This is also known as the ‘down-gradient assumption’ that assumes a local behavior because momentum fluxes are only a function of the local gradients. However, important characteristics of nonlocal behavior are coherent structures such as buoyant vertical plumes and LC observed in the PBL, in which heat and momentum fluxes can be observed in the presence of very small gradients (Large et al. 1994). The gradient transport, or (local) K-theory approach is a parameterization for the momentum flux (Reynold stress) that works reasonably well when only small eddies are present in the flow, but behaves poorly when large-eddy coherent structures are present (Stull, 1988, p. 204). In the non-local KPP model of LMD, this is corrected by adding an additional non-local

term (equation 5), to account for counter-gradient fluxes, observed in laboratory BL (Deardorff 1966) and LES experiments (Holtslag and Moeng 1991) in the central region of convective BL.

In LES turbulent momentum fluxes are mostly solved, and the turbulent viscosity (ν_t), usually based on the Smagorinsky model, is used to parameterize the sub-grid scale turbulence that is smaller than the resolved part. In this report the eddy viscosity estimated from LES results is the bulk or scalar eddy viscosity, defined as:

$$K_m = \frac{|\langle \mathbf{u}_\perp w \rangle|}{|\partial_z \langle \mathbf{u}_\perp \rangle|} \quad (11)$$

In equation 11, $|\langle \mathbf{u}_\perp w \rangle|$ is the magnitude of the total (resolved + SGS) turbulent momentum flux and $|\partial_z \langle \mathbf{u}_\perp \rangle|$ is the magnitude of the vertical Eulerian shear. This definition is similar to the one adopted in Noh et al. (2011) and McWilliams et al. (2012), except we use the magnitude of the Eulerian shear instead of the Lagrangian (Eulerian + Stokes) shear. We adopt this definition, using the Eulerian shear instead of the Lagrangian shear, because we want to parameterize an adjustment for the existing turbulent mixing schemes, which are based on the traditional current shear. Furthermore, the K-profiles from this definition are found to be strictly convex while other definitions (Noh et al. 2011, p. 478) yield negative values of eddy viscosity in our simulations. This alternative definition of eddy viscosity is apt for analysis of simulations under steady conditions when the shear production is always positive, but in our simulations the changing wind direction and magnitude will further stir the system and generate instability that yield negative shear production. The negative values in the eddy viscosity from this alternative definition reflect the non-local nature of vertical mixing by LC (Noh et al. 2011, p. 479). Similarly, the presence of significant momentum fluxes in the presence of very small vertical gradients (i.e., non-local flux) is represented in equation (11) as a spike of the eddy viscosity, which is observed in our simulations.

Stokes e-folding scale ($1/\beta$): The Stokes e-folding scale is the depth at which the Stokes drift decreases by a factor of e (i.e., Euler's number) compared to its value at the surface ($U_s = u_s(z = 0)$). It is also known as the Stokes drift penetration or decay scale, which for the case of a monochromatic wave is related to the wavelength as $1/\beta = \delta = 1/2k$.

3.2 Large Eddy Simulations at Station Papa

LES simulations have been performed at OWS-P. The LES model used here solves the filtered Craik-Leibovich momentum and continuity equations:

$$\frac{Dv}{Dt} + f\hat{z} \times (v + u_s) = -\nabla\pi - g\hat{z} \left(\frac{\rho}{\rho_0} \right) + u_s \times \omega + SGS \quad (12)$$

$$\frac{D\rho}{Dt} + u_s \cdot \nabla\rho = SGS \quad (13)$$

$$\nabla \cdot v = 0 \quad (14)$$

Where SGS refers to the sub-grid scale forcing. For a detailed description of the governing equations of the LES simulations performed here refer to the papers by McWilliams et al. (1997) and Liu et al. (2018). For a discussion on the parameterization of the SGS model used, refer to the paper by Sullivan et al. (2007).

OWS-P is a well-known site for having one of the longest records measuring ocean-atmosphere interactions, carbon uptake and ocean acidification and is frequently used to test ML models due to moderately low mesoscale activity, such that the horizontal homogeneity assumption is a good approximation, with strong winds, currents and Stokes drift.

The site is shown in Figure 1 and is located 850 miles off the British Columbia, Canadian coast at longitude -145 degrees and latitude 50 degrees north. Simulations span a period of 20 days, starting on November 14, 2011 at 1 UTC and ending on December 4, 2011 at 1 UTC.

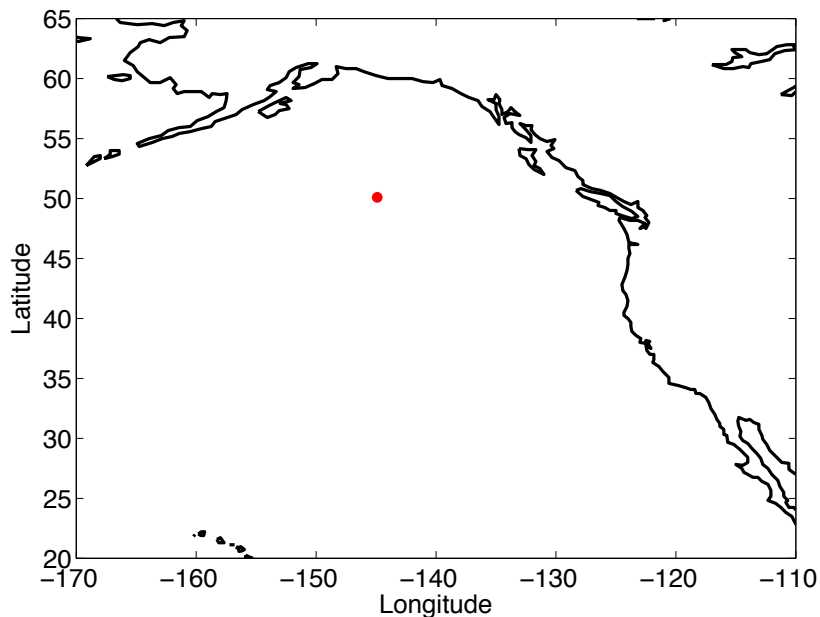


Figure 1: Location of Ocean Water Station Papa.

Horizontally the LES domain is square with 160 grid points over 360 meters, an effective resolution of 2.25 meters. There are 128 layers in the vertical direction from a depth of 200m and stretched towards the surface, as shown in Figure 2.

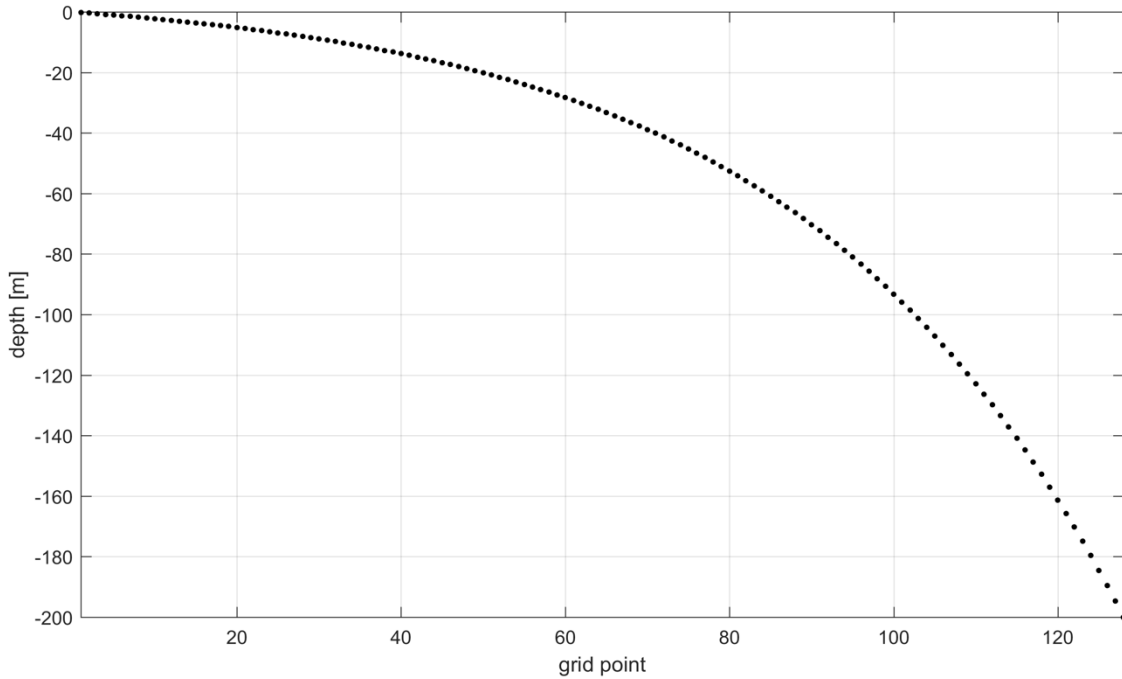


Figure 2: Vertical grid for Large Eddy Simulation at Ocean Water Station Papa

The velocity field is initialized from rest ($u = 0, v = 0, w = 0$), while temperature and salinity are initialized from observed profiles. Temperature and salinity are measured at 17 levels from 1 to 300 meter depth, and are then linearly interpolated to the vertical grid (Figure 3).

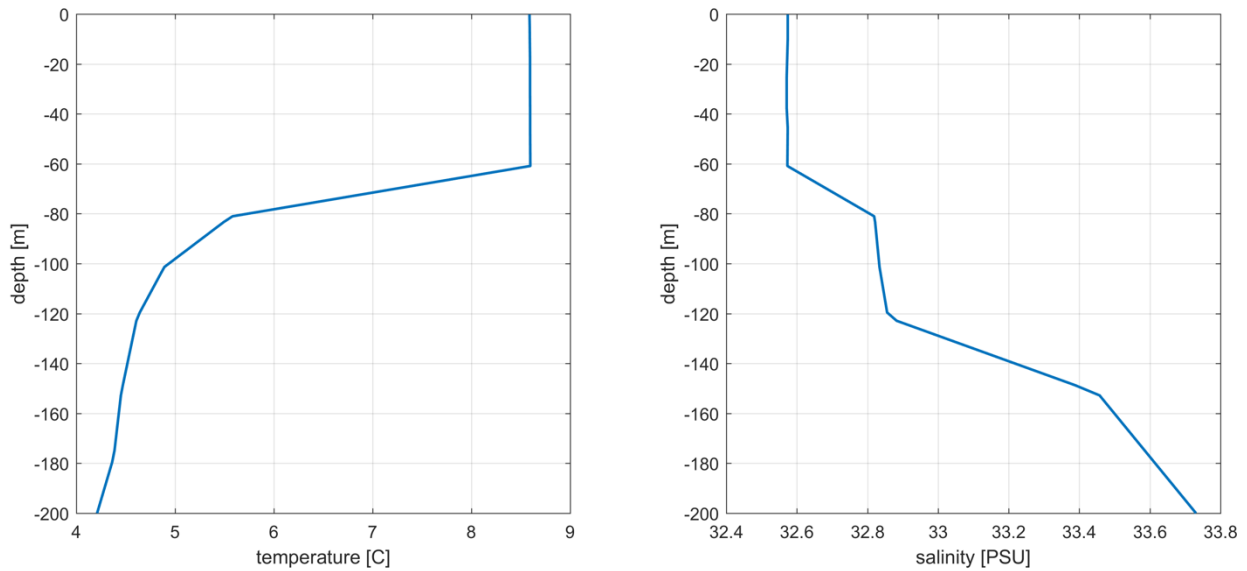


Figure 3: Initial temperature and salinity profiles for Large Eddy Simulation at Ocean Water Station Papa

As observed in the figure above, the ocean is well mixed in the upper 60m at initialization. Observed wind and heat flux are used to force the model, and a time series is shown in Figure 4.

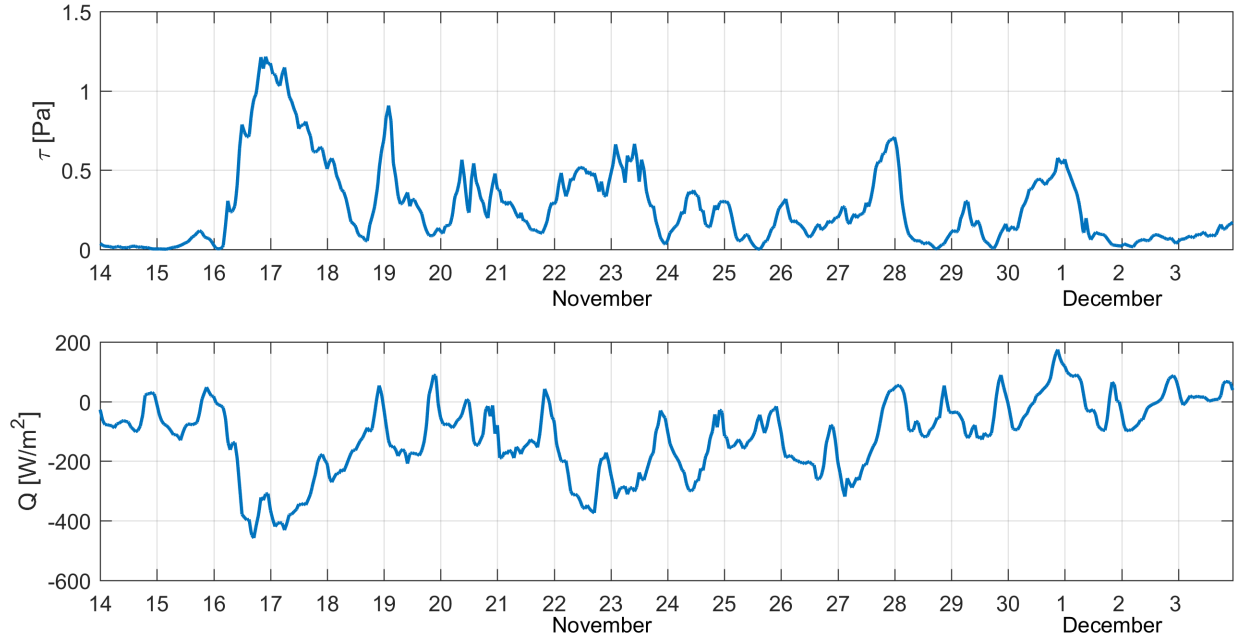


Figure 4: Surface forcing at OWS-P. (Top) Wind stress magnitude in Pascals. (Bottom) Surface heat flux in Watts per square meter.

The Stokes drift current (SDC) is computed using observed directional wave spectra, and the time series of surface values and vertical profile at initial time are given in Figure 5 for illustration.

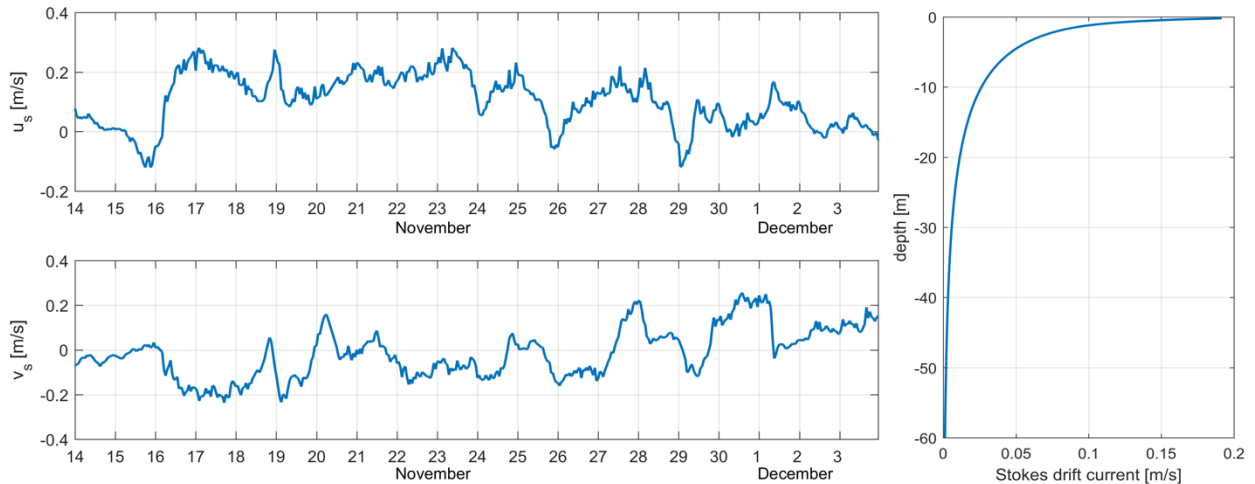


Figure 5: Stokes drift at OWS-P. (Top-left) Time series of Eastward surface Stokes drift. (Bottom left) Time series of Northward Stokes drift. (Right) Stokes drift current profile at initialization.

The mean profile of Stokes drift current (SDC), computed over the 20 day period penetrates deep into the ocean.

3.3 Statistics and Averaging

Model statistics for the LES experiments at Station Papa are computed by averaging over an inertial period for 10 alternating inertial periods (Figure 6). Station Papa is at latitude 50 degrees north, which yields an inertial period of 15.62 hours, so the averaging period spans roughly 6.5 days from November 16 at 07:12 UTC to November 22 at 19:25 UTC. This period is chosen on the basis of having a wide range of wind stress and heat flux, a long enough spin-up period from initialization and rapid ML deepening. In this report, all figures from here to section 3.6 are averages over these 10 inertial period, and all figures from section 3.7 and beyond are averages over individual inertial periods as defined in Figure 6. Figure 6 shows a time series of the characteristic velocity scales for wind, wave, and heat forcing, namely friction velocity, surface Stokes drift, and surface buoyancy flux respectively, for the 6.5-day period. The shaded rectangles in the background denote each inertial period, which are labeled T1 to T10 to discuss averaged of a particular period.

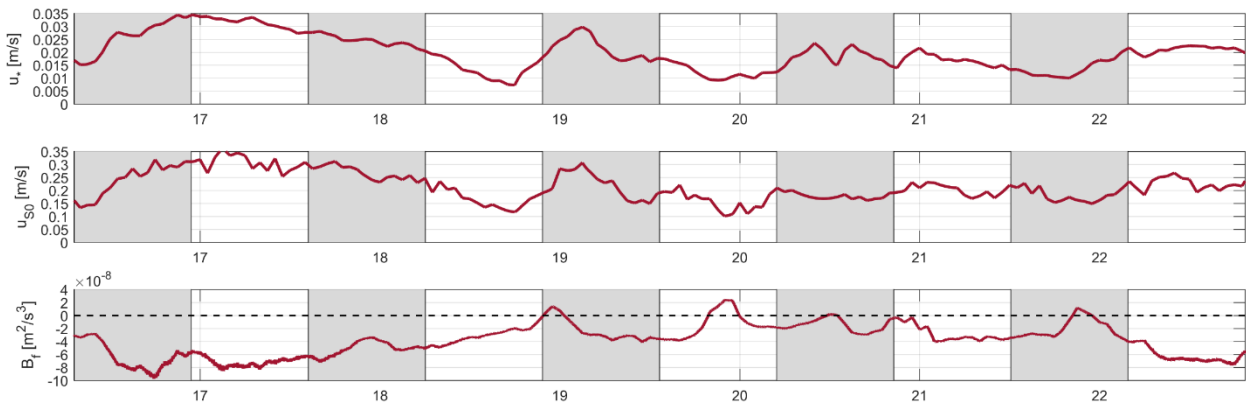


Figure 6: (Top) Water side friction velocity. (Middle) Surface Stokes drift. (Bottom) Surface buoyancy flux at Ocean Water Station Papa for the 6.5 day averaging period. Background shaded rectangles are used to denote different inertial periods.

Surface conditions vary considerably during this period: wind speeds range from $\sim 5[m/s]$ ($0.037[Pa]$ or $u_* = 0.006[m/s]$) to $\sim 23[m/s]$ ($1.25[Pa]$ or $u_* = 0.035[m/s]$), surface Stokes drift ranges from $0.1[m/s]$ to $0.36[m/s]$ and surface buoyancy flux ranges from very convective $-1 \times 10^{-7}[m^2/s^3]$ to stable $2 \times 10^{-8}[m^2/s^3]$. This period also exhibits variations of the Stokes drift penetration (e-folding depth) and wind-wave misalignment (Figure 7).

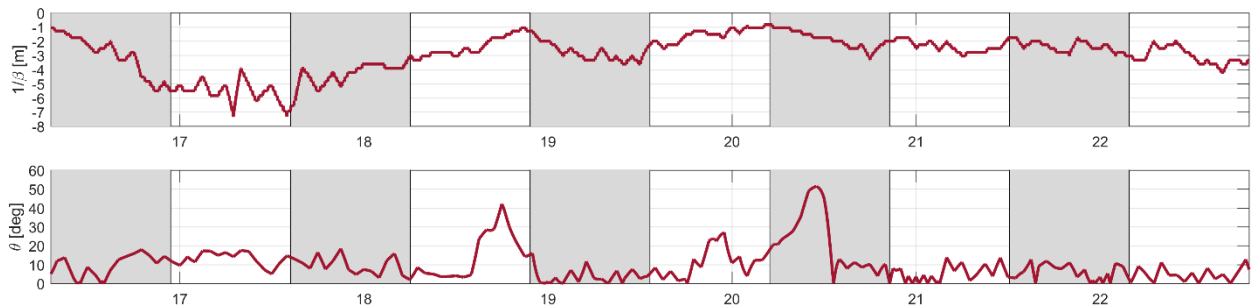


Figure 7: (Top) Stoke drift e-folding depth. (Bottom) wind-wave misalignment angle at Ocean Water Station Papa from November 16, 2011 at 7:12:01 to November 22, 2011 at 19:25:19.

In the figure above we can observe that periods T4, T6 and T7 show large degrees of wind-wave misalignment. We defer detailed discussion on the effect of the Stokes e-folding depth and the wind-wave misalignment, but both have a measurable impact on the LT parameterization.

3.4 Dimensional Analysis for LT

Dimensional analysis is a simple but powerful tool to analyze physical systems in a broad and simplified way, ideal for model parameterizations. It can be used to analyze the properties of physical phenomena (e.g., Langmuir circulation) which can be expressed by a physical equation. Additionally, expressing this physical equation in non-dimensional form greatly reduces the degrees of freedom necessary to characterize the physical system. Since our interest is in parameterizing turbulent mixing due to LT, our variable of interest is eddy viscosity (K_m) which has dimensions [m^2/s]. Therefore, we want to find an equation which relates the *additional* eddy viscosity caused by LT to surface forcing, namely wind shear, surface buoyancy flux and surface gravity waves.

The questions we want to answer are:

- What are the relevant physical parameters which represent the physics we are interested in?
- What are the relevant non-dimensional parameters we can use to describe the system?
- How do these non-dimensional numbers relate to previously suggested parameters (e.g., turbulent Langmuir number, Hoenikker number)?

In our specific problem, our physical variable of interest (Ω) is the *additional vertical mixing* brought by the inclusion of LT to the governing equations according to CL theory. Turbulent vertical mixing is represented in RANS ocean models by the eddy viscosity (K_m), so our variable of interest is the difference in eddy diffusivity between simulations neglecting and including the effect of LT:

$$\Omega = \Delta K_m = K_{LT} - K_{noLT} \quad (15)$$

For the time being, we will assume this parameterization applies only to the turbulent eddy viscosity (i.e., turbulent momentum diffusivity), but results for other diffusivities (e.g., heat) are analogous since they involve the same units [m^2/s]. The difference (Δ) in K_m is measured with respect to results from LES simulations with and without the addition of the Stokes drift, included in the CL-VF terms of the governing equations. However, note that (K_m) is not a resolved quantity in LES, so its definition has important implications on this parameterization (see section 3.1).

3.5 Parameter Development

An essential part of this parameterization is to determine which physical parameters are the most relevant in vertical mixing processes of the OSBL. These parameters should condense information from physical phenomena, namely wind shear, surface buoyancy flux and wave forcing, into a variable which can be used as the basis for the parameterization. Some physical parameters have been used extensively in different fields, such as friction velocity, which has been used in turbulence and similarity theories of shear flows and convective PBL. Wave forcing and the associated Stokes drift has proved more elusive, partially because there is a natural correlation between wind stress and surface Stokes drift but remote swells can also generate Stokes drift currents which penetrate deeper into the ocean regardless of local wind conditions. In this section we use physical reasoning and dimensional arguments to support our initial choice of these parameters, which will then be supported by theory and simulations. Note that this process required several iterations in order to achieve an acceptable scaling of non-dimensional parameters, where the error as measured by the spread of the correlation was optimized. The goal is to develop a parameterization which is useful over a large range of realistic oceanic conditions.

We start by considering the vertical TKE budget to gain insight on the relative importance of each term responsible for vertical mixing. The equation of vertical TKE for the OSBL may be derived by performing Reynold's decomposition of the Craik-Leibovich momentum equations, and taking half the trace of the Reynolds stress tensor (Pope 2000) and is given by:

$$\frac{\partial \bar{e}}{\partial t} + \bar{U}_j \frac{\partial \bar{e}}{\partial x_j} = \delta_{i3} \frac{g}{\theta} (\overline{u'_i \theta'}) - \overline{u'_i u'_j} \frac{\partial \bar{U}_i}{\partial x_j} - \overline{u'_i u'_j} \frac{\partial \bar{U}_i^s}{\partial x_j} - \frac{\partial (\overline{u'_i e})}{\partial x_j} - \frac{1}{\rho} \frac{\partial (\overline{u'_i p'})}{\partial x_i} - \epsilon \quad (16)$$

From left to right, the terms represent: local change in TKE, advection of TKE, buoyancy flux, shear production by wind stress, shear production by Stokes drift, energy transport, pressure transport and dissipation. In this equation, three physical phenomena are responsible for the turbulent production: wind shear, buoyancy flux and Stokes drift. The rest of the terms account only for transport or sinks of energy. The TKE budget for the LES experiments with and without the effect of LT at station Papa are shown in Figure 8

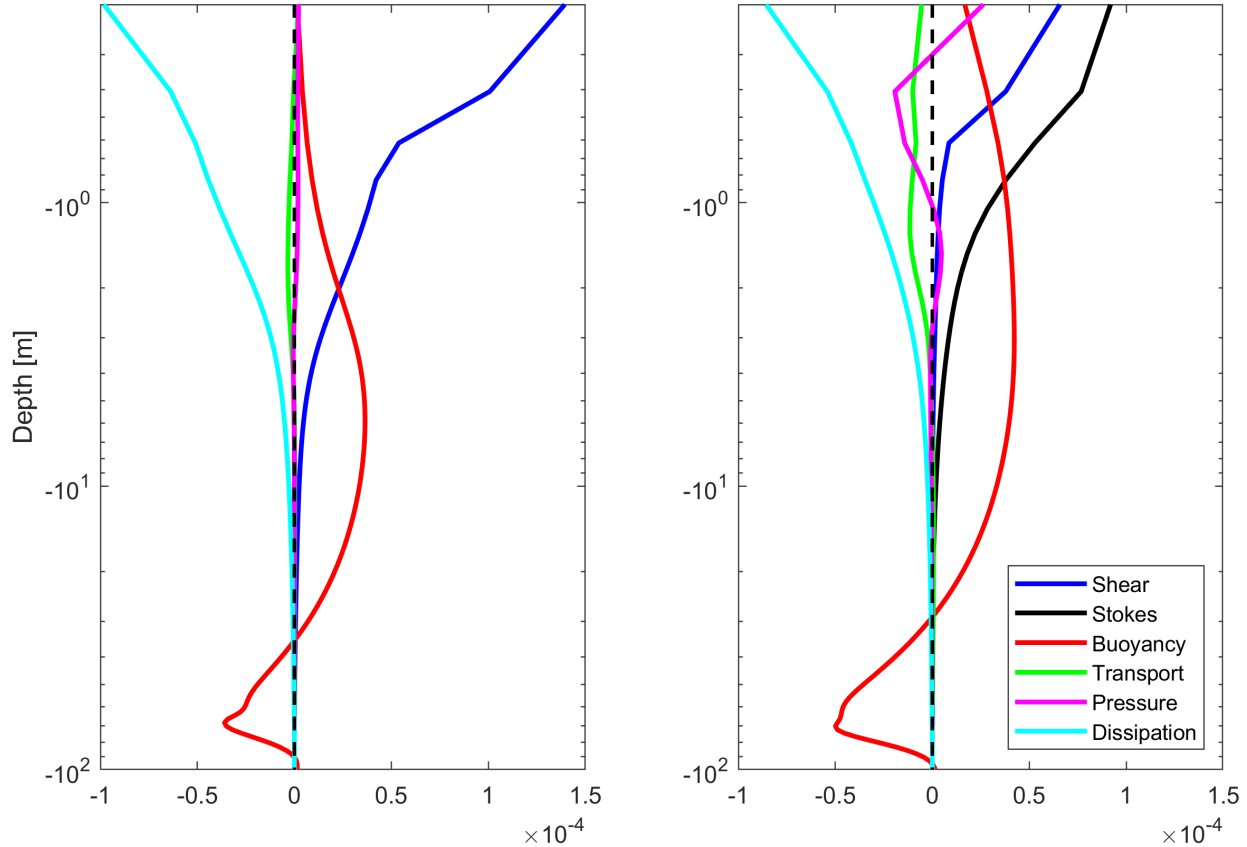


Figure 8: Vertical Turbulent Kinetic Energy budget at Ocean Water Station Papa from the LES model averaged over 10 inertial oscillations (6.5 day period). (Left) Without LT. (Right) With LT

In the figure above, we can observe that the relative importance of each term in the TKE budget is different when LT is present. In the absence of LT, the balance is between shear production, buoyancy and dissipation (similar to the ABL), but in the presence of LT turbulent transport has a more significant contribution while shear production from the wind is reduced. The contribution from shear production when LT is present decreases because vertical gradients of velocity decrease faster than the increase in turbulent fluxes. The transport and pressure terms are also significantly larger in the simulation with LT while the dissipation is slightly reduced, suggesting that the excess of available energy at the near surface is transported downwards instead of being dissipated at the surface. In the surface layer, Stokes production is the largest source of TKE but buoyancy production is larger in the bulk of the mixed layer. Buoyancy production also increases slightly, suggesting Stokes shear and buoyancy work together to increase vertical mixing. Figure 9 shows the difference between the right and left panels in Figure 8. The difference in TKE between simulations with and without Stokes drift clearly shows that the inclusion of LT results in a significant reduction of the shear production component. Most importantly, it also shows that LT increases buoyancy production in the surface layer and entrainment at the base of the ML, which suggests that the effects of LT on the MLD depend on the strength of convection as proposed most recently by Li and Fox-Kemper (2017).

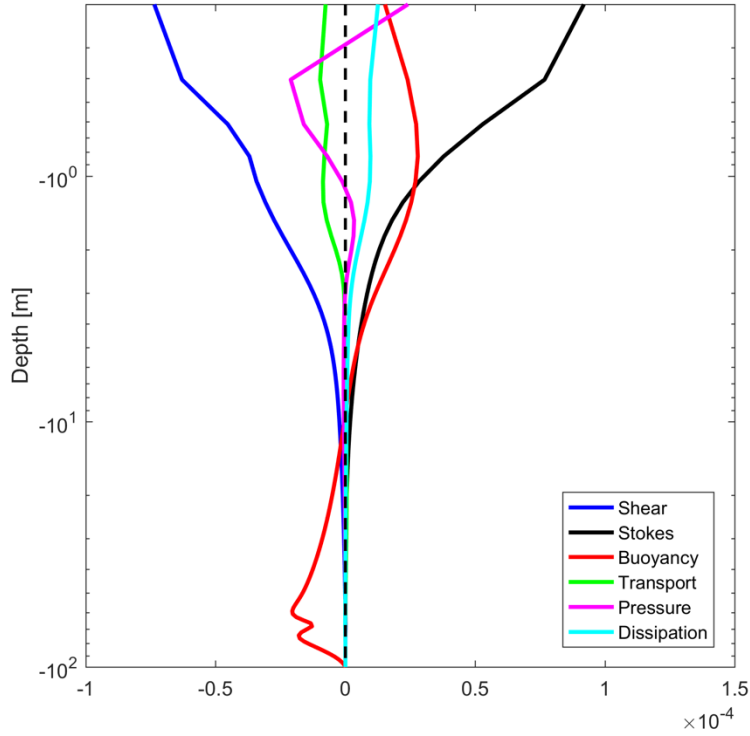


Figure 9: Difference in the Vertical Turbulent Kinetic Energy budget, between simulations with and without LT.

Using these observations and dimensional analysis, we now consider various physical parameters that may contribute to the enhanced vertical mixing by LT.

Eddy viscosity $K_m [m^2/s]$ involves only two fundamental units, length and time, so it may be characterized using any combination of length and time scales. These characteristic scales have been used in turbulence theory, such as in the ABL, to form similarity theories which can be then used as parameterizations of vertical turbulent mixing in numerical models as function of surface quantities. For example, the semi-empirical Monin-Obukhov (MO) similarity theory argues that turbulent characteristics in the surface layer depend only on the surface kinematic fluxes and distance from the boundary. The fundamental turbulent parameters that can be formed from these quantities are the friction velocity, the scale of turbulent fluctuations of scalar (S), and the Obukhov length scale (L):

$$u_*^2 = (\overline{wu_0^2} + \overline{wv_0^2})^{1/2} \quad (17)$$

$$S^* = -\overline{ws_0}/u_* \quad (18)$$

$$L = u_*^3 / (\kappa B_0) \quad (19)$$

Where ($B_0 = -\alpha g \overline{w\theta_0}$) is the surface buoyancy flux and (κ) is Von Karman's constant.

An important length scale in the OSBL, often included as a prognostic variable in ML models, is the BLD (h), because it determines the depth at which turbulent fluctuations act to mix the upper layers of the ocean. Many length, time and velocity scales have been suggested to characterize the effects of wind shear, buoyancy and Stokes drift in the ocean, the table below shows some examples:

	Length	Time	Velocity
Wind Shear	Ekman depth (d_e)	Coriolis frequency (f) Shear frequency $M^2 = \frac{dU}{dz}$	Friction velocity u_*
Buoyancy	BLD (h) MLD (h_m)	B-V frequency $N^2 = -\frac{g}{\rho} \frac{d\rho}{dz}$	Surface buoyancy flux (B_0) Convective velocity (w_*)
Stokes drift	e-folding depth ($1/\beta$)	Stokes shear $S^2 = \frac{dU_s}{dz}$	Surface drift current (u_s)

Table 1: Length, time and velocity scales typically used to represent wind stress, buoyancy and Stokes drift.

Following this reasoning, we assume that the additional mixing by LT may be characterized using a characteristic length and time scales, or alternatively a characteristic velocity and length scales or velocity and time scales. To determine which of these scales should be used to parameterize LT, we can compute the correlation coefficient between the difference of the shear production term of LES results at OWS-P with and without the effect of Stokes drift with each of the physical parameters.

$$\Delta P_{shear} = \left(-\overline{u'w'} \frac{dU}{dz} - \overline{v'w'} \frac{dV}{dz} \right)_{Stokes} - \left(-\overline{u'w'} \frac{dU}{dz} - \overline{v'w'} \frac{dV}{dz} \right)_{Without Stokes} \quad (20)$$

Note that the difference in shear production above is a good measure of quantifying the difference in eddy viscosity with and without LT because the TKE budget (Figure 8) shows the shear production term is significantly affected by the inclusion of Stokes drift. Therefore it is reasonable to presume that the difference in shear production is proportional to difference in eddy viscosity.

The correlation coefficient is defined as:

$$CC = \frac{cov(\Delta P_{shear}, \omega)}{\sigma_{\Delta P_{shear}} \sigma_{\omega}} \quad (21)$$

Equation (21) represents the correlation coefficient between the difference in shear production (equation 20) and a physical parameter (ω), for example, $\omega = u_*$.

At each level of the vertical grid, the shear production is computed for the case including the Stokes drift and do the same for simulations without the Stokes drift. Then, we compute the CC of the difference of shear production at each level with our physical parameters (Figure 10).

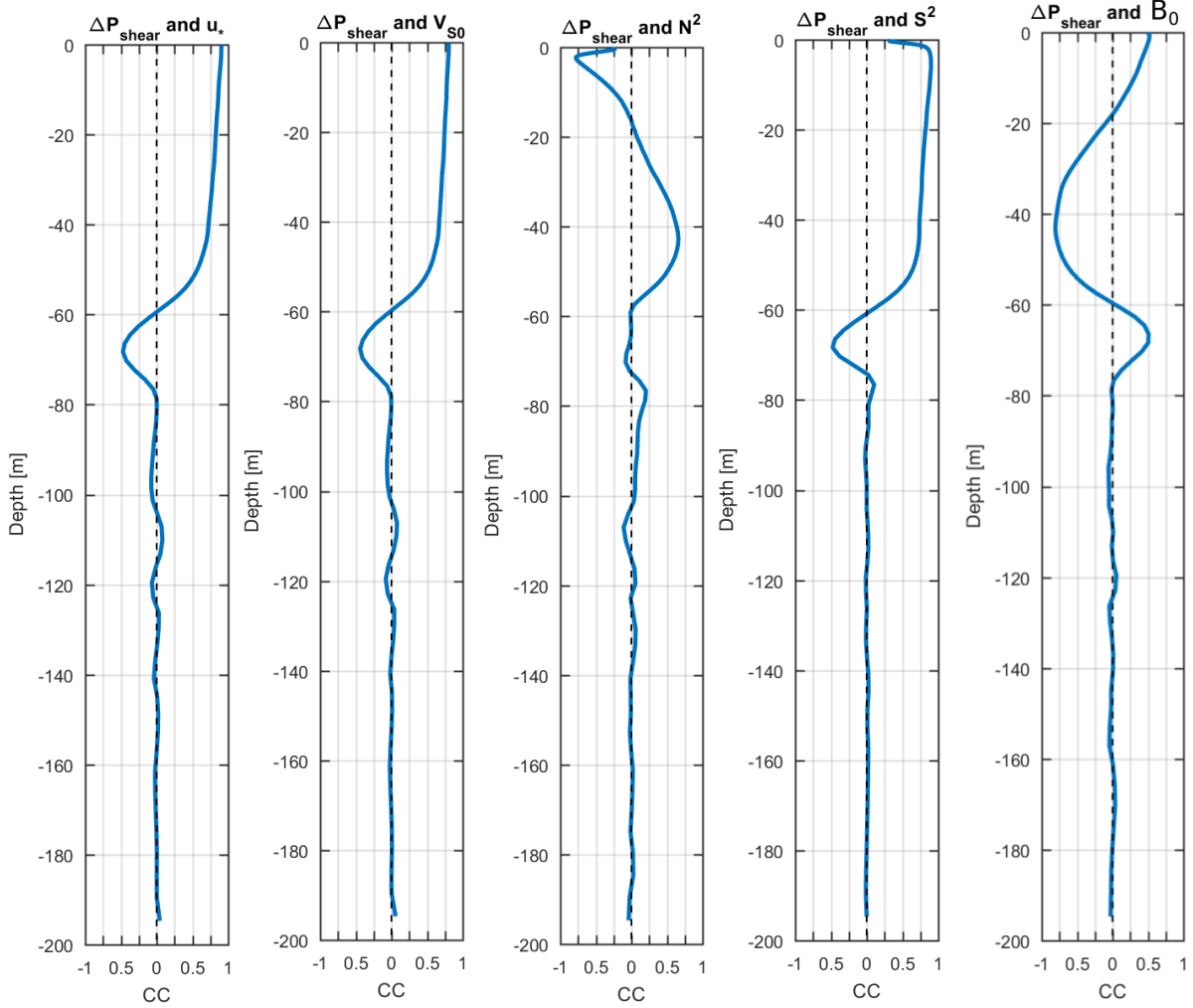


Figure 10: Correlation coefficient of physical parameters with the difference in shear production from simulations with and without Stokes drift.

As we can expect, the friction velocity correlates well with the difference of shear production.

Both the Surface Stokes drift (V_{S0}) and the surface Stokes shear ($S^2 = \left(\frac{\partial U_s}{\partial z}\right)^2 + \left(\frac{\partial V_s}{\partial z}\right)^2$) correlate well with shear production. Our initial hypothesis, then leads as to conclude that the most relevant physical parameters affecting the enhancement of eddy viscosity are:

$$\Delta K = f(u_*, V_{S0}, S^2, N^2, B_0) \quad (22)$$

Of course there are other parameters that may affect the enhancement of eddy viscosity in the presence of LT, but for now we are concerned on those parameters which have the most significant effect. For example, inertial oscillations may play a role in modulating LT, so the Coriolis parameter (f) may be taken into consideration. The Ekman depth can be estimated as a function of the turbulent eddy viscosity and Coriolis frequency.

The use of two parameters, instead of one, to describe the effect of Stokes drift is not trivial. Consider the following: for simplicity, let us assume the case of a steady, monochromatic deep-

water wave propagating in the (\hat{x}) direction. The Stokes drift is defined as (see equation 2.4 in McWilliams et al. (1997)):

$$u_s = \hat{x}V_{s0}e^{2kz} \quad (23)$$

Where (V_{s0}) is the Stokes drift velocity at the surface and ($k = 2\pi/\lambda$) is the wave number of this monochromatic wave where (λ) is the wave length. The Stokes drift vertical gradient (i.e., Stokes shear) is simply the vertical derivative of the Stokes drift:

$$\frac{du_s}{dz} = S = 2kV_{s0}e^{2kz} \quad (24)$$

Where ($\beta = 2k$) is the reciprocal of the Stokes e-folding depth, which measures how much the Stokes drift penetrates into the ocean. This is an important physical parameter related to the Stokes drift. In the study of Li et al. (2005), they assume a steady monochromatic wave field and find discrepancies in their idealized LES results when compared to observed open ocean conditions in the North Pacific, which they suggest may be due to the vertical decay scale of Stokes drift. To explore this, they perform two additional simulations changing only the e-folding depth (β), and find that having different depth ratios (βh_m) has a significant effect on the mean currents (section 3 in Li et al. 2005). Furthermore, Kukulka and Harcourt (2017) study the influence of the Stokes drift decay scale on LT and conclude that the dominant LC size scales with the depth penetration ratio (βh_m). The analytical expression for the Stokes shear (equation 23) involves Stokes shear (i.e., a time scale), surface Stokes drift (i.e., a velocity scale) and e-folding depth (i.e., a length scale). In this expression, there are only two linearly independent variables, that is, information about the Stokes e-folding depth and surface Stokes velocity automatically defines the Stokes shear. This analytical expression and idealized LES experiments (e.g., Li et al. 2005) suggest that two scales are needed to fully characterize the effects of Stokes drift. Using only one variable implies an assumption of the wave field, either a constant e-folding depth or a balance of the wave field with wind shear (i.e., fully developed seas). Under idealized conditions this assumption may be valid, but in the real ocean where the wave length and wave age change constantly this approximation is questionable. Consequently the turbulent Langmuir number by itself cannot be used to fully characterize ocean waves because the same surface Stokes drift velocity may be achieved with different combinations of e-folding depths and Stokes shear. Another concern is the assumption of aligned wind and waves, which will be addressed in later sections.

After our initial guess of the relevant physical parameters we are interested in reducing the degrees of freedom in our physical equation. We can achieve this by applying the Buckingham Pi theorem, which states that given a physically meaningful equation involving \mathbf{n} physical variables with \mathbf{k} physical dimensions (i.e., fundamental units), we can derive a non-dimensional equation in terms of $\mathbf{p}=\mathbf{n}-\mathbf{k}$ non-dimensional parameters constructed from the original physical parameters. This greatly reduces the parameter space over which experiments (laboratory, field, and modeling) need to be conducted to understand and characterize the phenomena under study and the non-dimensional numbers give us useful information about the system.

3.6 Non-dimensional variables

Non-dimensional variables are a succinct way to express complex physical phenomena, which lie at the core of the Buckingham Pi theorem. They provide useful information about the system as a function of our relevant physical parameters, and can be used to establish similarity relations between experiments where more than one variable is changed. In LT, perhaps the most relevant and certainly the most widely used non-dimensional parameter is the turbulent Langmuir number McWilliams et al. (1997):

$$La_t = \left(\frac{u_*}{V_{s0}} \right)^2 \quad (25)$$

In the context of an asymptotically large Reynolds number, the turbulent Langmuir number represents the ratio between shear instability of wind driven currents and the Craik-Leibovich vortex force due to Stokes drift. It has been widely used to characterize LT, and is also physically meaningful because it represents the ratio of turbulent shear production by the wind and wave forced production by Stokes drift. See equation 2 in Belcher et al. (2012).

$$\frac{P_{shear}}{P_{vf}} = \frac{\overline{u'w'} \frac{dU}{dz}}{\overline{u'w'} \frac{dU_S}{dz}} = \frac{\frac{u_*^2 u_*}{h}}{\frac{u_*^2 u_S}{h}} = La_t^2 \quad (26)$$

This equation (26) assumes that the vertical momentum flux is proportional to the square of the friction velocity, the vertical gradients of the mean velocity and Stokes drift are proportional to the friction velocity and Stokes drift surface velocity respectively, over a depth scale h , defined as the base of the mixed layer. In this paper the mixed layer depth is defined as the depth at which temperature and salinity profiles are approximately uniform capped below by a sharp pycnocline. Although a mathematical definition of MLD is not provided, it is clear from the schematic in figure 2 from Belcher et al. (2012) that the length scale over which the Stokes drift decays is smaller than the ML ($\delta < h$). As we will discuss later, we argue here that the Stokes shear and e-folding depth rather than the Stokes drift velocity at the surface, is a more relevant scale measuring the strength of the vortex force brought by wave forcing, which leads us to define a modified Langmuir number. This is in agreement with Li and Garrett (1995) who also uses $\delta = 1/2k$ as the relevant length scale for the CL-VF.

Another important non-dimensional number, suggested by Li and Garrett (1995), is the Hoenikker number:

$$Ho = \frac{4B_0}{u_s \beta u_*^2} \quad (27)$$

Where $\beta = 1/\delta$ is the reciprocal of the e-folding depth, also called penetration depth, of the Stokes drift. This non-dimensional number compares unstable buoyancy flux driving thermal convection with the vortex force driving LC (Li et al. 2005). Note that this number includes two physical variables to represent the influence of the Stokes drift: surface Stokes drift and e-folding depth. In the equation of Belcher et al. (2012) the vortex force production is assumed proportional to $u_s u_*^2/h$, while Li and Garrett (1995) assume the vortex force proportional to

$u_s \beta u_*^2$. The difference is important when characterizing ocean observations, because wind waves are associated with significant surface Stokes drift and relatively shallow penetration compared to swell waves. This distinction may be easily overlooked in idealized LES simulations, where the wave field is assumed steady, monochromatic and aligned with the wind.

Note also, that Belcher et al. (2012) propose the ratio:

$$\frac{\overline{w' b_s'}}{-u' w' \cdot \partial u_s / \partial z} \sim \frac{B_0}{u_s u_*^2 / h} = \frac{h}{L_L} \quad (28)$$

Measuring buoyancy forced production against wave forced production, which is analogous to the Hoenikker number proposed by Li et al. (2005), with the difference that the relevant length scale is h instead of β . From a physical standpoint, h is influenced by both convection and LT, while β depends only on the wave field, and therefore we consider the Hoenikker number to be a more relevant parameter.

Together, the turbulent Langmuir number and the Hoenikker number are two controlling dimensionless parameters in the OSBL. A time series of the turbulent Langmuir number (equation 25) and the Hoenikker number (equation 27) are shown in the figure below.

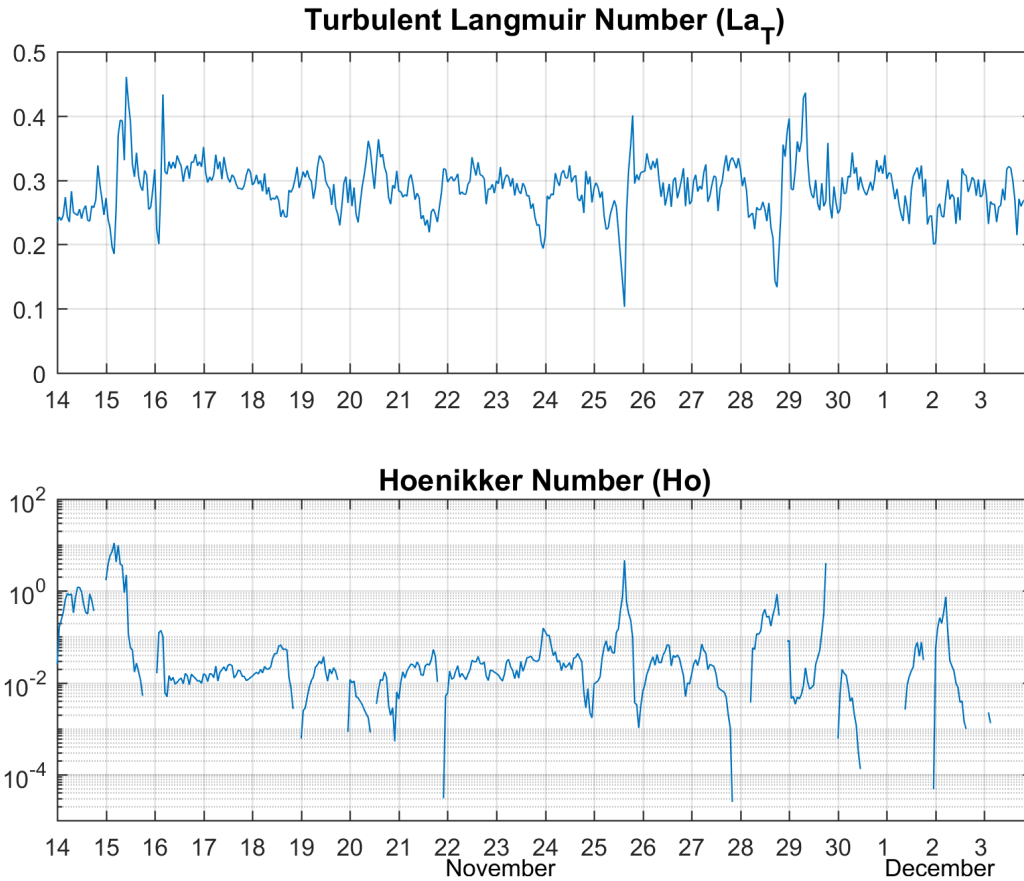


Figure 11: (Top) Turbulent Langmuir number. (Bottom) Hoenikker number for Ocean Water Station Papa simulations.

During the 6.5 day averaging period (Figure 6), the turbulent Langmuir number is in the range 0.22 – 0.36 and the Hoenikker number is in the range of 0.001 – 0.1 (Figure 11). This provides a considerable range typical of LT in the ocean.

In the study by Li et al. (2005), they propose using these two parameters to form a regime diagram for classifying turbulent large eddies in the upper ocean. Figure 12 shows the diagram of this parameter space for the entire simulation period at Station Papa. Later, we will discuss how our dimensionless numbers relate to the turbulent Langmuir and Hoenikker numbers.

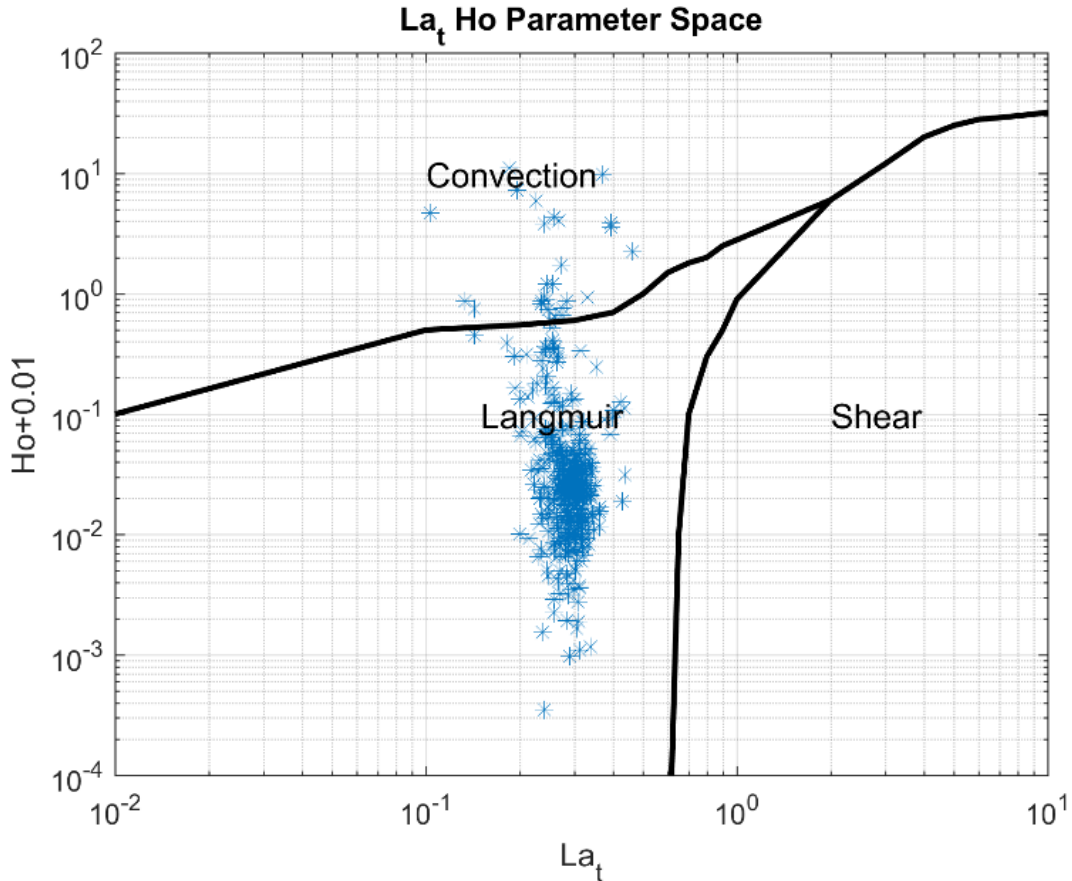


Figure 12: Parameter space (La_t - Ho) for OWS-P simulations.

We can observe that the turbulent Langmuir number is about 0.3 and the Hoenikker number is around $O(10^{-2})$, which falls under the regime dominated by LT. Note that the Hoenikker number (equation 27) is positive when the ocean loses heat (convective) and negative when the ocean gains heat. Since the y-scale in Figure 11 (bottom) is logarithmic, the Hoenikker number is not defined in this plot when there is a stabilizing total surface heat gain at the surface, hence the discontinuities. The wind shear has significant influence in the value of Ho , and for very light winds ($< 5[m/s]$) this parameter tends to 0, or 0.01 in the regime diagram in Figure 12.

In the following section, the physical parameters and dimensionless numbers are reconsidered in the context of the LES at OWS-P. The physical parameters and the non-dimensional numbers are redefined to yield a robust and accurate parameterization.

3.7 LT Surface Parameterization

In this section, we start by parameterizing LT at the surface using linear regression analysis. The first step towards developing the LT parameterization, is to find an equation expressing the relationship between our variable of interest and our relevant physical variables, in non-dimensional form. To do this, we need to start by normalizing (ΔK) , which can be expressed in terms of its fundamental dimensions as $[L^2 T^{-1}]$. By far the most widely used variable used to scale turbulent quantities that also correlates well with the difference of shear production (Figure 10) is the friction velocity, which has fundamental dimensions $[L^1 T^{-1}]$. We can then either multiply (u_*) by a length scale or square it and multiply it by a time scale to get the right units. Among our initial set of physical parameters $(u_*, V_{s0}, S^2, N^2, B_0)$, the Stokes shear $[T^{-2}]$ is the most relevant time scale affecting vertical mixing due to LT. Therefore, we choose to normalize the eddy viscosity difference as:

$$\Pi = \frac{\Delta K}{u_*^2/S_0} \quad (29)$$

Note that the normalization of our variable of interest is somehow trivial because only the choice of physical relevant variables affects the set of linearly independent dimensionless numbers (i.e., Pi groups) according to the Buckingham Pi theorem. However, the particular combination of variables chosen to normalize (ΔK) does affect the scaling in the non-dimensional equation.

Now, we need to find an appropriate scaling between our non-dimensional eddy viscosity $(\Pi = \frac{\Delta K}{u_*^2/S})$ and a set of non-dimensional numbers formed from relevant physical variables $(u_*, V_{s0}, S^2, N^2, B_0)$. We start with a first degree approximation, such that our non-dimensional eddy viscosity difference is a function of only one dimensionless number:

$$\frac{\Delta K}{u_*^2/S} = f(\Pi_1) \quad (30)$$

The obvious choice is to try to scale (Π) with the turbulent Langmuir number, $(\Pi_1 = \sqrt{u_*}/V_{s0})$.

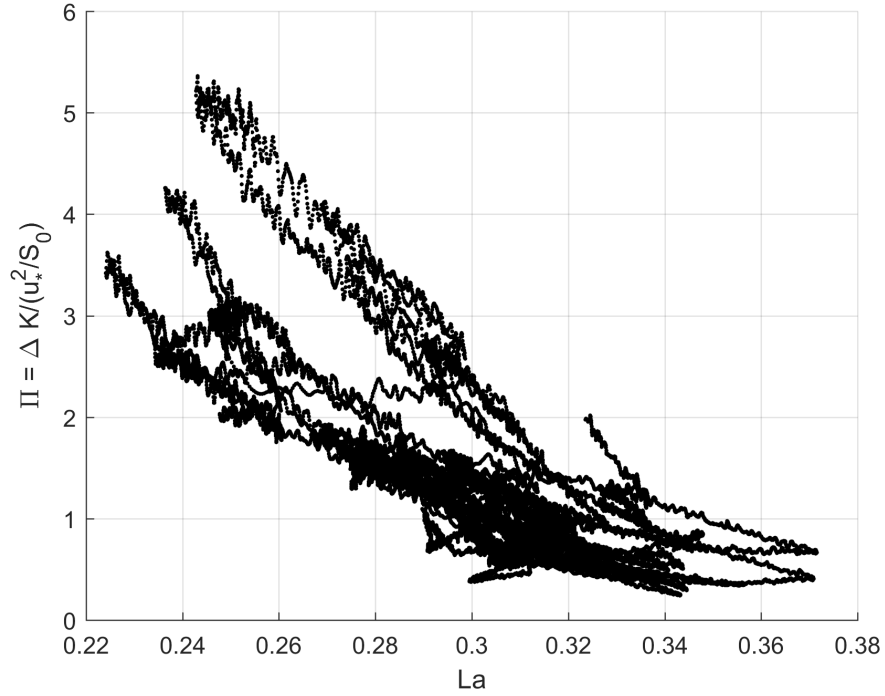


Figure 13: Scaling of turbulent Langmuir number and non-dimensional eddy viscosity difference.

Figure 13 shows a clear trend: as the relative strength of the CL-VF increases with relation to the wind shear (i.e., decreasing La) the vertical mixing due to LT increases. However, we can observe a separation in this scaling related to different penetration depths of the Stokes drift.

Figure 14 below shows the scaling of the turbulent Langmuir number with our non-dimensional eddy viscosity, colored by wind-wave angle of misalignment (left) and decay scale (right). In the right figure, for shallow penetration (dark blue) the scaling is linear and follows a different trend than for deeper waves.

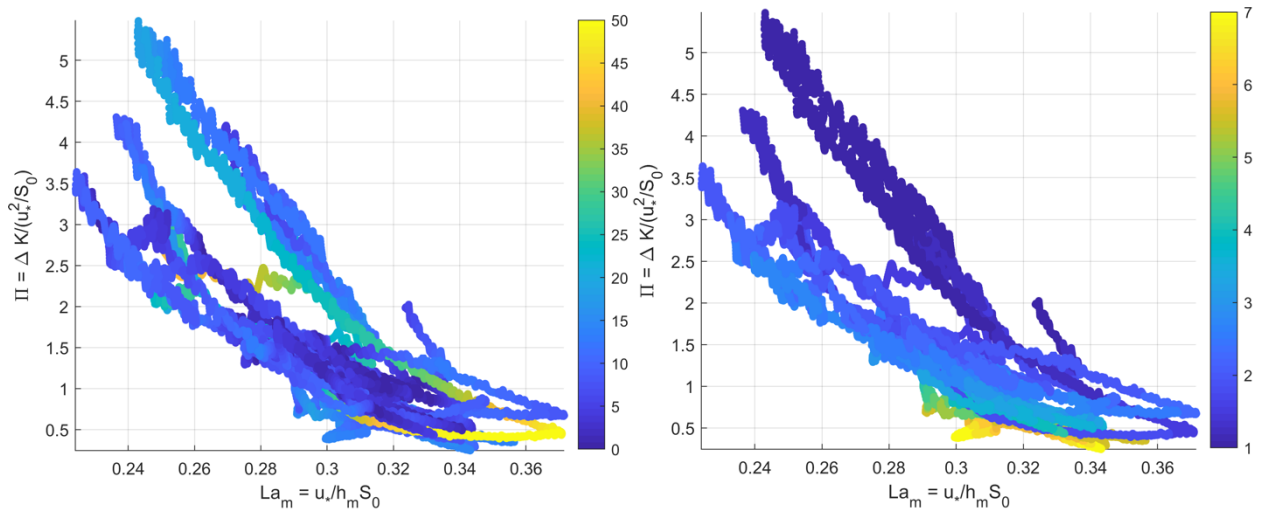


Figure 14: Scaling of turbulent Langmuir number and non-dimensional eddy viscosity difference. (Left) Colored by wind-wave misalignment angle. (Right) Colored by e-folding depth.

Using the turbulent Langmuir number to scale turbulent quantities is apt for stationary simulations under idealized conditions, where a steady monochromatic wave field implies a constant e-folding depth. The study of Harcourt and D'Asaro (2008) investigates the scaling of turbulent quantities in the OSBL under realistic forcing conditions (i.e., full wave spectrum) and conclude that the use of a (D_S^*) scale equivalent monochromatic wave does not accurately reproduce the results using a full-surface wave spectrum with the same e-folding depth. They propose using a surface layer Langmuir number:

$$La_{SL} = \sqrt{\frac{u_*}{\langle u_s \rangle_{SL} - u_{sref}}} \quad (31)$$

Where $\langle u_s \rangle_{SL}$ is the average Stokes drift in a surface layer $0 > z > -0.2H_{ML}$ relative to that of near the bottom of the mixed layer (u_{sref}). Besides accounting for different penetration depths of the Stokes drift, an important property of the surface layer averaged Langmuir number (equation 31) not exhibited by the turbulent Langmuir number (equation 25) observed in the North Atlantic and Artic Oceans is a seasonal variability in which the LT mixing is enhanced during summer and reduced during winter (Figure 1 in Ali et al. (2019)). This is a desirable property because LT parameterizations based on the turbulent Langmuir number (e.g., McWilliams and Sullivan (2000)) tend to overestimate the strength of mixing in winter and underestimate the strength of mixing in summer (Fan and Griffies (2014)).

In another study by Kukulka and Harcourt (2017), they use a simplified framework with a set of idealized LES simulations to investigate the effect of the Stokes drift decay scale on LT, and suggest using a modified Langmuir number to account for both Stokes drift velocity at the surface and its penetration. They define this modified Langmuir number as:

$$La_\phi = \left(\frac{u_*}{u_{s\phi}} \right)^{1/2} \quad (32)$$

Where $u_{s\phi}$ is a depth-integrated weighted Stokes drift shear or, equivalently, a spectrally filtered surface Stokes drift.

$$u_{s\phi} = 2 \int_0^\infty \phi(k) k \omega \Psi(k) dk \quad (33)$$

Where $\phi(k)$ is a spectral filter, $\Psi(k)$ is the surface height wavenumber spectrum, ω is the angular frequency and k is the wavenumber. This spectral Langmuir number is a generalized expression of the surface layer Langmuir number, and when the spatial filter is applied over the top 20% of the mixed layer the expressions are equivalent as discussed in Kukulka and Harcourt (2017). All of these suggested parameters attempt to address the deficiency of the turbulent Langmuir number in failing to characterize the effect different penetration depths.

We explore the possibility of scaling our non-dimensional eddy viscosity difference with the surface layer Langmuir number (La_{SL}) as well as a similar expression of this number we denote as (La_β), where the averaging is over the Stokes e-folding depth ($1/\beta$) instead of the surface layer.

$$La_{\beta} = \left(\frac{u_*}{\langle (u_{\beta}) - u_{ref} \rangle} \right)^{1/2} \quad (34)$$

For the 6.5 day period of the simulation at OWS-P, we test the scaling of the surface layer Langmuir number and e-folding layer Langmuir number and obtain the following:

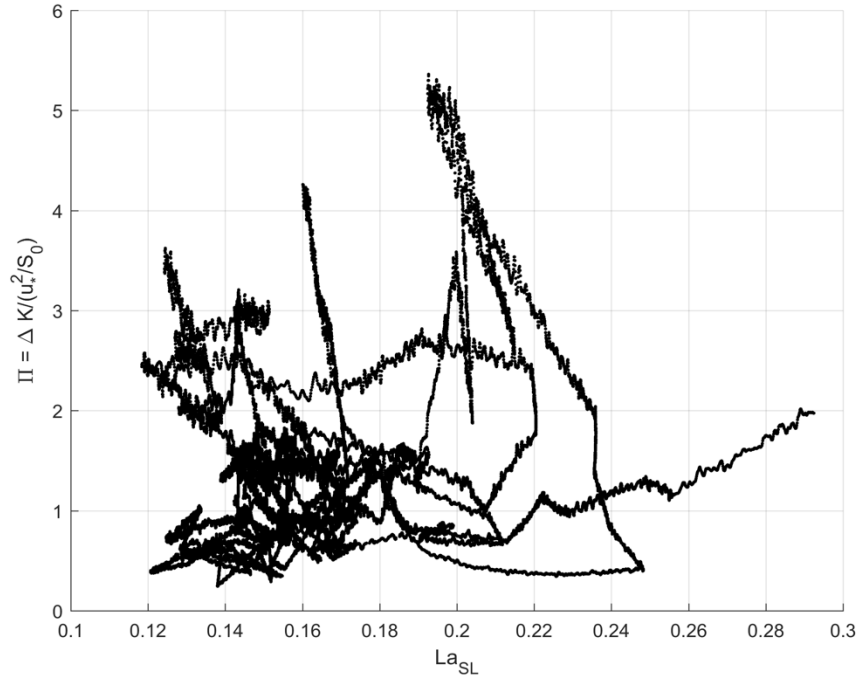


Figure 15: Scaling of surface layer Langmuir number and non-dimensional eddy viscosity difference.

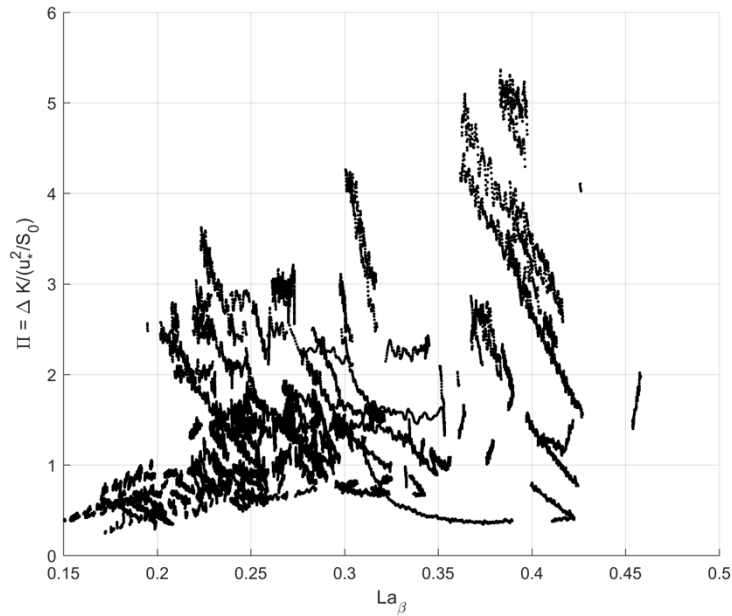


Figure 16: Scaling of e-folding depth averaged Langmuir number and non-dimensional eddy viscosity.

As we can observe, we do not find a good scaling of our non-dimensional eddy viscosity with the surface layer averaged Langmuir number. However, this does not contradict the results by (Harcourt & D'Asaro, 2008). They use the surface layer Langmuir number to scale TKE and bulk Vertical Kinetic Energy (VKE), while we are attempting to scale the shear production term which is proportional to the momentum fluxes and mean vertical gradients. This is a physically important distinction, because the normal stresses, that is, the diagonal components of the Reynolds stress tensor (i.e., TKE), are distinct from the shear stresses, the off diagonal components of the Reynolds stress tensor ($\overline{u'w'}$, $\overline{v'w'}$). Since our definition of eddy viscosity only involves the off-diagonal components of the Reynold stress tensor, parameterizing eddy viscosity with the surface layer Langmuir number is ineffective. More importantly, the scaling depends on the choice of the non-dimensional eddy viscosity which is somewhat trivial.

As discussed earlier, analytical and LESs suggest that we need two length, time or velocity scales to fully characterize the wave field. The studies by Li et al. (2005), Harcourt and D'Asaro (2008), and Kukulka and Harcourt (2017) suggest that the decay length of the Stokes drift ($1/\beta$) or rather the penetration depth ratio (βh_m) has a significant effect on mean profiles of velocity and turbulent quantities in the OSBL. Therefore, we re-consider our initial choice of physical parameters to include these two physical parameters.

$$\Delta K = f(u_*, \beta, S_0^2, B_0, h_m) \quad (35)$$

Instead of using the surface Stokes drift velocity and Stokes shear, we opt to use the Stokes e-folding depth and Stokes shear to characterize the wave field. Now, we attempt to scale the non-dimensional eddy viscosity using $\frac{u_*\beta}{S_0}$ and the penetration depth ratio:

$$\frac{\Delta K}{u_*^2/S_0} = f\left(\frac{u_*\beta}{S_0}, h_m\beta\right) \quad (36)$$

The scaling found is:

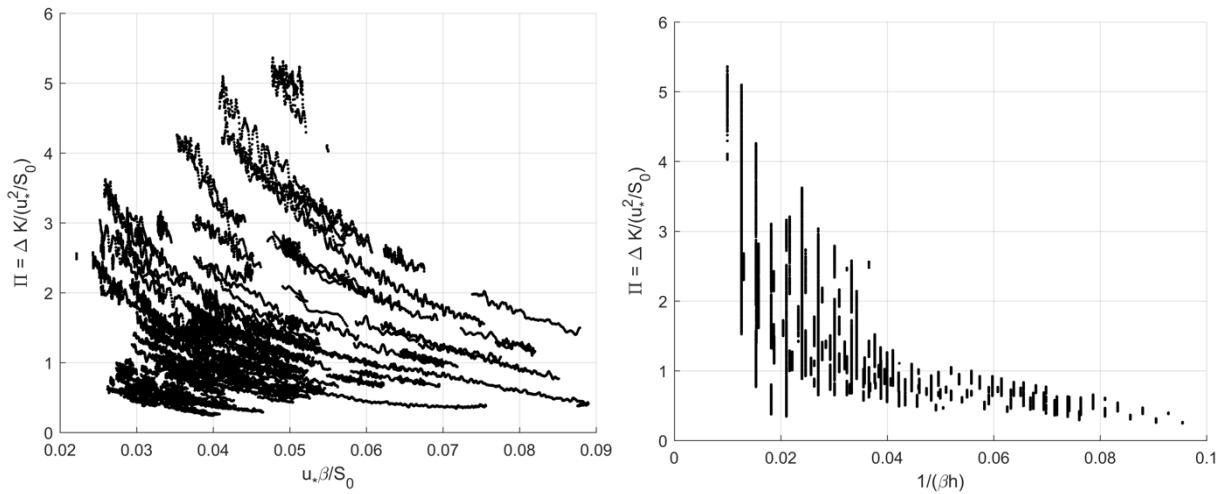


Figure 17: (Left) Scaling of modified Langmuir number $\left(\frac{u_*\beta}{S_0}\right)$. (Right) Scaling of penetration depth ratio ($h_m\beta$) with non-dimensional eddy viscosity difference.

We can observe a clear trend, but there is still a separation of scales. Furthermore, we want to simplify the problem as much as possible by scaling our non-dimensional eddy viscosity with only one non-dimensional parameter. Since the e-folding depth is present in both of these numbers, we can further simplify the problem by combining both of these numbers into one:

$$\left(\frac{u_*\beta}{S_0}\right)\left(\frac{1}{\beta h_m}\right) = \left(\frac{u_*}{S_0 h_m}\right) \quad (37)$$

The scaling we obtain is:

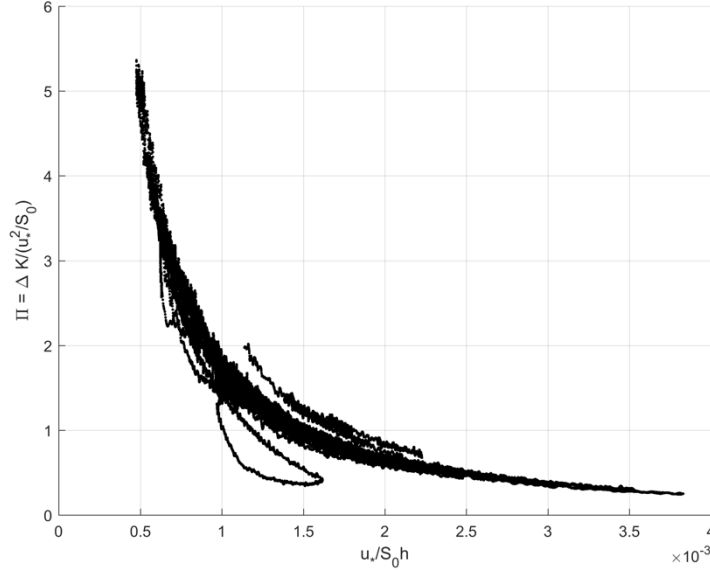


Figure 18: Scaling of modified Langmuir $\left(\frac{u_*}{S_0 h_m}\right)$ number and non-dimensional eddy viscosity difference.

Clearly, the scaling of the eddy viscosity is much improved when compared to the turbulent Langmuir number (McWilliams et al. 1997) or the surface Langmuir number (Harcourt and D’Asaro 2008). Moreover, we do not need to use the e-folding depth which we have replaced by the mixed layer depth (h_m).

$$\frac{\Delta K S_0}{u_*^2} = f\left(\frac{u_*}{S_0 h_m}, \Pi_2(B_0, \dots)\right) \quad (38)$$

Here, we formally define our modified Langmuir number as:

$$\Pi_1 = \frac{u_*}{S_0 h_m} \quad (39)$$

We can parameterize the difference in eddy viscosity as a function of this modified Langmuir number and another dimensionless number (Π_2) function of the surface buoyancy flux. In the OSBL, the mixed layer depth is the most relevant length scale to characterize vertical mixing, which is affected by surface convection and LT. In the figure above, the points which are found to be off the scaling coincide with periods of high wind-wave misalignment, which we are still not taking into account. This implies that the difference in eddy viscosity at the surface is a function of friction velocity, MLD, Stokes shear and on the wind-wave misalignment angle. To

finalize this section, we perform a linear regression analysis, using a power fit to parameterize our non-dimensional equation.

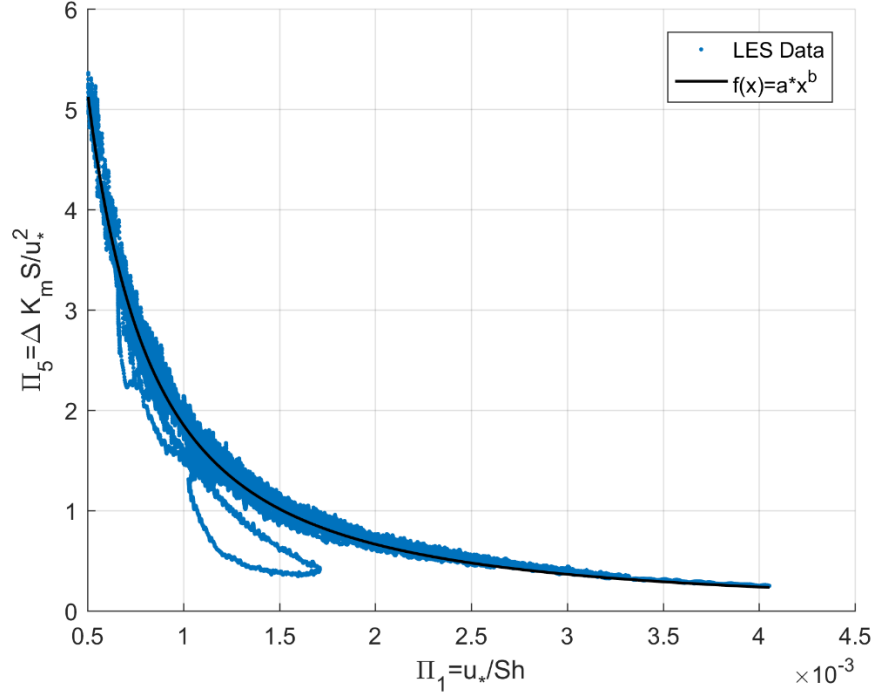


Figure 19: Surface layer parameterization showing the scaling between modified Langmuir number and non-dimensional eddy viscosity difference. The black line is the non-linear regression (power fit).

The equation relating our non-dimensional eddy viscosity to our modified Langmuir number is:

$$\frac{\Delta K_m}{u_*^2/S} = 6.64 * 10^{-5} \left(\frac{u_*}{S_0 h} \right)^{-1.482} \quad (40)$$

Going back to the physical meaning of the turbulent Langmuir number, as the ratio of turbulent shear production by the wind and wave forced production by Stokes drift (Belcher et al. 2012):

$$\frac{P_{shear}}{P_{vf}} = \frac{\overline{u'w'} \frac{dU}{dz}}{\overline{u'w'} \frac{dU_S}{dz}} = \frac{\frac{u_*^2 u_*}{h}}{\frac{u_*^2 u_S}{h}} = La_t^2 \quad (41)$$

Our scaling suggests that a more accurate representation is given by:

$$\frac{P_{shear}}{P_{vf}} = \frac{\overline{u'w'} \frac{dU}{dz}}{\overline{u'w'} \frac{dU_S}{dz}} = \frac{\frac{u_*^2 u_*}{h}}{u_*^2 S_0} = La_m = \frac{u_*}{S_0 h} \quad (42)$$

This is because the Stokes shear at the surface, is affected by both the surface Stokes drift and penetration into the OSBL.

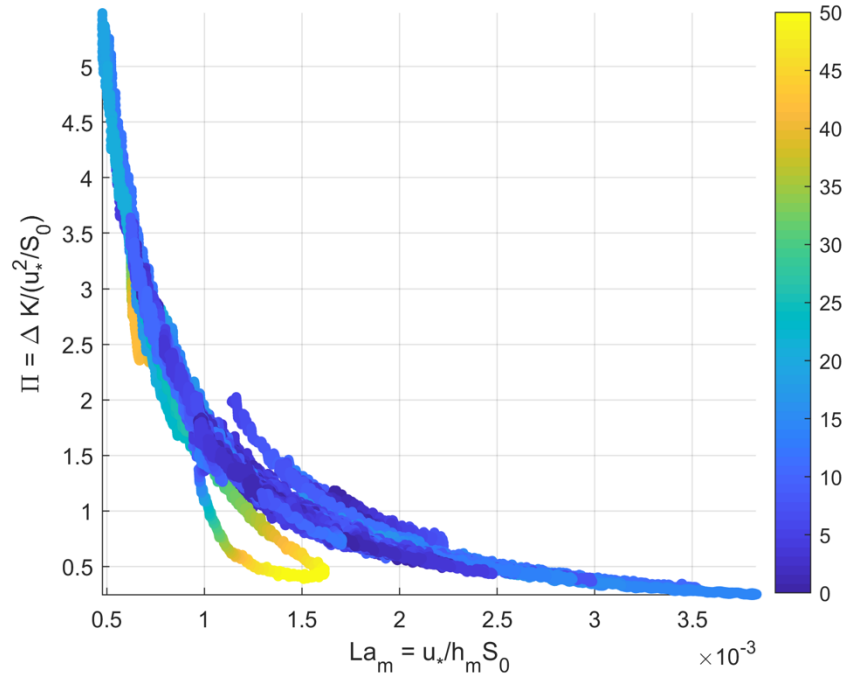


Figure 20: Scaling of modified Langmuir number with non-dimensional eddy viscosity colored by wind-wave misalignment angle.

The figure above shows a good scaling with our modified Langmuir number when the wind-wave angle of misalignment is less than 20 degrees. For higher wind-wave angles at a fixed modified Langmuir numbers the difference in eddy viscosity is reduced. This will be taken into account in the full parameterization discussed in the following section.

3.8 LT Boundary Layer Parameterization

The ultimate goal of this parameterization is to model the profile of eddy viscosity from the surface to the bottom of the BL. As discussed in section 2, ocean models already include parameterizations of the turbulent motions under the influence of wind shear and buoyancy flux but lack the effect of LT. Estimating the scalar eddy viscosity from LESs at Station Papa we can see that the eddy viscosity profiles are significantly different when LT is present, both in shape and magnitude.

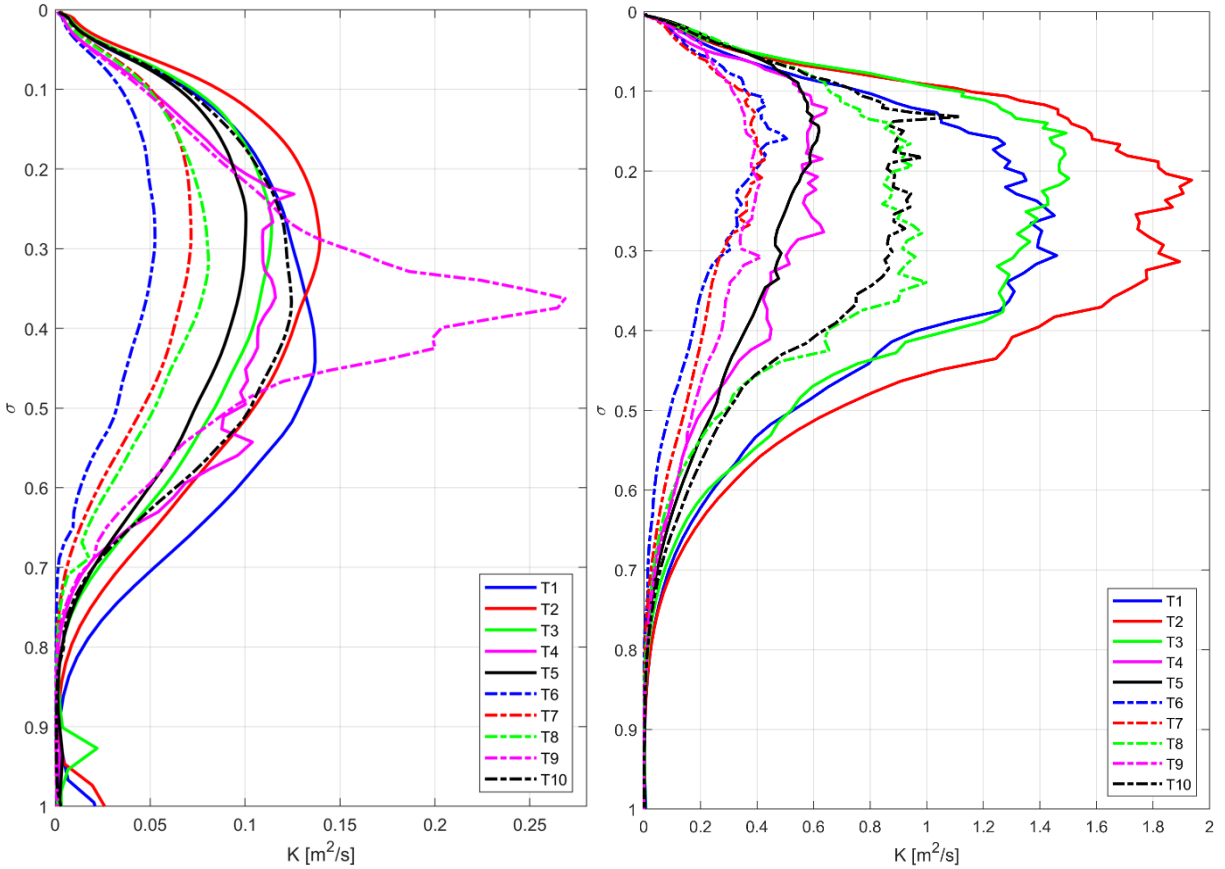


Figure 21: Profiles of inertially averaged scalar eddy viscosity from estimated from LES at Station Papa. (Left) Without LT. (Right) With LT.

The figure above shows the inertially averaged scalar eddy viscosity, computed in equation (11).

Note that using this definition guarantees that the eddy viscosity is always non-negative, but does not provide information on the direction of the turbulent fluxes or velocity gradients.

Additionally, in the presence of small vertical velocity gradients, the eddy viscosity have unusual spikes (e.g., T9). Figure xx shows significant enhancement of the eddy viscosity due to LT, in the range of 3-8 times as much as the case without LT. Additionally, the shape of the inertially averaged eddy viscosity profiles is also significantly different. For the case without LT the maximum eddy viscosity is close to $\sigma = 0.3$, while in the cases with LT the maximum is more variable and ranges from $\sigma = 0.12$ to $\sigma = 0.3$.

The focus of this report is in parameterizing the additional effect of LT on the vertical eddy viscosity profiles. Figure xx below shows the difference (ΔK) between the simulation with and without Stokes drift.

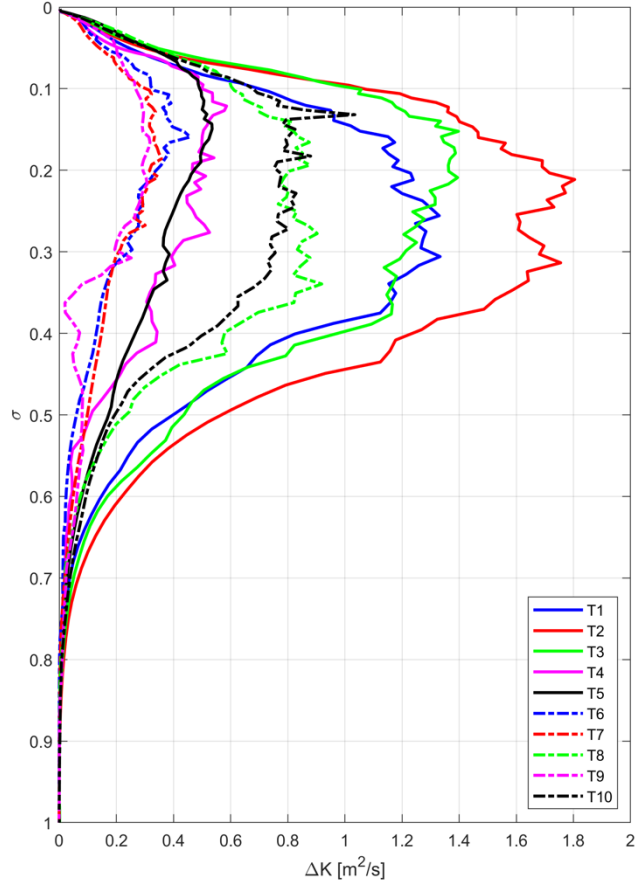


Figure 22: Profiles of inertially averaged eddy viscosity difference, between LES with and without LT.

Comparing the profiles of eddy viscosity (Figure 22), it is clear that the enhancement due to LT for this period is significant and consequently the profiles of eddy viscosity difference (Figure 22) and the profiles of eddy viscosity with LT are very similar. In the following sub-sections we will take a close look at these ten inertial periods to assess previous model suggestions and compare them with our proposed model. We choose the K Profile Parameterization scheme because it is computationally inexpensive compared to SMC models, and may be easily modified to include the effects of LT.

3.8.1 The KPP model

The KPP model offers several advantages over other parameterizations: it is based on semi-empirical theories, it is computationally inexpensive (compared to solving additional transport equations) and it is fairly simple to implement. The non-local KPP model for ocean applications was introduced by Large et al. (1994), and the model will be described just briefly to highlight the derivation and modifications made for this parameterization.

In the KPP model, the eddy viscosity is modeled using equation (6), shown below:

$$K(\sigma) = hw(\sigma)G(\sigma)$$

Where h is the BLD, w is a turbulent velocity scale and G is a shape function. The BLD is computed as the shallowest depth at which the bulk Richardson number exceeds a critical value.

$$Ri_b = \frac{B_{sl} - B}{|\vec{u}_{sl} - \vec{u}|^2 + V_t^2} (z_{sl} - z) \quad (43)$$

Here the subscript (sl) denotes an integral over the surface layer, B is the buoyancy, U is the velocity and V_t is a velocity scale represents the turbulent velocity shear. Integrating over the surface layer makes this number insensitive to vertical grid resolution, making it more robust and better suited for applications. In practice, computing the BLD is perhaps the most problematic part of this parameterization so it will be discussed in detail in the next chapter of implementation.

The turbulent velocity scale $w(\sigma)$ accounts for the enhancement due to convection, and is based in the semi-empirical Monin-Obukhov theory derived initially for the ABL, computed as:

$$w(\sigma) = \frac{\kappa u_*}{\phi} \quad (44)$$

Where κ is Von Karman's constant and ϕ is the non-dimensional flux profiles described in detail in appendix B of Large et al. (1994).

Finally, the shape function is a third degree polynomial which determines the overall shape of the K-profile, including the point of maximum eddy viscosity.

$$G(\sigma) = a_0 + a_1\sigma + a_2\sigma^2 + a_3\sigma^3 \quad (45)$$

A third degree polynomial was chosen so that there are 4 coefficients with which to control the values and derivatives of the eddy viscosity at the surface and bottom part of the boundary layer. The assumptions made are: 1) surface eddy viscosity is zero at the surface, since turbulent eddies do not cross the surface, 2) a linear reduction of momentum flux in the surface layer, 3/4) the value and gradient of the eddy viscosity go to zero at the bottom boundary layer. These assumptions fix the values of the 4 coefficients and yield:

$$G(\sigma) = \sigma - 2\sigma^2 + \sigma^3 \quad (46)$$

This function has a maximum at $\sigma = 0.33$, which roughly coincides with the maximum point of the scalar eddy viscosity in the LES without LT.

3.8.2 The enhanced KPP model

Other studies have suggested modifications to the KPP model to account for the enhancement due to LT. Here we briefly discuss the enhancement by McWilliams and Sullivan (2000), and Smyth et al. (2002), which suggest an enhancement using the turbulent Langmuir number.

$$f = \left(1 + \frac{c_w}{La_t^4}\right)^{1/2} \quad (47)$$

Where La_t is the turbulent Langmuir number and C_w is a function that accounts for convection. In the study of McWilliams and Sullivan (2000), they assign C_w a value of 0.08 on the basis of fits to large eddy simulations of quasistationary, weakly convective turbulence. When Langmuir turbulence is significant ($La_t < 1$) the enhancement becomes proportional to the surface Stokes drift. As mentioned earlier, this poses a problem when the decay length scale measured by the e-folding depth is different with similar surface Stokes drift. Longer waves with similar surface Stokes drift velocities and deeper decay lengths will have lower magnitudes of the Stokes shear which is proportional to the CL-VF. Additionally, convection plays an important role in vertical mixing and is not completely decoupled to LT. Accordingly, Smyth et al. (2002) formulate C_w to reflect the influence of convection when LT is also present:

$$C_w = c_{w0} \left(\frac{u_*^3}{u_*^3 + 0.6w_*^3} \right)^l \quad (48)$$

Where c_{w0} and l are constants to be determined, found to be equal to 0.15 and 2 respectively in Smyth et al. (2002). It is not clear where the value 0.6 comes from, but it has an effect on the influence of surface buoyancy flux on the parameterization. In the case of ($u_*^3 = -0.6w_*^3$) we get a singularity in which $C_w \rightarrow \infty$ as does the enhancement.

As mentioned earlier, we are interested in parameterizing the difference, or additional effect of LT in the K-profiles. By parameterizing the additional eddy viscosity due to LT, we can then add this parameterization to current models regardless of the method used.

$$\Delta K = K_{LT} - K \quad \rightarrow \quad K_{LT} = K + \Delta K \quad (49)$$

For example, we can use the well-known Mellor-Yamada scheme to model the eddy viscosity under the influence of wind shear and convection (K) and then add the difference (ΔK) to obtain the full profile (K_{LT}). This makes the enhancement due to LT easier to formulate since the difference can go to zero in the absence of Stokes drift, and it may even be negative when there is a high degree of wind-wave misalignment angle.

We choose the benchmark for our parameterization to be the suggestion by Smyth et al. (2002), discussed above, which leads to the following K-profiles.

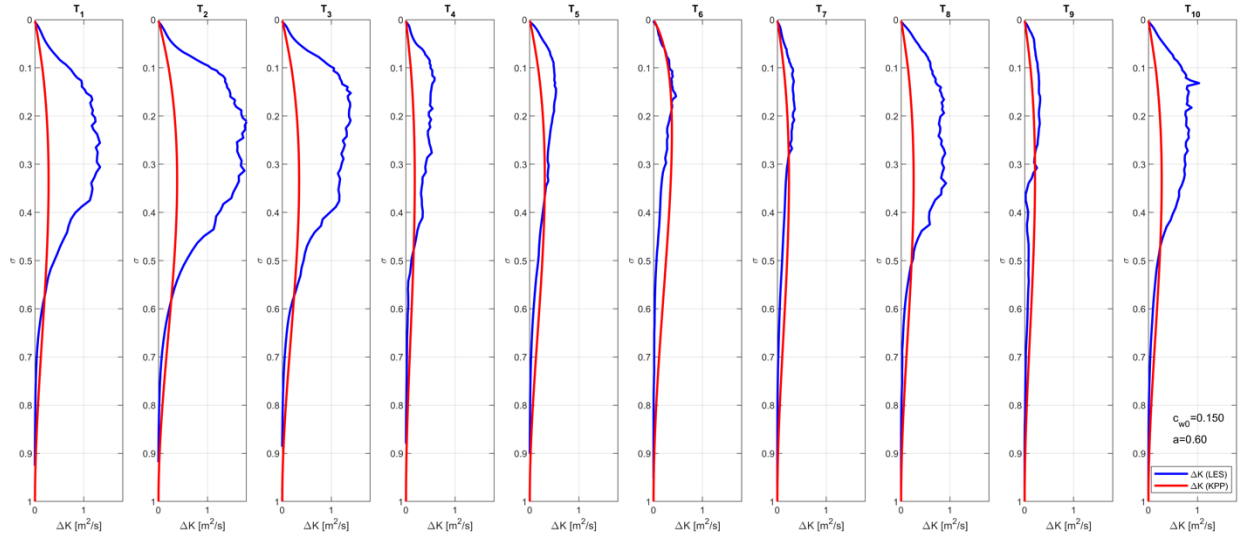


Figure 23: Profiles of inertially averaged eddy viscosity for 10 periods estimated from LES (blue) and from the KPP model of Smyth et al. (2002) (red).

The figure above shows the enhancement from the KPP model significantly underestimates the enhancement in the LES during most inertial periods, doing worse when convection is significant during the first 3 inertial periods. Adjusting convection constants (c_{w0}, l) to match the first three inertial periods results in an overestimation of the latter more neutral periods. This is ameliorated by changing the constant 0.6 value controlling the importance of surface heating, but an accurate representation for the 10 inertial periods could not be reached using the simple enhancement suggested above. The two major limitations of this suggested model is that it is independent of wind-wave misalignment and penetration depth (e-folding depth), resulting in the failure to reproduce or attempt to reproduce the shape of the eddy viscosity profiles, which are observed to be significantly different in the cases with and without LT in our LES (Figure 21).

In the next sub-sections, we present modifications of the KPP model that target the 2 limitations mentioned above.

3.8.3 The new KPP model

The vast majority of numerical studies of LT make the assumption of aligned wind and wave directions, which is a good approximation in situations when local winds and waves are in equilibrium. The structure of Langmuir circulations is thought to change significantly when the misalignment becomes very large (Var Roeckel et al. 2012) and vertical mixing rates may change significantly as a consequence of this misalignment.

In order to quantify the difference in vertical mixing rates in simulations with and without the effects of LT, a set of idealized LES has been performed with different wind-wave misalignment angles ($\theta = 0, 30, 60, 90, 120, 150$), totaling 7 different cases: 1 without LT and 6 with LT at the angles mentioned. Stratified ocean initial conditions are prescribed for the idealized experiments with a constant density layer from the surface to a depth of 20m. Below that layer, stable stratification of $d\theta/dz = 0.01$ K/m is prescribed with the thermal expansion coefficient $\alpha = 2 \times 10^{-4}$ K⁻¹. Constant forcing is applied for all experiments following McWilliams et al. (1997)

with wind stress $\tau = 0.037 Nm^{-2}$ (corresponding to a wind speed of about 5 m s⁻¹), a weak heat flux into the ocean of $Q_* = -5 Wm^{-2}$, and a Stokes drift profile corresponding to a sinusoidal wave with an amplitude of 0.8 m and length of 60 m (corresponding surface Stokes drift is $U_s = 0.068 m s^{-1}$). The boundary layer is uniformly rotating with a Coriolis force $f = 8.5867 \times 10^{-5} s^{-1}$, corresponding to 36.17° N latitude. The wave direction is kept aligned with the wind during the first inertial oscillation period to spin up turbulence and then changed to a certain angle depending on the case.

The figure below shows the scalar eddy viscosity profiles for the 7 LES. More detailed analysis of these idealized experiments can be found in Fan et al. (2019).

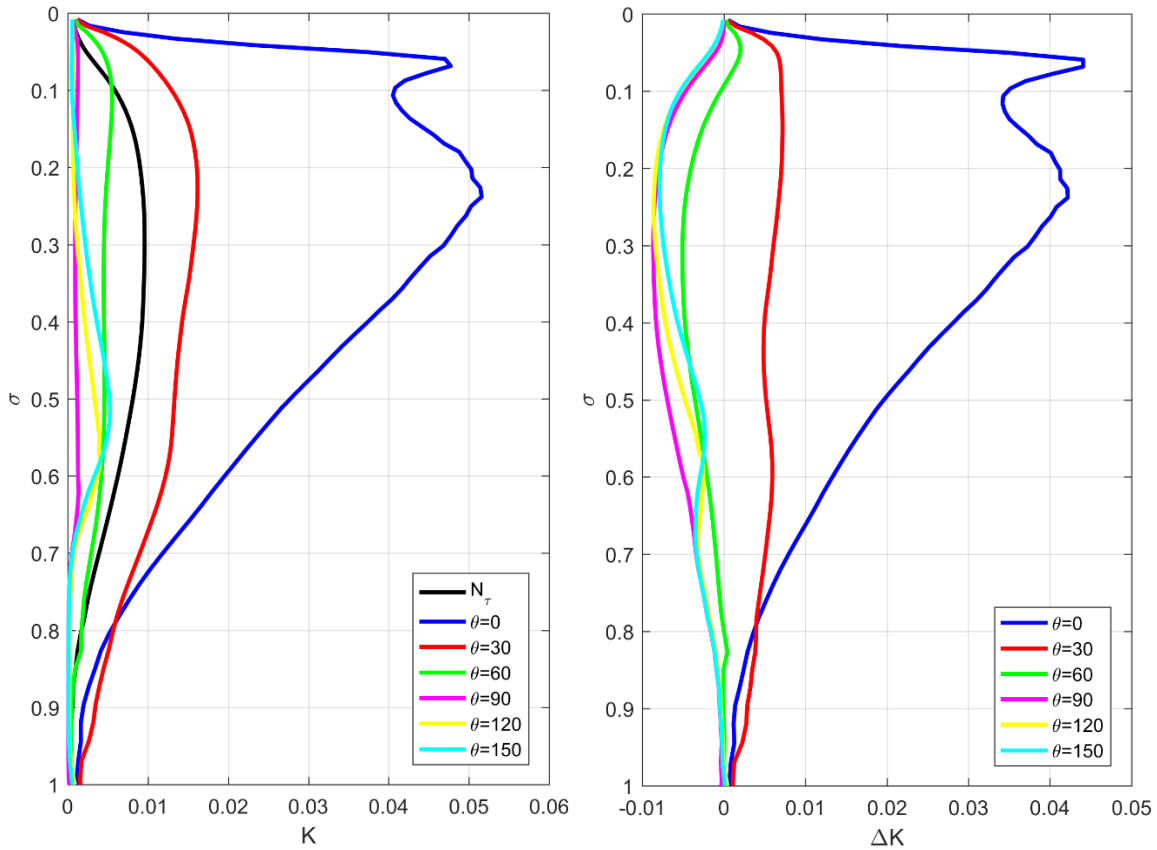


Figure 24: (Left) Profiles of scalar eddy viscosity and (Right) eddy viscosity difference for idealized LES under different wind-wave angles.

These figures show that the wind wave misalignment has a significant effect on the form and magnitude of the eddy viscosity profiles. The maximum magnitude of eddy viscosity is observed at the case of aligned wind and waves, roughly 5 times the magnitude of the case without LT. As the angle of wind-wave misalignment increases the magnitude of this enhancement decreases exponentially, such that the difference of eddy viscosity profile for the case of $\theta = 30^\circ$ is much less than the case of aligned wind-waves. The case of $\theta = 60^\circ$ shows that the eddy viscosity difference is negative throughout most the BL, implying that somewhere between $\theta = 30^\circ$ and $\theta = 60^\circ$ of misalignment there is no enhancement in vertical mixing compared to the case without LT.

Based on these simulations we want to quantify the enhancement in vertical mixing rates as a function of wind-wave misalignment. In other words, we want to parameterize the difference in eddy viscosity using the KPP model:

$$K_{LT} - K = hw(\sigma)G(\sigma)\mathbf{F}(\sigma, \theta) \quad (50)$$

Where $F(\sigma, \theta) = (f(\sigma) - 1)g(\theta)$ is the modification of the difference in scalar eddy viscosity. The function $f(\sigma)$ is the enhancement due to LT for the case of aligned wind-waves and $g(\theta)$ accounts only for the wind-wave misalignment angle. Because the simple enhancement (McWilliams and Sullivan 2001) is a good approximation for steady forcing conditions with aligned wind-waves, we take f equal to equation (47), which yields:

$$F(\sigma, \theta) = \left(\frac{c_w(u_* w_*)}{La_t^4} \right)^{\frac{1}{2}} \times \mathbf{g}(\theta) \quad (51)$$

The enhancement of the difference F should be zero as the effect of LT decreases ($La_t \rightarrow \infty$), and should increase as proportionally to the Stokes drift. The term in parenthesis is similar to the simple enhancement proposed by McWilliams and Sullivan minus the one, since we are parameterizing the difference, and is equal to 4.47 in the idealized simulation with aligned wind-waves ($\theta = 0$) presented here.

Now we can deduct a general form of the wind-wave modulation function ($g(\theta)$) by looking at the K-profiles of the idealized LES experiments. From the difference in eddy viscosity profiles (Figure 24), it is clear that the maximum enhancement is found for the case of aligned wind-waves and that this enhancement is clearly not linear since the difference in the K-profiles for cases $\theta = 0$ and $\theta = 30$ is larger than for $\theta = 30$ and $\theta = 60$, suggesting an exponential behavior. More importantly, the difference in eddy viscosity is positive for the case of $\theta = 30$ and negative for $\theta = 60$, so that the difference must be zero somewhere in between. Finally, it seems that for cases $\theta > 30$ LT works to decrease the rate of mixing compared to the case without LT, such that at high angles of wind-wave misalignment LT decreases mixing rates instead of enhancing them. The reduction in vertical mixing is maximum at $\theta = 90$. Consequently, we make the following assumptions to make an analytical prediction of the wind-wave modulation function (g).

- Enhancement of the difference is maximum at 0 degrees, so $g(0) = 1$
- Enhancement of the difference is 0 at 45 degrees, so $g(45) = 0$
- Maximum reduction is at 90 degrees, so $g(90) = \min(g) < 0$

Here we also assume symmetry around the direction of the wind, so that a 30 degree misalignment of the waves to the right is equal to a misalignment to the left. Using the assumptions listed above, we derive a general form:

$$g(\theta) = ae^{-|\theta|} \cos(b\theta + c) \quad (52)$$

Where a , b and c are constants to be determined, and θ is the angle of wind-wave misalignment. The absolute value on the exponential makes the function even, necessary to accommodate the symmetry constraint mentioned in the previous paragraph. This function displays an exponential decay observed in the K-profiles of the idealized LES and the sinusoidal function reflects the periodic nature of the observed profiles. We now adjust constants a , b and c using parameterization of the difference as mentioned above so that the modeled values match the ‘observed’ quantities in the LES experiments.

$$g(\theta) = \frac{e^{-|\theta|}}{\cos(3\pi/8)} \cos\left(\frac{\theta}{2} + \frac{3\pi}{8}\right) \quad (53)$$

The function is normalized at $\theta = 0$ to comply with the constraint on the first bullet. The wind-wave modulation form is shown along its entire range ($-\pi < \theta < \pi$) in the figure below.

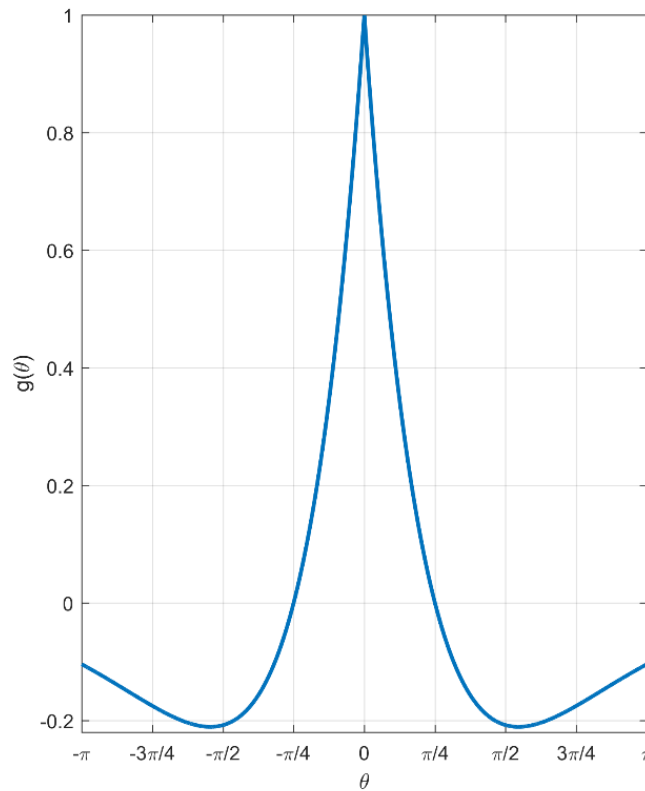


Figure 25: Wind-wave modulation function $g(\theta)$ in range $-\pi < \theta < \pi$.

Using this function, we obtain a parameterization of the eddy viscosity difference.

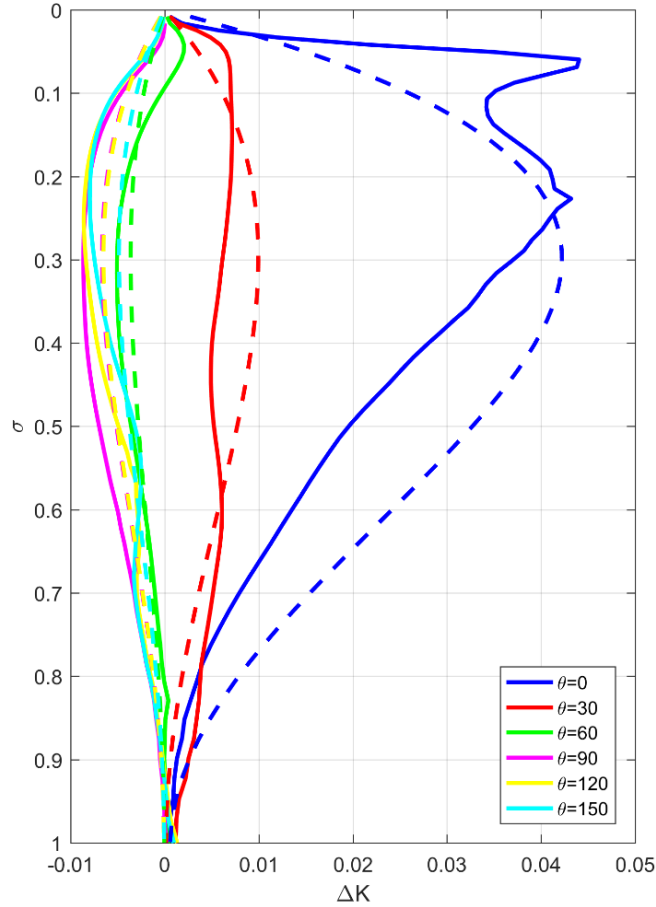


Figure 26: Profiles of eddy viscosity difference between simulations with and without LT at different wind-wave misalignment angles. Solid lines are estimated from LES and dashed lines are calculated using the wind-wave modulation function.

The wind wave modulation function shows good agreement with the idealized eddy viscosity profiles. Including this function as part of the parameterization should decrease the enhancement due to LT for misaligned wind and wave directions, which should be important in real ocean applications.

A notable drawback of the KPP scheme to parameterize LT is that the shape, or K-profiles of the cases with and without LT are significantly different. In shear dominated flows, even with significant convection the shape function ($G(\sigma)$) proposed in Large et al. (1994) is a good representation of the observed K-profiles for the case without LT. However, when LT is present the shapes of the K-profiles are significantly different to those without LT. To address this problem we take a closer look at the original shape function (equation 46)

The assumptions made in the original formulation of the non-local KPP scheme are still valid when LT is present, namely zero eddy viscosity at top/bottom of the BL, zero gradient at the bottom and linear gradient at the top; the *minimum* degree of the polynomial needs to be 3 to accommodate for the 4 necessary constraints. However, there is no reason not to increase the degree of the polynomial. By expressing the shape function $G = \sigma(1 - \sigma)^n$ as a binomial expansion of degree n , we can generalize and use some of its properties.

$$G(\sigma) = \sigma(1 - \sigma)^n \tag{54}$$

$$\frac{\partial G}{\partial \sigma} = (1 - \sigma) \left[1 - \frac{n\sigma}{1-\sigma} \right] \tag{55}$$

For any value of n , the 4 necessary constraints are met.

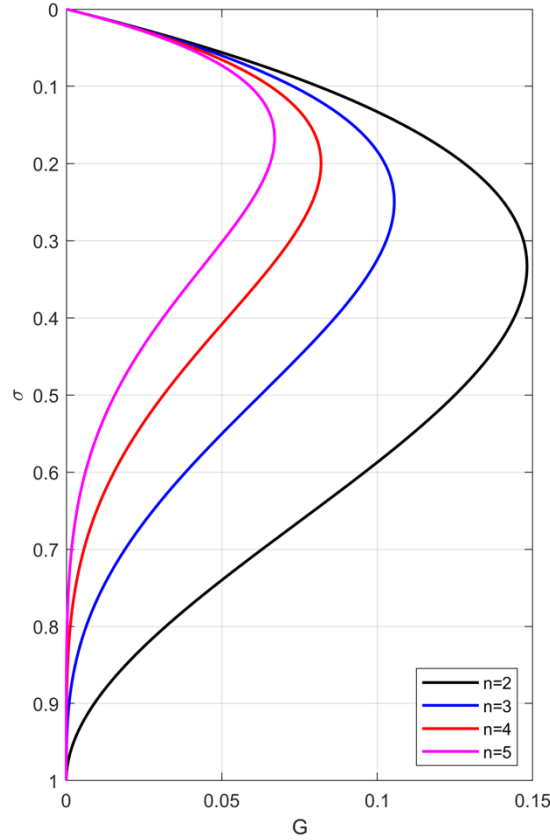


Figure 27: Generalized shape function $G(\sigma) = \sigma(1 - \sigma)^n$ with different degrees (n).

By increasing the degree of the binomial expansion we can control the magnitude and shape of the K-profiles. As a matter of fact the point at which the maximum happens is only a function of the degree of the expansion $\max(G) = \frac{1}{n+1}$.

Looking at the inertially averaged profiles of the difference in eddy viscosity (Figure 22) we can observe that periods in which convection is significant yield a maxima of eddy viscosity at deeper depths and the opposite is true for periods closer to neutral surface stratification. As observed in the TKE budget (Figure 8) simulations with LT have a larger contribution of turbulent transport, such that any excess in turbulent production near the surface is transported downwards by convective buoyant plumes. Consequently, it is hypothesized that surface buoyancy flux plays an important role in the magnitude and shape of the K-profiles and we can modify the degree of the binomial expansion of the shape function to alter the shape and magnitude of the eddy viscosity profiles without violating the constraints in Large et al. (1994, p. 371) which are still applicable to the OSBL. To do so, we make the shape function:

$$G(\sigma, \Pi_2) = \sigma(1 - \sigma)^n \quad (56)$$

Where n is a function of Π_2 , a dimensionless parameter proportional to surface buoyancy flux. Due to the correlation of the Coriolis parameter on the MLD, we can determine this dimensionless parameter to be:

$$\Pi_2 = \frac{B_0 f^3}{h^2} \quad (57)$$

Considering the observed range of surface heat fluxes in our LES, we determine the degree of the shape function to be:

$$n = -\frac{\Pi_2}{15} + 5 \quad (58)$$

The final step towards the parameterization is the use of our modified Langmuir number (equation 39) and the adjustment of the constants to match our LES results. The new KPP model presented here is a function of the wind wave angle (θ), the modified Langmuir number (Π_1) and our non-dimensional surface buoyancy flux (Π_2). We can express the relationship between vertical mixing as measured by the eddy viscosity as:

$$\Delta K = f(u_*, B_0, S_0/\beta, h_m, f, z) \quad (59)$$

The enhancement due to LT is a function of the wind shear, surface buoyancy flux, Stokes shear, Stokes' e-folding depth, wind-wave misalignment, mixed layer depth and Coriolis frequency. The mixed layer depth is a function of the stratification, so the relevant variable here is actually the potential density. Note that the Stokes shear and e-folding depth are expressed as a ratio because it is used as a substitute to the Stokes surface velocity and also to be consistent with Buckingham Pi theory ($p=n-k$). The wind-wave angle of misalignment is implicit in equation (59), since it may be computed from the directions of the wind stress (u_*) and the Stokes drift (S_0/β). In dimensionless form we can write this relationship as:

$$\frac{\Delta K}{u_*^2/S_0} = f(\Pi_1, \Pi_2, \sigma, \theta) \quad (60)$$

Where Π_1 is the modified Langmuir number, a measure of the relative strength of the CL-VF, Π_2 is the non-dimensional surface buoyancy flux, a measure of the relative strength of convection, σ is the non-dimensional vertical coordinate and θ is the wind-wave angle of misalignment in radians.

In order to test our parameterization, we start by looking at preliminary results using the LES simulation without LT to attempt to recreate the eddy viscosity from simulations with LT. Wind stress, surface buoyancy flux and the Stokes drift are boundary and forcing conditions to the model, so they are the same for simulations with and without LT. The main difference lies in the temperature and salinity fields, which are expected to be different in the two simulations. To emphasize the importance of the surface buoyancy flux in the enhancement of LT, we first perform the K-profile parameterization without the modification of the shape function.

$$\Delta K = hw(\sigma)G(\sigma)F(\sigma, \Pi_1, \theta) \quad (61)$$

Where $F(\sigma, \Pi_1, \theta)$ is the parameterization of the difference in eddy viscosity, defined as:

$$F(\sigma, \Pi_1, \theta) = \left(\frac{c_w}{\Pi_1^2}\right)^{\frac{1}{2}} \frac{e^{-|\theta|}}{\cos(3\pi/8)} \cos\left(\frac{\theta}{2} + \frac{3\pi}{8}\right) \quad (62)$$

Note that this number is somewhat different to the one used for the final surface parameterization because the model is already a function of the MLD through the KPP scheme. Recall that $\Pi_1 = \left(\frac{u_*\beta}{s_0}\right)\left(\frac{1}{\beta h}\right)$ is the number used for the final surface parameterization, but since $F \propto h\beta$ the BL parameterization already includes the penetration ratio ($h\beta$).

Adjusting constants ($c_{w0} = 0.8, l = 2$) and using the original shape function we obtain:

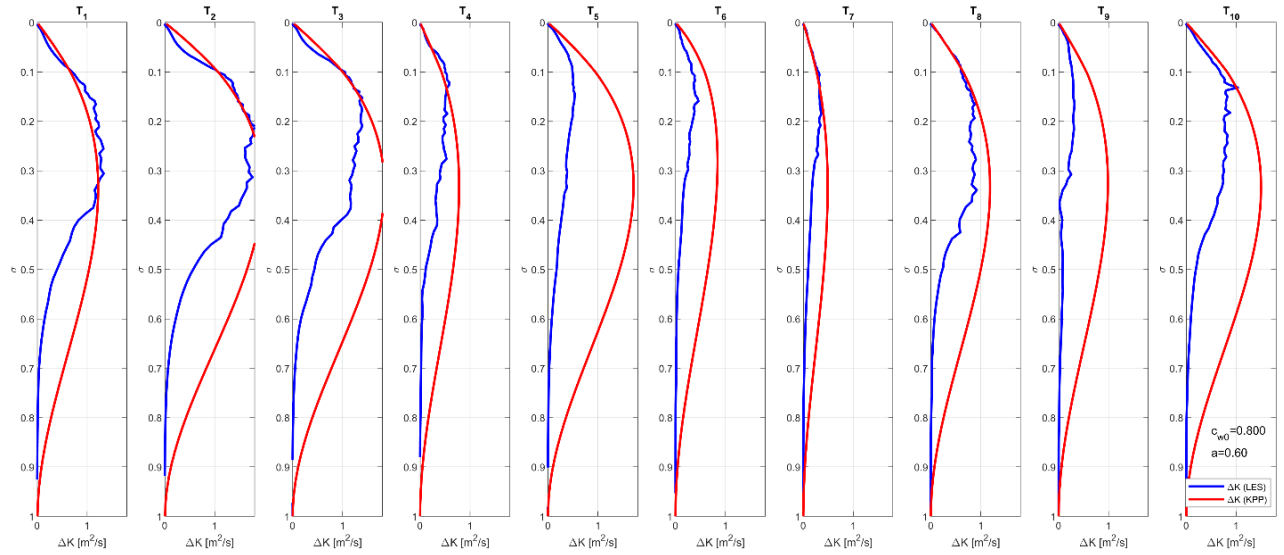


Figure 28: Preliminary BL parameterization without modification of shape function using values from LES at OWS-P.

This result significantly improved the simple enhancement suggested by McWilliams and Sullivan (2001), by making the eddy viscosity sensitive to wind-wave misalignment angle through the wind-wave modulation function ($g(\theta)$) and the penetration ratio.

The final parameterization also includes the modification of the shape function

$$\Delta K = hw(\sigma)G(\sigma, \Pi_2)F(\sigma, \Pi_1, \theta) \quad (63)$$

Using this formulation, we obtain

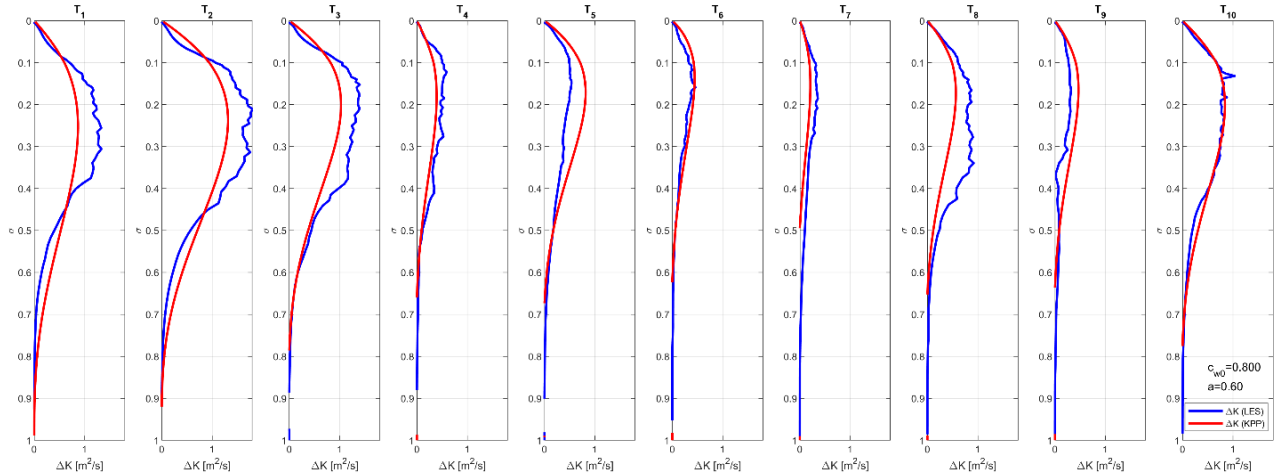


Figure 29: Final BL parameterization using preliminary values computed from LES at OWS-P.

The figure above shows that making the shape function dependent on the surface buoyancy flux significantly improves the accuracy of the K-profiles. In the following section we will explain the technical aspects behind the implementation of this parameterization in NCOM.

4. Implementation

The enhanced KPP model presented here has been implemented in the latest available version of NCOM, found in (/home/martin/model_ncom1/NCOM_SVN_branch_ice3m) from April 2019. NCOM uses an input flag (indzk) which controls the vertical scheme used to compute momentum and scalar diffusivities. The available options are:

4. Mellor-Yamada level 2 (indzk=2)
5. Mellor-Yamada level 2.5 (indzk=4)
6. Kantha and Clayson (indzk=5)
7. Harcourt (indzk=6)
8. KPP (indzk=7)

In practice, implementing the original KPP (Large, McWilliams, & Doney, 1994) and the enhanced KPP model presented here is basically the same, because it involves the calculation of MLD and the dimensionless Monin-Obukhov profiles. Furthermore, it is shown that for simulations without wave forcing, the KPP scheme yields more accurate profiles of eddy viscosity relative to estimated values of LES simulations without LT.

Vertical mixing schemes are found in file:

/NCOM_SVN_branch_ice3m/libsrc/ncom/ncom1vmix_sz.f where a subroutine is created for each of the schemes mentioned. The implementation is done by adding an additional subroutine (profq7_sz). This subroutine consists on:

1. The relevant physical parameters are computed from input values.

$$u_* = \sqrt{usflx^2 + vsflx^2}$$

$$B_0 = g\alpha(hsflx)$$

$$L = \frac{u_*^3}{\kappa B_0}$$

Note that in NCOM, the wind stress is divided by the constant seawater density ($\tau_{NCOM} = \frac{\tau}{\rho_0}$) and the surface heat flux is divided by seawater density and the specific heat of water ($Q_{NCOM} = \frac{Q}{\rho_0 c_p}$), both of which are set in the input file.

2. The MLD is computed based on a temperature criteria: a change of 0.125 degrees from the surface value. This yields the most consistent results in the initial testing at Station Papa, with the use of potential density yielding values that are significantly shallower than the values computed from LES.
3. The vertical coordinate (σ) is defined as the vertical z-coordinate normalized by the computed MLD:

$$\sigma_m = \frac{z_m}{h} \quad \sigma_w = \frac{z_w}{h}$$

This vertical coordinate is different from the σ -coordinate in NCOM, and is used to compute the non-dimensional flux profiles (ϕ_m, ϕ_s).

4. Non-dimensional flux profiles are computed exactly as specified in Large et al. (1994), appendix B. Using these values the turbulent velocities scales are computed as:

$$w_x(\sigma) = \frac{\kappa u_*}{\phi_x \left(\frac{\epsilon h}{L} \right)} \quad \epsilon < \sigma < 1 \quad \zeta < 0$$

$$w_x(\sigma) = \frac{\kappa u_*}{\phi_x \left(\frac{\sigma h}{L} \right)}$$

For unstable forcing conditions ($\zeta < 0$) the turbulent velocity scale below the surface layer is kept at this value to avoid exponentially large values. Note that here the subscript x denotes a generalized value, which is $x = s$ for scalars (salinity and temperature) and $x = m$ for momentum. The ratio of the scalar to momentum fluxes determines the Prandtl number, so the vertical momentum diffusivity is a scale of the scalar diffusivity.

5. The Stokes shear is calculated at the surface.

$$S_0 = \frac{\sqrt{u_s(z_w(2))^2 + v_s(z_w(2))^2} - \sqrt{u_s(z_w(1))^2 + v_s(z_w(1))^2}}{z_w(2) - z_w(1)}$$

This value yields good agreement with the Stokes shear computed from LES. However, in order to avoid vertical grid resolution dependence the Stokes shear should be either computed using an exponential profile or averaged over a certain depth.

6. The wind-wave angle is computed.
7. The non-dimensional functions (Π_1, Π_2) are computed.
8. The convective velocity scale $w_*^3 = \kappa h B_0$ and the convective function (C_w) is computed.
9. The K-profiles are computed.

Note that we opt to use the MLD throughout the entire parameterization instead of the BLD. This part is the most crucial and hardest part to get right.

As discussed in section 3, mixed and boundary layer depths are often defined using different criteria. In this section we show the MLD and BLD computed different criteria in our LES experiments at OWS-P.

In the next section we present results from the NCOM simulations, comparing LES estimated values and the other available schemes in NCOM.

5. Results and Discussion

In this section, we analyze results from 1-D NCOM simulations at OWS-P using the turbulent parameterizations discussed in chapter 2, as well as the newly implemented KPP scheme and the proposed parameterization of the enhancement due to LT described in chapter 3 and 4.

Two sets of experiments are presented. The first set replicates the LES simulations at OWS-P discussed in chapter 3, which spans 20 days during the fall of 2011. Accordingly, initial conditions and surface forcing are the same for the LES and NCOM simulations. The setup for all NCOM cases (Table 2) is identical (e.g., vertical grid, surface forcing) with the only difference being the turbulent mixing scheme used. NCOM results are compared to the LES results and observations, with emphasis on the eddy viscosity and temperature (e.g., SST). The goal of this set of experiments is to validate the KPP implementation and LT parameterization in NCOM and compare its performance to the SMC models already available in NCOM.

The second set of experiments consists of a one year long simulation at OWS-P for 1961. This simulation allows us to test the model's performance during an annual cycle that consists of seasonal variable surface forcing, i.e. testing the ability of the different parameterizations in both deepening and shallowing of the MLD. Additionally, the annual simulations at station Papa have been used extensively to test the performance of different ML models (Martin (1985); Large et al. (1994)), which provides a good benchmark for our results. However, there is no spectral wave data available for this year and the Stokes drift used for the simulation was estimated from observed wind stress, which is assumed to be aligned with the Stokes drift direction essentially neglecting the presence of remotely generated swells.

5.1 Computing MLD and BLD

In this sub-section we briefly discuss the computation of BLD using the bulk Richardson number, and how it compares to LES estimates using turbulent quantities (e.g., TKE and dissipation).

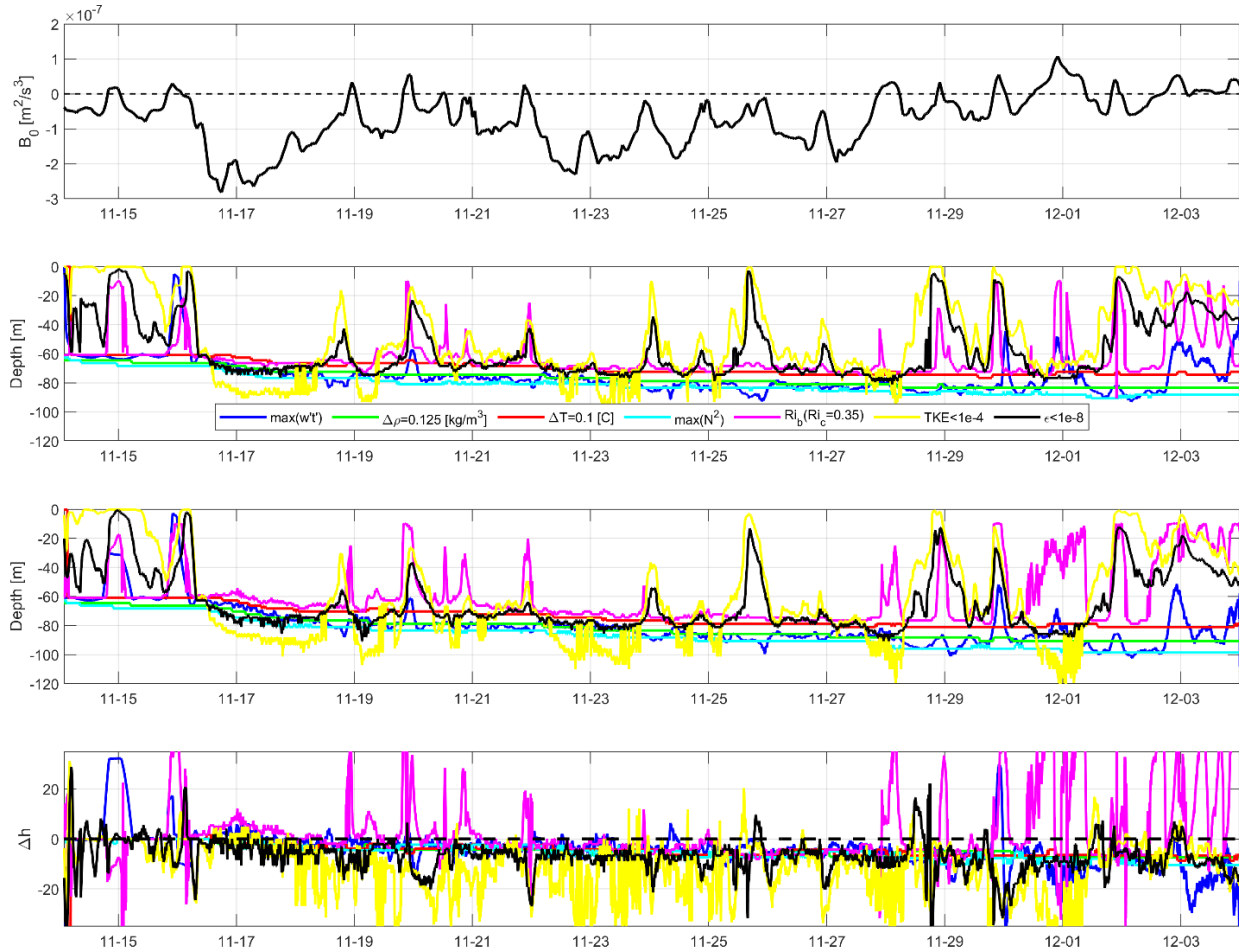


Figure 30: (Top) Surface buoyancy flux at OWS-P. (mid-top) MLD and BLD from LES without LT. (mid-bottom) MLD and BLD from LES with LT. (bottom) MLD and BLD difference, from LES with LT minus LES without LT.

The figure above shows the different MLD and BLD based on different criteria, namely the minimum turbulent heat flux, change of potential density from the surface, change of temperature from the surface, maximum stratification frequency, bulk Richardson number, TKE and dissipation. The boundary layer depths based on TKE and dissipation seem to be highly correlated as would be expected (i.e., same periods of shallowing/deepening) but the difference in depth based on the chosen thresholds, less than 10^{-4} for TKE and less than 10^{-8} for dissipation, is significant for some periods up to 20 meters. During periods of significant convection and shear (e.g., November 17-18) the BLD based on TKE is deeper than the definition based on dissipation, while for more stable periods (December 1, 4) the opposite is true. This suggests that the additional turbulent energy is converted to potential energy which effectively deepens the pycnocline.

The BLD based on the bulk Richardson number and using a critical Richardson number of 0.3 is slightly shallower than the other definitions and is more sensitive to stable surface forcing. This definition also poses a problem for comparison between LES simulations with and without the effect of LT, because it is a strong function of the vertical mean shear but does not account for the Stokes shear so that BLD is shallower for simulations with LT when Langmuir turbulence is significant ($La_t < 1$). A modified definition of BLD based the bulk Richardson number may be found by including the Stokes shear. Here, we test three different definitions of the bulk Richardson number.

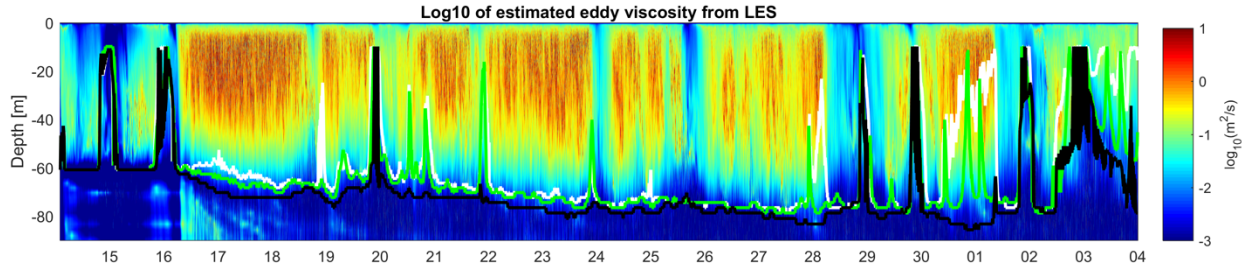


Figure 31: Color contours of \log_{10} of eddy viscosity from LES with LT, superimposed with the BLD estimated from the bulk Richardson number ($Ri_c = 0.3$) using the mean velocity (white line), Lagrangian velocity (green line) and the parameterization suggested by Li and Fox-Kemper (2017; black line).

Figure 31 shows color contours of the logarithm of eddy viscosity estimated from LES with the BLD computed from the bulk Richardson number using the mean velocity (Ri1; equation 9), the Lagrangian velocity (Ri2; mean + Stokes) and the parameterization suggested by Li and Fox-Kemper (Ri3; (2017)). During periods of strong destabilizing convection (November 17), Ri1 is slightly underestimated relative to the other two, while for periods of weak convection (November 19-30) Ri1 and Ri2 are almost identical, and Ri3 is slightly deeper. However, during periods of stabilizing buoyancy flux (December 1), the Ri1 and Ri2 estimated BLD are shallower than the Ri3 estimated BLD. If we take the BLD as where the eddy viscosity vanishes, this qualitative assessment suggests that including the Stokes drift in the bulk Richardson number generally improves the estimation of the BLD, especially during stable forcing, which is an essential prognostic variable in models based on the KPP scheme.

The entrainment depth $z(\min(w't'))$ is very similar to the depth of maximum stratification frequency $z(\max(N^2))$ but shallows during periods of stable surface forcing. The MLD based on maximum stratification frequency, a change of $0.125[kg/m^3]$ and $0.1^\circ C$ from the surface are all very similar, with the maximum stratification frequency criteria being the deepest, followed by the change in density and then temperature criteria.

From a physical standpoint the region of maximum stratification frequency provides a good measure of the MLD where kinetic energy from surface fluxes is converted to potential energy by raising dense water from the bottom to the top layers. This definition also correlates well with the entrainment depth, and MLD based on a change of density and temperature from the surface. All definitions based on potential density and temperature show mixed layer deepening in simulations with LT compared to simulations without it (Figure 30). Furthermore, definitions

based on potential density are found to be generally more robust (Harcourt & D'Asaro, 2008) and therefore MLD is defined in terms of potential density.

On the other hand, BLD is sometimes also defined as the point of maximum stratification frequency (Li & Fox-Kemper, 2017) or maximum temperature gradient (Sullivan & McWilliams, 2010), which do not show the same sensitivity to surface forcing in our simulations as definitions based on turbulent quantities (e.g., TKE). However, under destabilizing surface heat flux and significant wind/wave shear BLD estimations based on maximum stratification frequency and dissipation coincide closely to each other.

5.2 NCOM simulation set-up

The goal of the NCOM simulations is to test the LT parameterization developed here and compare its performance to other vertical schemes. Currently, NCOM includes the parameterizations by Mellor-Yamada, Kantha-Clayson and Harcourt, which are all second moment closure models. The Kantha-Clayson and Harcourt schemes have modifications to account for the CL-VF so that simulations with the effect of LT can be simulated. To facilitate the discussion, each mixing scheme is given a unique model name to indicate the scheme and whether or not it includes enhancements due to LT. The cases used for this report are summarized in the table below (Table 2).

Model Name	Mixing Scheme	Wave Forcing
MY	Mellor-Yamada level 2.5	No
KC	Kantha-Clayson	No
KCLT	Kantha-Clayson with LT	Yes
HC	Harcourt	No
HCLT	Harcourt with LT	Yes
KPP	K-Profile Parameterization	No
KPPLT	Enhanced KPP	Yes

Table 2: List of NCOM simulations at OWS-P.

The NCOM model was configured to simulate ML dynamics, and since our interest is to investigate vertical mixing under different surface forcing conditions we assume horizontal homogeneity by using a quasi-1D grid, dimensions 150 x 2 x 2, and double periodic boundary conditions in the horizontal directions.

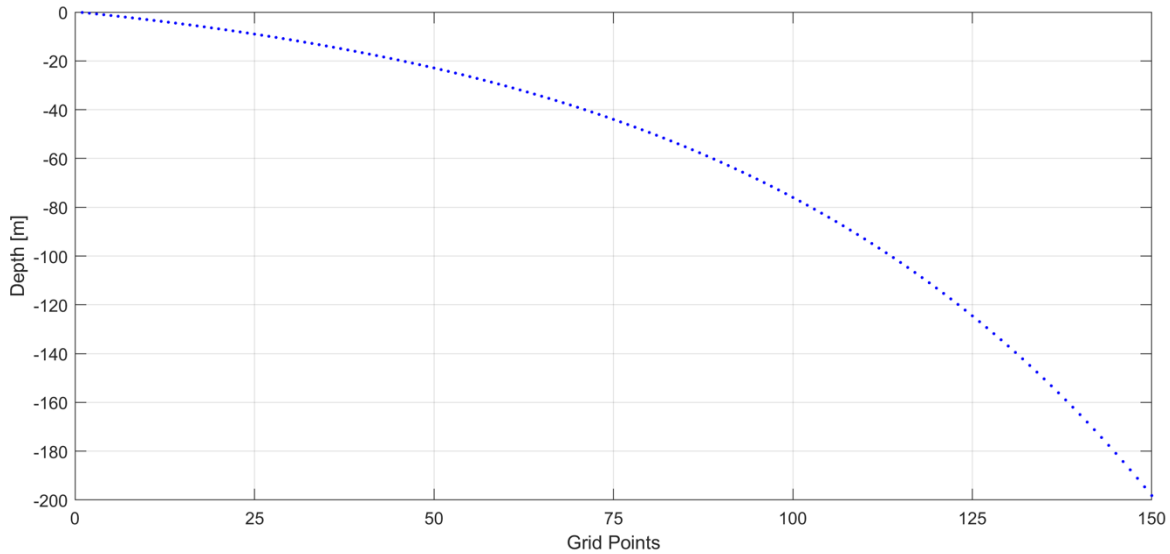


Figure 32: Vertical grid with 150 layers used for NCOM simulations.

The vertical grid (Figure 32) has a minimum thickness of 0.3m at the surface and has a logarithmic profile with the next grid being a constant multiple of the previous one. It is stretched towards the surface to capture the larger gradients expected from surface fluxes. All simulations were initialized from rest, that is, all velocities are set to zero ($u/v/w=0$) as well as initial surface elevation ($e=0$).

Initial conditions for temperature and salinity are obtained from OWS-P measurements and interpolated onto the vertical NCOM grid. The upper ML penetrates to a depth of roughly 60 meters, below which the thermocline and halocline may be clearly observed.

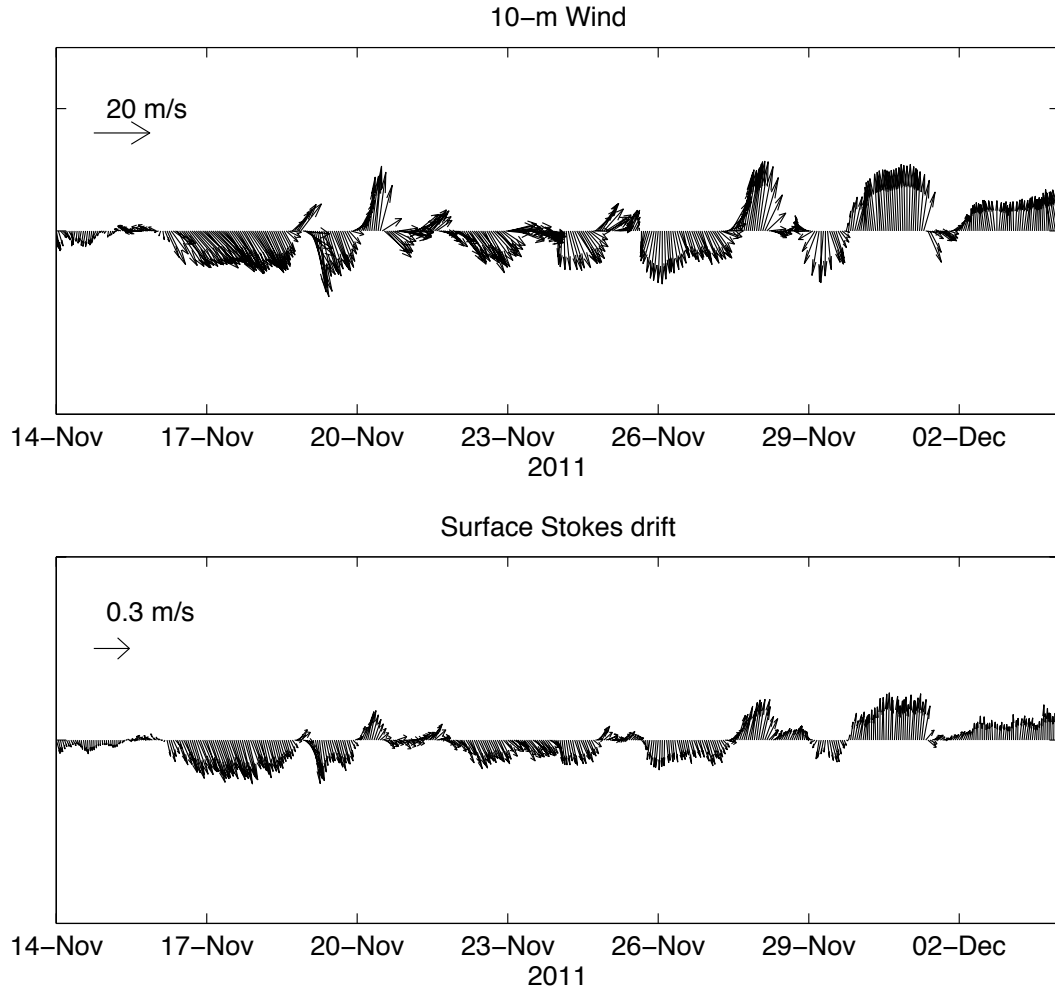


Figure 33:(Top) wind vectors at 10m height. (Bottom) Surface Stoke drift vectors at OWS-P.

The figure above shows wind velocity and surface Stokes drift during the duration of the experiment. As we can see, wind and waves are roughly aligned, although short periods of high wind-wave misalignment angles are observed. Observed 10-m wind and heat flux are used to force the model. In the NCOM simulations the total surface heat flux (Q_t), composed of latent heat flux (Q_e), sensible heat flux (Q_s), long (Q_b) and short (Q_{sol}) wave solar radiation, is prescribed at the surface. The solar penetration by short-wave solar radiation is not taken into account, instead the total heat flux is imposed at the surface.

5.3 Simulations without LT

As a starting point, simulations without wave forcing are performed to test the vertical schemes where they are expected to perform best.

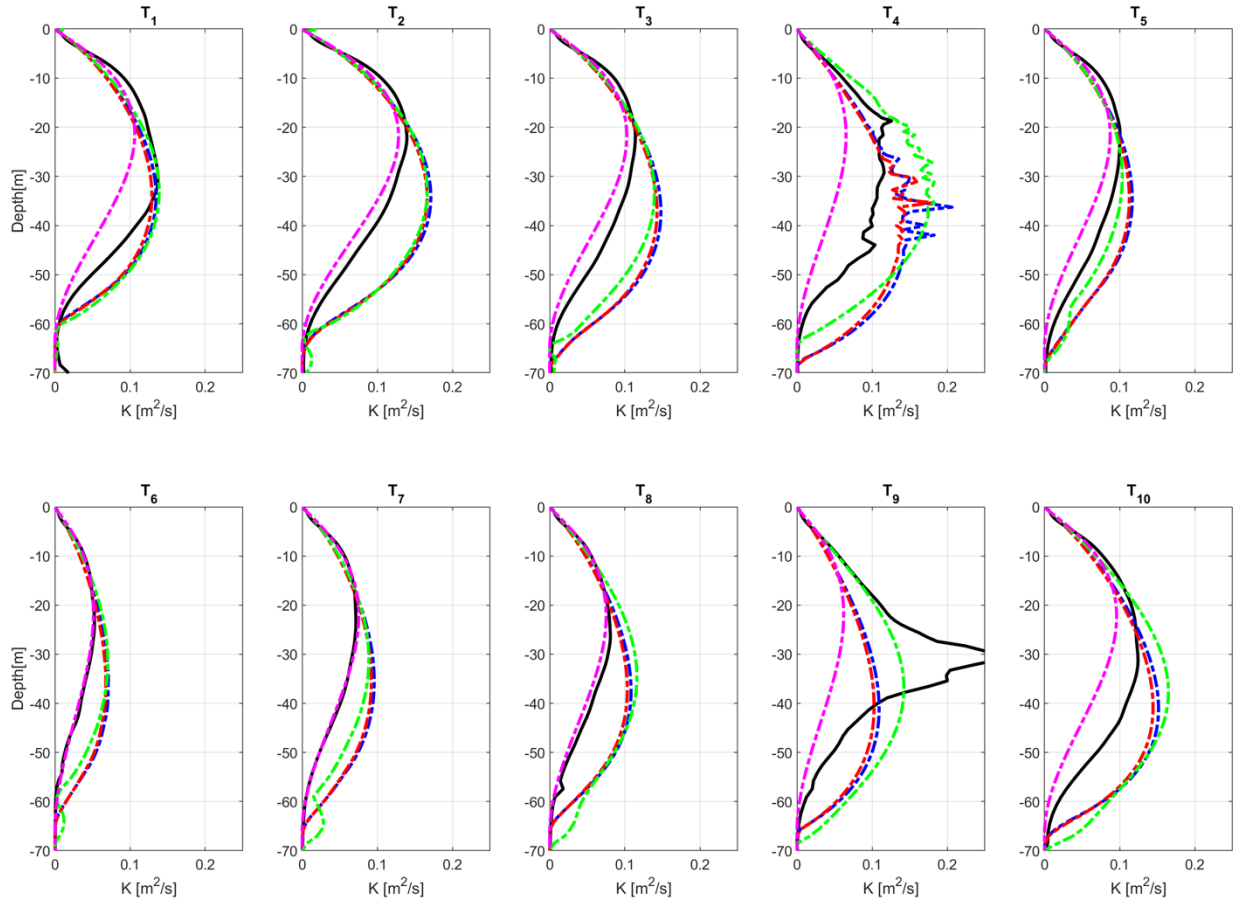


Figure 34: Inertially averaged eddy viscosity profiles from LES (black), MY (blue), KC (red), HC (green) and KPP (magenta).

Vertical profiles of eddy viscosity are averaged over inertial periods to remove inertial oscillations. The profiles shown in Figure 34 show that SMC schemes (MY, KC, HC) perform similarly, as can be expected from their derivations. The Harcourt scheme does have some significant deviations from the MY and KC profiles, most notably at inertial periods (T4 and T9), which also show unusual profile shapes from LES. At the bottom of the ML, there are elevated mixing rates found in using the Harcourt scheme, most notably on periods 7 and 8. The KPP model implemented in NCOM does significantly better at simulating the shape of the K-profiles for most periods, with significant differences found most notably on period T9. The shortcomings of the KPP model may be attributed to the fact that the current implementation uses MLD instead of BLD, but the approximation seems to work well over this period. A more detailed representation of the performance of the vertical mixing can be observed in color contours.

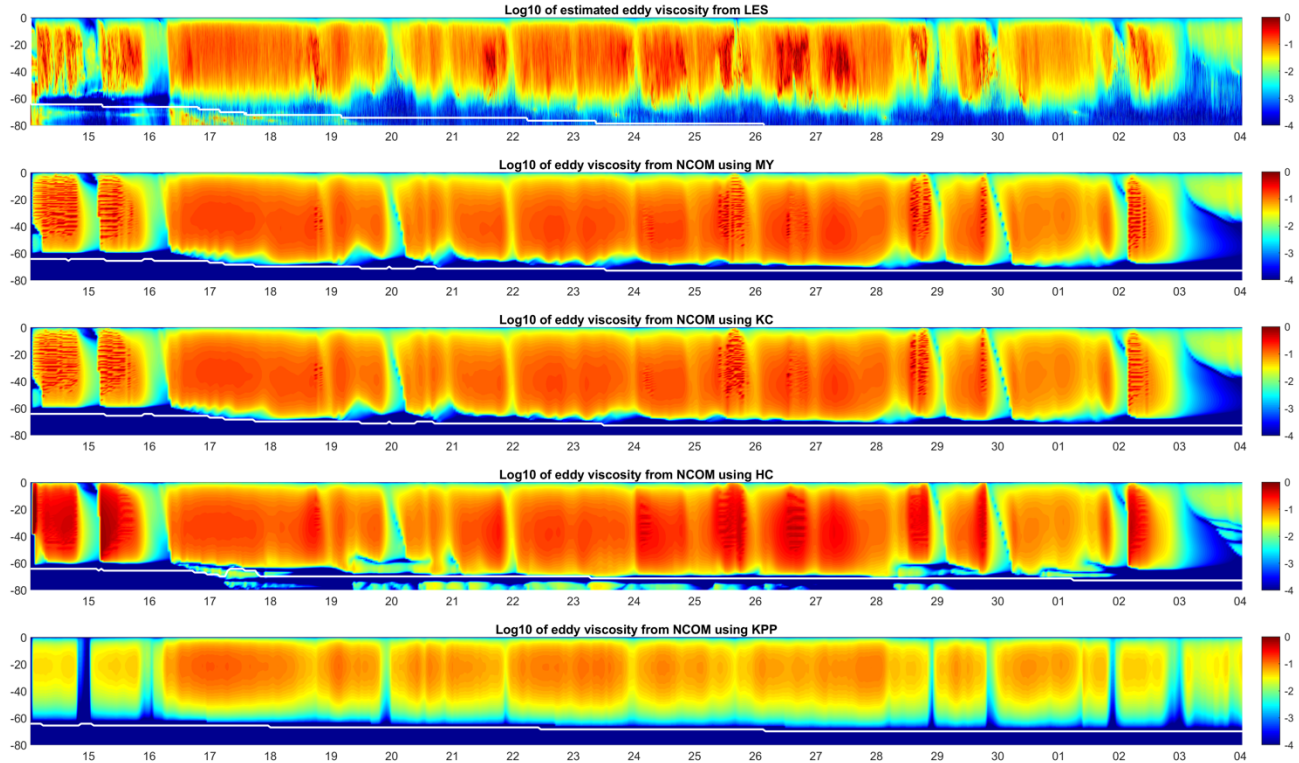


Figure 35: Color contours of \log_{10} of eddy viscosity from LES and NCOM simulations.

The color contours above show two important differences between the KPP and SMC schemes. First, the magnitude of the eddy viscosity is slightly underestimated in the KPP, and slightly overestimated in the SMC schemes. Second, the maximum of the profiles for LES and KPP is found around one third of the ML from the top (around 20m), while the maximum from the SMC schemes is found around two thirds of the ML (around 40m). Looking at the last day of the simulation, some important differences are observed between the SMC models and the KPP. During this period surface heat flux is stabilizing, and vertical mixing rates become significantly more shallow and this is not well represented in the KPP scheme. This is attributed to the use of the MLD instead of BLD to compute turbulent velocity scale, and additionally the eddy viscosity itself is also proportional to h .

5.4 Simulations with LT

In this section, we compare simulations with the effect of the CL-VF. In these simulations we omit the Mellor-Yamada scheme since it is not modified to account for the vortex force. The Kantha-Clayson and Harcourt schemes are both modified to account for LT, with important differences in their constants and derivation of the stability functions which should result in significantly different results. Below, we show the inertially averaged eddy viscosity profiles for the 10 inertial periods shown in Figure 6: (Top) Water side friction velocity. (Middle) Surface Stokes drift. (Bottom) Surface buoyancy flux at Ocean Water Station Papa for the 6.5 day averaging period. Background shaded rectangles are used to denote different inertial periods.

of the simulations with LT.

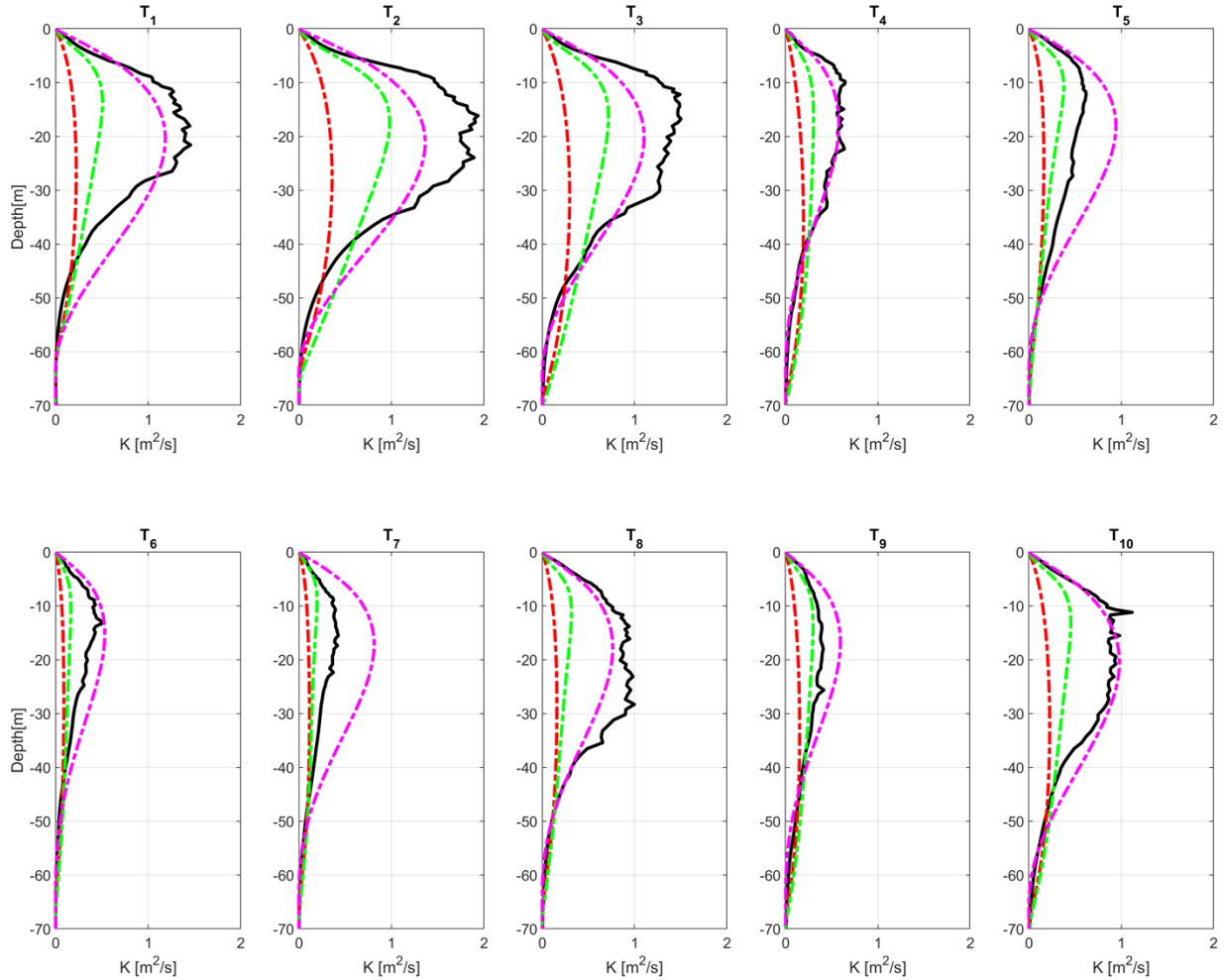


Figure 36: Inertially averaged eddy viscosity profiles from LES (black), KC (red), HC (green) and KPP (magenta)

The inertial eddy viscosity profiles show significant differences between the SMC and KPP models. Both the magnitude and shape of the LT parameterization presented here show good agreement with LES profiles, and significant improvement over the other schemes. The Harcourt and Kantha-Clayson schemes also show significant differences between each other, with the Harcourt scheme being generally larger in magnitude. The Harcourt scheme shows elevated mixing rates close to the surface, where the Stokes drift is more significant, and deepens with the Stokes penetration (e-folding depth). The enhanced KPP scheme shows greater sensitivity to surface momentum and heat fluxes, which characterize the first 3 inertial periods shown here.

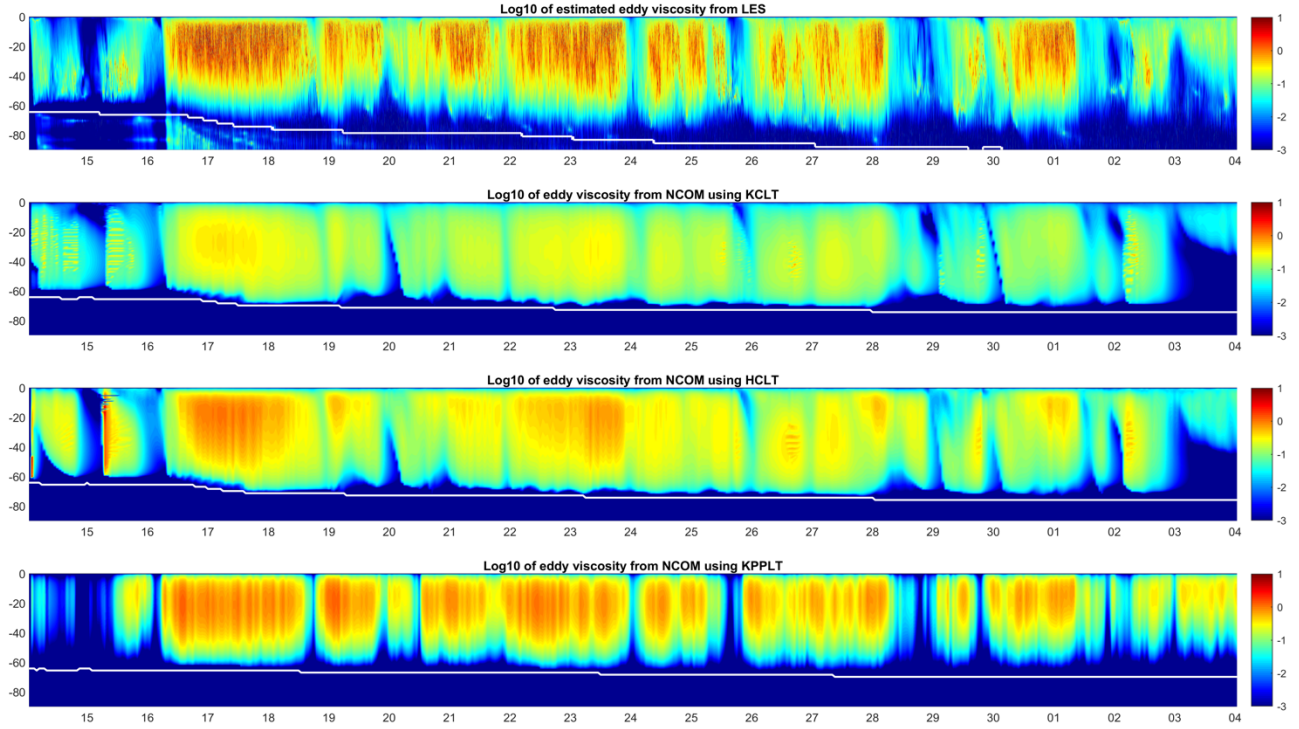


Figure 37: Color contours of \log_{10} of eddy viscosity from LES and NCOM simulations.

Color contours of the base 10 logarithm of eddy viscosity show good agreement between LES and NCOM simulations using the enhanced KPP scheme (Figure 37). The shape and magnitude agree well throughout most of the 20 day period. As in the case without LT, during the last day of simulation there are significant differences due to the use of MLD instead of BLD. Turbulent motions and their effect on BLD respond much more quickly to a stabilizing surface heat flux, while the ML takes longer to become shallow. This results in deeper penetration of modeled vertical mixing rates in this implementation of the enhanced KPP, but should not be observed if an acceptable BLD is found. Consequently, it is expected that this implementation perform better under convective forcing conditions than in stabilizing conditions. The main reason the enhanced KPP performs better than the other SMC schemes compared to the performance of the simulations without LT, is because in the presence of LT the *enhancement*, that is, the difference between the eddy viscosity with LT and without, is much greater than the eddy viscosity without LT. The enhancement is modeled as:

$$F(\sigma, \Pi_1, \theta) = \left(\frac{C_w}{\Pi_1^2} \right)^{\frac{1}{2}} \frac{e^{-|\theta|}}{\cos(3\pi/8)} \cos\left(\frac{\theta}{2} + \frac{3\pi}{8}\right)$$

As Langmuir Turbulence becomes more significant ($\Pi_1 \rightarrow \infty$) and the enhancement becomes a larger proportion of the total eddy viscosity. Alternatively, the enhancement may be added to the eddy viscosity from Mellor-Yamada or other schemes without the effect of LT. However, the enhancement implemented here was optimized to the original KPP scheme (Large et al. 1994), which shows better agreement in shape and magnitude than the other schemes implemented in

NCOM. In the following subsection we wrap-up with the most significant results from the parameterization.

5.5 OWS Papa (1961)

1-D NCOM simulations were performed at OWS-P for the entire year of 1961. The details for the estimation of surface fluxes and initialization of this simulation can be found in Martin (1985, p. 908), and here we only briefly discuss the setup of the vertical grid, time stepping and the estimation of the Stokes drift.

The setup used here, can be found in `\home\martin\model_ncom1\run_pap`. The vertical grid uses 100 levels in the vertical direction, starting at 0.5m and extending to a maximum depth of over 5000m, and uses the same logarithmic stretching towards the surface used in our previous experiment (Figure 32). The time step is set at 1 hour and the model is integrated from January 1st to December 31st, 1961.

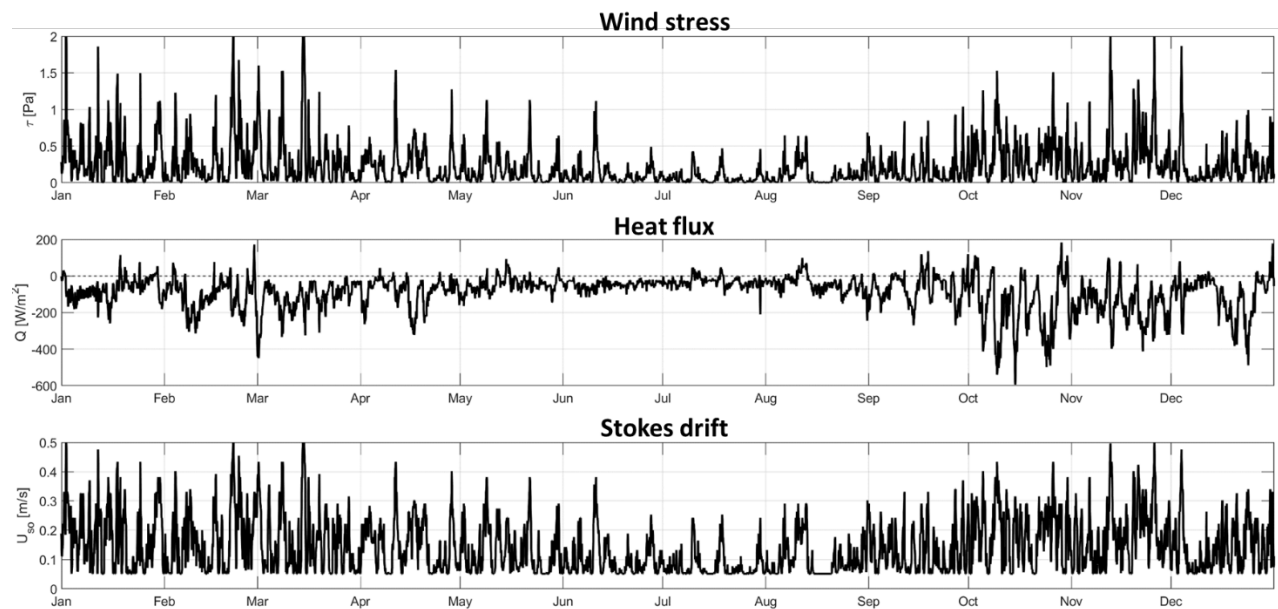


Figure 38: Surface forcing used for the OWS-P simulations during 1961. (Top) Wind stress, (middle) surface heat flux, and (bottom) surface Stokes drift velocity magnitude.

Figure 38 shows the wind stress, heat flux and surface Stokes drift used for the simulation. As mentioned before, the Stokes drift is estimated from the wind stress assuming these two vectors are aligned and neglecting the presence of remote swells. Consequently, the surface Stokes drift velocity might be overestimated, for example the minimum magnitude of the Stokes drift at the surface over the entire year is 5.1cm/s (Figure 38).

In this section, we only discuss the results of the NCOM simulations with LT. We can assess the general performance of each parameterization by comparing the simulated and observed SST (Figure 39).

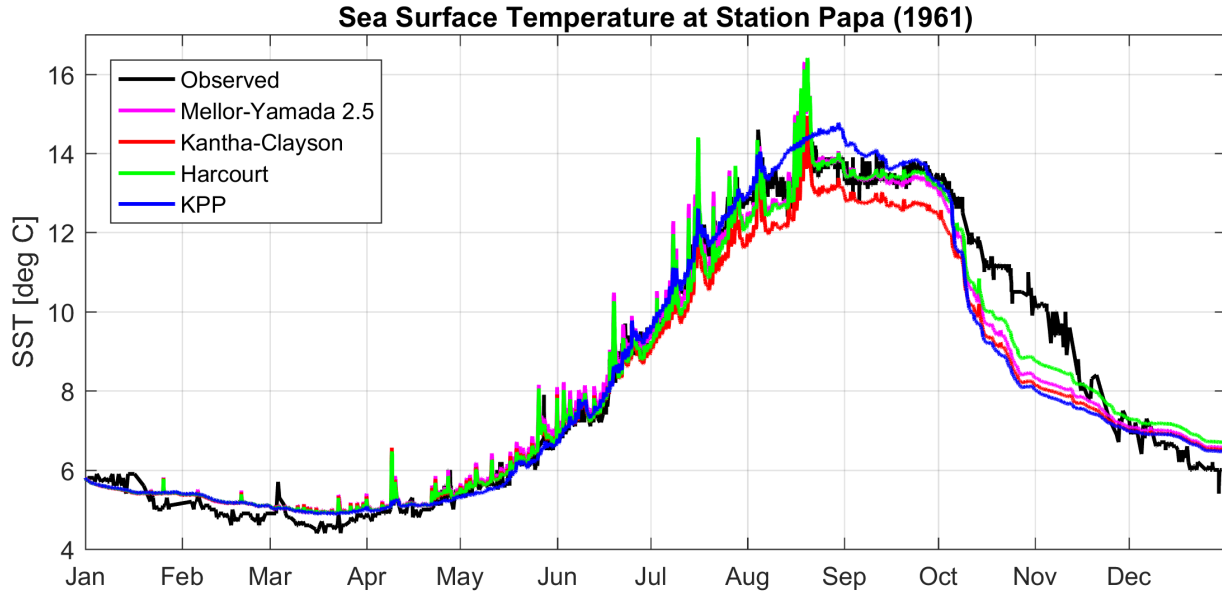


Figure 39: SST at station Papa during 1961 from BT observations (black) and NCOM simulations with LT using Mellor-Yamada 2.5 (magenta), Kantha-Clayson (red), Harcourt (green) and our enhanced KPP model (blue).

Comparing the observed SST with our results we find that the performance of the different LT parameterizations is very similar during winter and most of the differences arise in the summer, especially in August. Overall, the Kantha-Clayson scheme over-predicts the eddy viscosity in this simulation resulting in an underestimation of SST during the months August to September, while the KPP model slightly overestimates the SST during August. An interesting observation is that the Mellor-Yamada 2.5 model, which does not simulate the effects of LT, shows good agreement during most of the year including summer, suggesting that tuning the model turbulence parameters to observations may implicitly parameterize the effects of LT. During the period of July to mid-August, the Harcourt scheme slightly over predicts the SST while the KPP model shows better agreement. The contrary is true for the latter half of August, where Harcourt and Kantha-Clayson show better agreement with observations, and the KPP model slightly overestimates the SST by about half a degree Celsius.

The maximum observed SST happens around mid-August, during which the wind stress is almost zero, the Stokes drift is minimum and the buoyancy flux is near neutral stability. During this period the SMC models show vertical mixing rates on the order of the background mixing ($10^{-4} [m^2/s]$), while the eddy viscosity from the KPP model is significantly overestimated. This is due to the fact that we use the Lagrangian velocity (mean + Stokes) to compute the BLD, which is overestimated due to the Stokes drift that has a minimum surface value of 5cm/s. However, this is only observed during this short period of very low wind stress and is likely a consequence of the assumption made to estimate the Stokes drift.

During the winter months, the SMC models exhibit significant temperature fluctuations (up to 1 degree) at the surface, especially in the Harcourt scheme. Since the Harcourt scheme treats the momentum fluxes due to shear/convection separately from the Stokes drift, it is very likely that

these fluctuations are also a consequence of the estimation of the Stokes drift. The period after October shows a poor agreement between the NCOM results and the observed values, which is attributed to increased horizontal advection not modeled in our 1-D simulations.

5.6 Closing remarks

A parameterization for the enhanced effects of Langmuir Turbulence was developed from physical, dimensional and regression analysis from Large Eddy Simulations at OWS-P under realistic forcing conditions as well as idealized LES experiments. The parameterization is based on previous suggestions of the non-local K Profile Parameterization (Large et al. 1994), with enhancements by McWilliams and Sullivan (2001) and Smyth et al. (2002). In practice, implementing the original KPP scheme and the enhancement was virtually the same, so both were implemented in the latest version of the Navy Coastal Ocean Model as a subroutine of the vertical mixing code. The vertical mixing scheme may be chosen by changing a flag in the input parameter file, between the Second Moment Closure Models (Mellor-Yamada 2.5, Kantha-Clayson and Harcourt) as well as the newly implemented KPP scheme.

An NCOM simulation at OWS-P spanning a 20 day period, between November 14 and December 4, 2011 was used to test the implementation of the LT parameterization, and compared with LES results and the other NCOM schemes. Good agreement was found in the shape and magnitude of the inertially averaged eddy viscosity profiles between the LES results and NCOM simulations with the enhanced KPP scheme. The most challenging part of this parameterization is the accurate representation and computation of the BLD, which is estimated as the MLD in this case. The BLD computed based on the bulk Richardson number and using LES values shows rapid response to stabilizing surface forcing becoming significantly more shallow. An accurate representation of the BLD computed in NCOM, should yield improvements over the current implementation. The problem in the computation seems to lie specifically in the potential density, which is significantly different than the one computed from LES. Nevertheless, estimating the BLD as the MLD based on the difference in temperature from the surface yields good results for the parameterization developed here.

6. Summary and Conclusions

A new Langmuir turbulence parameterization with improved physics is developed based on recent scientific discoveries through the NRL 6.1 project “The Effect of Langmuir turbulence in upper ocean mixing”: 1. Strong horizontal density gradient can inhibit turbulence in the boundary layer and reduce mean flow in the mixed layer; 2. Large wind-wave misalignment can lead to strong reductions of turbulence in the boundary layer and traps the momentum in shallower surface layers; and 3. Enhanced upwelling due to LT can counteract on the deep convection and reduce the total turbulence level in the water column.

The parameterizations includes the effect of Buoyancy fluxes and wind-wave misalignment and is a function of the mixed layer depth which is proved to be significant in the eddy viscosity scaling in real case simulations, and is implemented in NCOM. 1D Numerical experiments show that the new formula is able to adequately represent eddy viscosity profiles within the mixed layer when compared to LES results. Although model comparisons at the Ocean Weather Station Papa show comparable skill between the newly developed parameterization and the turbulence closure models by Kantha-Clayson (2004) and Harcourt (2015), given the relative simple ocean dynamics at the station, we expect better performance from the new parameterization in more complicated atmospheric and ocean conditions.

7. Glossary

NCOM: Navy Coastal Ocean Model

NCAR: National Center for Atmospheric Research

CL-VF: Craik-Leibovich Vortex Force

LT: Langmuir Turbulence

LC: Langmuir Circulations (or Langmuir Cells)

LES: Large Eddy Simulation

SGS: Sub-Grid Stress

TKE: Turbulent Kinetic Energy

VKE: Vertical Kinetic Energy

RANS: Reynolds Averaged Navier-Stokes

ARSM: Algebraic Reynold Stress Model

PDE: Partial Differential Equation

SMC: Second Moment Closure

MY: Mellor-Yamada

KC: Kantha-Clayson

HC: Harcourt

GLS: General Length Scale

SST: Sea Surface Temperature

SDC: Stokes Drift Current

LMD: Large, McWilliams and Doney

KPP: K-Profile Parameterization

MO: Monin-Obukhov

ML: Mixed Layer

BL: Boundary Layer

MLD: Mixed Layer Depth

PBL: Planetary Boundary Layer

ABL: Atmospheric Boundary Layer

OSBL: Oceanic Surface Boundary Layer

BLD: Boundary Layer Depth

CC: Correlation Coefficient

UTC: Coordinated Universal Time

OWS-P: Ocean Water Station Papa

Acknowledgements

The original MATLAB functions to read and write NCOM data were provided by Tim Campbell (NRL Code 7322), and modified by the lead author, Miguel Solano, for the OWS-P simulations. We thank Dr. Campbell for providing these functions.

This research was performed while the lead author, Miguel Solano, held an NRC Research Associateship award at the Naval Research Laboratory at Stennis Space Center.

References

- Ali, A., Christensen, K., Breivik, O., Malila, M., Raj, R., Bertino, L., . . . Bakhoday-Paskyabi, M. (2019). A comparison of Langmuir turbulence parameterizations and key wave effects in a numerical model of the North Atlantic and Arctic Oceans. *Ocean Modelling*, 137, 76-97.
- Belcher, S., Grant, A., Hanley, K., Fox-Kemper, B., Van Roekel, L., Sullivan, P., . . . Polton, J. (2012). A global perspective on Langmuir turbulence in the ocean surface boundary layer. *Geophysical Research Letters*, 39, 1-9.
- Craik, A., & Leibovich, S. (1976). A Rational Model for Langmuir Circulations. *Journal of Fluid Mechanics*, 73, 401-426.
- Crow, S. (1968). Viscoelastic Properties of Fine-Grained Incompressible Turbulence. *Fluid Mechanics*, 33, 1-20.
- D'Asaro, E., Thomson, J., Shcherbina, A., Harcourt, R., Cronin, M. H., & Fox-Kemper, B. (2014). Quantifying upper ocean turbulence driven by surface waves. *Geophysical Research Letters*, 41, 102-107.
- Deardorff, J. (1966). The counter gradient heat flux in the lower atmosphere and in the laboratory. *Journal of Atmospheric Sciences*, 503-506.
- Fan, Y., & Griffies, S. (2014). Impacts of parameterized Langmuir turbulence and Nonbreaking wave mixing in global climate simulations. *Journal of Climate*, 27, 4752-4775.
- Galperin, B., Kantha, L., Hassid, S., & Rosati, A. (1988). A Quasi-equilibrium Turbulent Energy Model for Geophysical Flows. *Journal of the Atmospheric Sciences*, 45(No. 1), 55-62.
- Gargett, A. E., & Wells, J. R. (2007). Langmuir turbulence in shallow water. Part 1. Observations. *Fluid Mechanics*, 576, 27-61.
- Harcourt, R. (2013). A Second-Moment Closure Model of Langmuir Turbulence. *Journal of Physical Oceanography*, 43, 673-697.
- Harcourt, R. (2015). An Improved Second-Moment Closure Model of Langmuir Turbulence. *Journal of Physical Oceanography*, 45, 84-103.
- Harcourt, R., & D'Asaro, E. (2008). Large-eddy simulation of Langmuir turbulence in pure wind seas. *Journal of Physical Oceanography*, 38, 1542-1562.
- Holtslag, A., & Moeng, C.-H. (1991). Eddy diffusivity and countergradient transport in the convective atmospheric boundary layer. *Journal of Atmospheric Sciences*, 48, 1690-1698.
- Kantha, L., & Clayson, C. A. (1994). An improved mixed layer model for geophysical application. *Journal of Geophysical Research*, 99(C12), 25235-25266.

- Kantha, L., & Clayson, C. A. (2004). On the effect of surface gravity waves on mixing in the oceanic mixed layer. *Ocean Modelling*, 6, 101-124.
- Kukulka, T., & Harcourt, R. (2017). Influence of Stokes Drift Decay Scale on Langmuir Turbulence. *Physical Oceanography*, 47, 1637-1656.
- Langmuir, I. (1938). Surface Motion of Water Induced by Wind. *Science*, 87, 118-123.
- Large, W., McWilliams, J., & Doney, S. (1994). Oceanic Vertical Mixing: a Review and a Model with a Nonlocal Boundary Layer Parameterization. *Reviews of Geophysics*, 32(4), 363-403.
- Leibovich, S. (1983). The form and dynamics of Langmuir circulations. *Annual Review of Fluid Mechanics*, 15, 391-427.
- Li, M., & Garrett, C. (1995). Is Langmuir circulation Driven by Surface Wave or Surface Cooling. *Journal of Physical Oceanography*, 25, 64-76.
- Li, M., Garrett, C., & Skillingstad, E. (2005). A Regime Diagram for Classifying Turbulent Large Eddies in the Upper Ocean. *Deep Sea Research Part I*, 52, 259-278.
- Li, Q., & Fox-Kemper, B. (2017). Assessing the effects of Langmuir turbulence on the entrainment buoyancy flux in the ocean surface boundary layer. *Journal of Physical Oceanography*, 47, 2863-2886.
- Liu, J., Liang, J.-H., McWilliams, J., Sullivan, P., Fan, Y., & Chen, Q. (2018). Effect of rotation on oceanic surface boundary layer turbulence. *Journal of Physical Oceanography*, 48, 2,057-2,080.
- Mahrt, L., & Gibson, W. (1976). Flux decomposition into coherent structures. *Monthly Weather Review*, 60, 1,403-1,418.
- McWilliams, J., & Sullivan, P. (2000). Vertical Mixing by Langmuir Circulations. *Spill Science & Technology Bulletin*, 6, 225-237.
- McWilliams, J., Huckle, E., & Liang, J. (2014). Langmuir Turbulence in Swell. *Physical Oceanography*, 44, 870-890.
- McWilliams, J., Huckle, E., Liang, J.-H., & Sullivan, P. (2012). The wavy Ekman layer: Langmuir circulations, breaking waves, and Reynolds stress. *Journal of Physical Oceanography*, 42, 1,793-1,816.
- McWilliams, J., Sullivan, P., & Moeng, C.-h. (1997). Langmuir Turbulence in the Ocean. *Fluid Mechanics*, 334, 1-30.
- Mellor, G. (2006). On theories dealing with the interaction of surface waves and ocean circulation. *Geophysical Research: Oceans*, 121, 4474-4486.
- Mellor, G., & Yamada, T. (1974). A Hierarchy of Turbulence Closure Models for Planetary Boundary Layers. *Journal of the Atmospheric Sciences*, 31, 1791-1806.

- Mellor, G., & Yamada, T. (1984). Development of a Turbulence Closure Model for Geophysical Applications. *Reviews of Geophysics*, 20, 851-875.
- Moeng, C.-H. (1984). A Large-Eddy-Simulation Model for the Study of the Planetary Boundary Layer Turbulence. *Journal of the Atmospheric Sciences*, 41, 2052-2062.
- Moeng, C.-H., & Wyngaard, J. (1986). An analysis of closures for pressure-scalar covariances in the convective boundary layer. *Journal of Atmospheric Sciences*, 34, 2,499-2,513.
- Niiler, P., & Kraus, E. (1977). One-dimensional models of the upper ocean. *Modelling and Prediction of the Upper Layers of the Ocean*, 143-172.
- Noh, Y., Goh, G., & Raasch, S. (2011). Influence of Langmuir circulation on the deepening of the wind-mixed layer. *Journal of Physical Oceanography*, 41, 472-484.
- Pearson, B., Grant, A., Polton, J., & Belcher, S. (2018). Reply to "Comments on 'Langmuir Turbulence and Surface Heating in the Ocean Surface Boundary Layer'". *Journal of Physical Oceanography*, 48, 459-462.
- Pope, S. (2000). *Turbulent Flows*. Cambridge: Cambridge University Press.
- Price, J., Weller, R., & Pinkel, R. (1986). Diurnal cycling: Observations and models of the upper ocean response to diurnal heating, cooling and wind mixing. *Journal of Geophysical Research*, 91, 8411-8427.
- Rotta, J. (1951). Statistische Theorie nichthomogener Turbulenz. *Z. Physik*, 129, 547-572.
- Skyllingstad, E., & Denbo, D. (1995). An ocean large-eddy simulation of Langmuir circulations and convection in the surface mixed layer. *Journal of Geophysical Research*, 100, 8,501-8,522.
- Smyth, W., Skyllingstad, E., Crawford, G., & Wisejekera, H. (2002). Nonlocal Fluxes and Stoke Drift Effects in the K Profile Parameterization. *Ocean Dynamics*, 104-115.
- Stull, R. B. (1988). *An Introduction to Boundary Layer Meteorology*. Dordrecht: Kluwer Academic Publishers.
- Sullivan, P., & McWilliams, J. (2007). Surface gravity wave effects in the oceanic boundary layer: Large-eddy simulation with vortex force and stochastic breakers. *Fluid Mechanics*, 593, 405-452.
- Sullivan, P., & McWilliams, J. (2010). Dynamics of winds and currents coupled to surface waves. *Annual Review of Fluid Mechanics*, 42, 19-42.
- Sullivan, P., McWilliams, J., & Melville, W. (2007). Surface gravity wave effects in the oceanic boundary layer: Large-eddy simulation with vortex force and stochastic breakers. *Journal of Fluid Mechanics*, 593, 405-452.

- Sutherland, G., Christensen, K., & Ward, B. (2014). Evaluating Langmuir turbulence parameterizations in the ocean surface boundary layer. *Journal of Geophysical Research: Oceans*, *119*, 1,899-1,910.
- Var Roeckel, L., Fox-Kemper, B., Sullivan, P., Hamlington, P., & Haney, S. (2012). The form and orientation of Langmuir cells for misaligned wind-waves. *Journal of Geophysical Research*, *117*, 1-22.
- Wyngaard, J., & Brost, R. (1984). Top-down and bottom-up diffusion in the convective boundary layer. *Journal of Atmospheric Sciences*, *41*, 102-112.